GENESIS OF THE VOLCAN COPIAPO SULPHUR DEPOSITS, MARICUNGA DISTRICT, CHILE.

Allen Stark

Submitted in Partial Fulfillment of the Requirements

for the Degree of Bachelor of Science, Honours

Dalhousie University,

Halifax, Nova Scotia

May, 1991

Distribution License

DalSpace requires agreement to this non-exclusive distribution license before your item can appear on DalSpace.

NON-EXCLUSIVE DISTRIBUTION LICENSE

You (the author(s) or copyright owner) grant to Dalhousie University the non-exclusive right to reproduce and distribute your submission worldwide in any medium.

You agree that Dalhousie University may, without changing the content, reformat the submission for the purpose of preservation.

You also agree that Dalhousie University may keep more than one copy of this submission for purposes of security, back-up and preservation.

You agree that the submission is your original work, and that you have the right to grant the rights contained in this license. You also agree that your submission does not, to the best of your knowledge, infringe upon anyone's copyright.

If the submission contains material for which you do not hold copyright, you agree that you have obtained the unrestricted permission of the copyright owner to grant Dalhousie University the rights required by this license, and that such third-party owned material is clearly identified and acknowledged within the text or content of the submission.

If the submission is based upon work that has been sponsored or supported by an agency or organization other than Dalhousie University, you assert that you have fulfilled any right of review or other obligations required by such contract or agreement.

Dalhousie University will clearly identify your name(s) as the author(s) or owner(s) of the submission, and will not make any alteration to the content of the files that you have submitted.

If you have questions regarding this license please contact the repository manager at dalspace@dal.ca.

Grant the distribution license by signing and dating below.

_____ _____

Name of signatory Date

ABSTRACT

The Miocene age Copiapo Volcanic Complex is located in the heart of the Maricunga gold mining district in the southernmost part (Latitude 27°S) of the Andean Central Volcanic Zone. The largest cone in this complex, Volcan Copiapo or Azufre, has many voluminous sulphur deposits which contain porous sulphur impregnated bodies, hydrothermal breccia vents, silica sinter, and silica caps. Ore deposits in this district are formed by epithermal acid-sulphate (high-sulphur) alteration processes (e.g Marte, Lobo).

Petrographic, X-ray diffraction, chemical, and microprobe studies indicate that the sulphur deposits contain the alteration mineral assemblage: native sulphur +/- alunite +/- quartz +/- gypsum +/- tridymite +/- minimiite +/- cinnabar. Clay minerals are generally rare. This assemblage resembles the surficial expression of an epithermal high-sulphur ore deposit.

Sulphur isotope, thin section, and hand sample studies indicate that: 1.) native sulphur in Copiapo sulphur deposits formed from ^{34}S-depleted $H_2S_{(g)}$ which was generated by the disproportionation of magmatic $SO_{2(g)}$; 2.) these sulphur deposits contain supergene sulphate minerals from the partial oxidation of ^{34}S-depleted $H_2S_{(g)}$ which is formed by the disproportionation of magmatic $SO_{2(g)}$; 3.) hypogene alunite in gold-bearing quartz veins at Marte formed form ^{34}S-enriched sulphuric acid which is formed by the disproportionation of magmatic $SO_{2(g)}$.

A conventional K-Ar date on alunite from the sulphur deposits within the Copiapo Volcanic Complex gave an age of 13.3 +/-0.5 M.Y. This date is coeval with the gold mineralization at Marte and Lobo in the periphery of the complex and much lower elevation. A $^{40}Ar/^{39}Ar$ date on an andesite flow, which partially covers and thus preserves the soft sulphur deposits, gives an age of 6.6 +/-0.3 M.Y. This constitutes the youngest known volcanism in the Copiapo Volcanic Complex.

This work seems to confirm the hypothesis that native sulphur accumulations in the Volcan Copiapo Complex represent the surficial crown of high-sulphur epithermal precious metal deposits at depth.

KEYWORDS: Acid-Sulphate Alteration, Epithermal, Gold, Native Sulphur, Alunite, Sulphur Isotopes, Geochronology, Volcanic.

TABLE OF CONTENTS

ABSTRACT i
TABLE OF CONTENTS ii
LIST OF TABLES iii
LIST OF FIGURES iv
LIST OF PLATES iv
LIST OF APPENDICES iv
ACKNOWLEDGEMENTS v

CHAPTER 1: INTRODUCTION

1.1 Introduction 1
1.2 Location of Study Area 2
1.3 Purpose 2
1.4 Previous Work 2
1.5 Methods 4
1.6 Organization of the Thesis 5
1.7 Scope and Limitations 5

CHAPTER 2: BACKGROUND OF EPITHERMAL VOLCANIC SYSTEMS

2.1 Introduction 7
2.2 Volcanoes of Precious and Base-Metal Deposits 7
2.2.1 Structural Relations of Ore Forming Volcanoes . . . 13
2.3 Epithermal Volcanic-Hosted Deposit Models 13
2.4 High Sulphur Model 15
2.4.1 Phase Relations of Acid-Sulphate Alteration 18
2.4.2 Source of Sulphur in High-Sulphur Model 20

CHAPTER 3: GEOLOGICAL SETTING

3.1 Introduction 21
3.2 Tectonic Setting 21
3.2.1 Geology of the Central Volcanic Zone 23
3.3 Southern Central Volcanic Zone Discontinuity 24
3.4 Maricunga Metallogenic Belt 26
3.4.1 Sub-Belts of the Maricunga Metallogenic Belt . . . 26
3.4.2 Maricunga Basement and Structural Geology 29
3.5 Copiapo Volcanic Complex Geology 29
3.5.1 Copiapo Volcanic Complex Basement Geology 31
3.5.2 The Geology of Volcan Copiapo 31
3.6 Summary 33

CHAPTER 4: VOLCAN COPIAPO SULPHUR DEPOSITS GEOLOGY

4.1 Introduction 34
4.2 Sulphur Deposit Geology at Volcan Copiapo 34
4.2.1 Hydrothermal Vent at Quebra Azufre Sur 36
4.2.2 Silica Sinter 37
4.3 Sulphur Intruded Host-Rocks at Volcan Copiapo 37
4.4 Mineralogy of Volcan Copiapo Sulphur Deposits 38
4.5 Semi-Quantitive Geochemistry 38
4.6 Volcan Copiapo Sulphur Deposit Formation 39

4.7 Comparison of Sulphur Deposits to High Sulphur Ore Model 39

CHAPTER 5: THE GENESIS OF THE SULPHUR DEPOSITS

5.1 Introduction 43
5.2 Volcan Copiapo $\delta^{34}S$ Samples 43
5.3 Review on Sulphur Isotopes in Hydrothermal Environments 47
5.3.1 Sulphur Isotope Geothermometry 47
5.3.2 Effect of pH on Sulphur Isotopic Equilibrium Rate . 48
5.3.3 Effect of Oxygen Fugacity on $\delta^{34}S$ Values 48
5.3.4 Source of Sulphur 49
5.3.5 Sulphur Concentration 51
5.3.6 Controlling Parameters for Volcan Copiapo $\delta^{34}S$ . . 51
5.4 Hypogene Acid-Sulphate Alteration at Volcan Copiapo . . 52
5.4.1 Primary Hypogene Alunite Veins at Volcan Copiapo . 52
5.4.2 Secondary Hypogene Sulphur Deposits at Volcan Copiapo 53
5.5 Supergene Acid-Sulphate Alteration at Volcan Copiapo . 54
5.5.1 Primary Supergene Acid-Sulphate Alteration 55
5.5.2 Secondary Supergene Acid-Sulphate Alteration . . . 56
5.6 Summary on the Genesis of Alteration at Volcan Copiapo 57

CHAPTER 6: GEOCHRONOLOGY

6.1 Introduction 59
6.2 Copiapo Volcanic Complex Geochronology Data 59
6.2.1 New $^{40}Ar/^{39}Ar$ Copiapo Volcanic Complex Data 63
6.2.2 New K-Ar Data for Copiapo Volcanic Complex 65
6.2.3 Atmosphere Contamination 66
6.2.4 Grouping of CVC Dates 69
6.3 Age of Volcan Copiapo Native Sulphur Deposits 69
6.4 Evolution of the Copiapo Volcanic Complex 70
6.5 Conclusions 71

CHAPTER 7: CONCLUSIONS

7.2 Conclusions 73

References 75

APPENDICES

Appendix A 86
Appendix B 90
Appendix C 108
Appendix D 112
Appendix E 113
Appendix F 114
Appendix G 119
Appendix H 121
Appendix I 123

LIST OF FIGURES

Figure 1.1 - Location Map of the study area 3
Figure 2.1 - Idealized model of stratovolcano ore types . . 8
Figure 2.2 - Mineralization associated with stratovolcanoes 10
Figure 2.3 - Mineralization associated with ash calderas . 11
Figure 2.4 - Mineralization associated with flow domes . . 12
Figure 2.5 - Sulphur minerals associated with magmatism . . 17
Figure 2.6 - Oxygen fugacity diagram 19
Figure 3.1 - Active volcanoes along the Andean Cordillera . 22
Figure 3.2 - Geological map of the Andes 25
Figure 3.3 - Map of the Maricunga metallogenic belt 27
Figure 3.4 - A map of the Volcan Copiapo geology 30
Figure 4.1 - Sample location map 35
Figure 4.2 - Relationship between sulphur mantos and vents 40
Figure 5.1 - $\delta^{34}S$ histogram for Volcan Copiapo Sulphur . . 46
Figure 5.2 - $\delta^{34}S$ and H_2S variation diagram 50
Figure 6.1 - Age date location map for the study area . . . 62
Figure 6.2 - Age spectrum plots for sample MZ-11-89 64
Figure 6.3 - Error in Ar as a function of atmospheric Ar . 67

LIST OF TABLES

Table 4.1 - Sulphur deposit mineralogy 39
Table 5.1 - Sulphur isotope samples 44
Table 6.1 - K-Ar data for CVC 60
Table 6.2 - $^{40}Ar/^{39}Ar$ data for CVC 61

LIST OF PLATES

Plate 1a & 1b - The western side of Volcan Copiapo summit . 80
Plate 2a - Hydrothermal breccia vent 81
Plate 2b - Hydrothermal breccia vent 81
Plate 3a - Hydrothermal explosion breccia 82
Plate 3b - The sulphur manto at Quebrada Azufre 82
Plate 4 - MZ-16a-89 hand sample from Quebrada Azufre . . . 83
Plate 5 - MZ-18-89 hand sample from Quebrada Azufre 83
Plate 6 - MZ-17-89 thin section 84
Plate 7 - MZ-18-89 thin section 84
Plate 8 - MZ-4-89 hand sample from Manto Volcan 85
Plate 9 - MZ-16a-89 photomicrograph of cinnabar 85

ACKNOWLEDGEMENTS

This thesis would not be possible without the supervision and support of Dr. Marcos Zentilli. The major funding for this thesis comes from the NSERC operating grant (No. A9036) to Dr. Zentilli.

The writer acknowledges Cuesta Research Ltd. for allowing the writer access to private reports.

The writer would also like to acknowledge assistance from the following individuals; Dr. P. Reynolds and K. Taylor: Geochronology, P. Stoffin: X-Ray Diffraction, S. Hinds: Text Editing, and numerous people in the geology department.

A special thank you is directed to my family and friends for their support and understanding.

CHAPTER 1: INTRODUCTION

1.1 Introduction

Volcanic-hosted native sulphur occurs in many Tertiary gold deposits formed near the surface. This association is established empirically from observations in North America, South America, New Guinea, the Dominican Republic, New Zealand, Australia, and Japan. (e.g. Bonham 1988; Sillitoe 1988; Sillitoe 1985). Despite the association of native sulphur with many hypogene gold deposits, most authors either ignore its presence, or consider it as superfluous in the formation of such deposits. However, in recent years an exploration model has evolved describing volcanic-hosted high-sulphur precious metal deposits. This model suggests that native sulphur deposits may be the little eroded crown or cap of precious metal-bearing epithermal systems.

At Volcan Copiapo, in northern Chile, hypogene native sulphur deposits and advanced argillic alteration occur together in andesitic volcanic rock. The geology of these sulphur deposits are limited to reports dating from the turn of the century and field observations made during sampling by Dr. M. Zentilli in December of 1989. These epithermal sulphur deposits have not been previously described in terms of their mineralogy. This thesis investigates the mineralogy of the Volcan Copiapo sulphur deposits and their geology in terms of genetic models for volcanic-hosted epithermal precious metal deposits.

1.2 Location of the Study Area

Volcan Copiapo is in the Copiapo Province, Region III of Chile, in the southern part of the Central Andean volcanic belt of South America, between 27°16'-27°24' South Latitude and 69°07'-69°10' West Longitude. Volcan Copiapo is 170 km east of the city of Copiapo and 700 km North of Santiago (Fig. 1.1). Altitudes in the immediate area are between 4500 and 6052 m above sea level with Volcan Copiapo dominating the topography.

1.3 Purpose

The purpose of this thesis is to improve the understanding of processes responsible for native sulphur deposit formation in the upper parts of hydrothermal systems associated with calc-alkaline volcanoes. In particular, this study explores a probable genetic relationship between sulphur deposition and precious metal mineralization at shallow depths in the Copiapo Volcanic Complex in northern Chile.

1.4 Previous Work

Abundant literature exists on the regional geology between 26°S and 29°S but there is very little specific information on the Copiapo Volcanic Complex.

Volcan Copiapo has resources of sulphur (Sayago 1874), and sulphates of aluminum, iron, potassium, and calcium (Guerra 1901). Estimated reserves of native sulphur at Volcan Copiapo range widely: the largest estimated reserve is 30 million

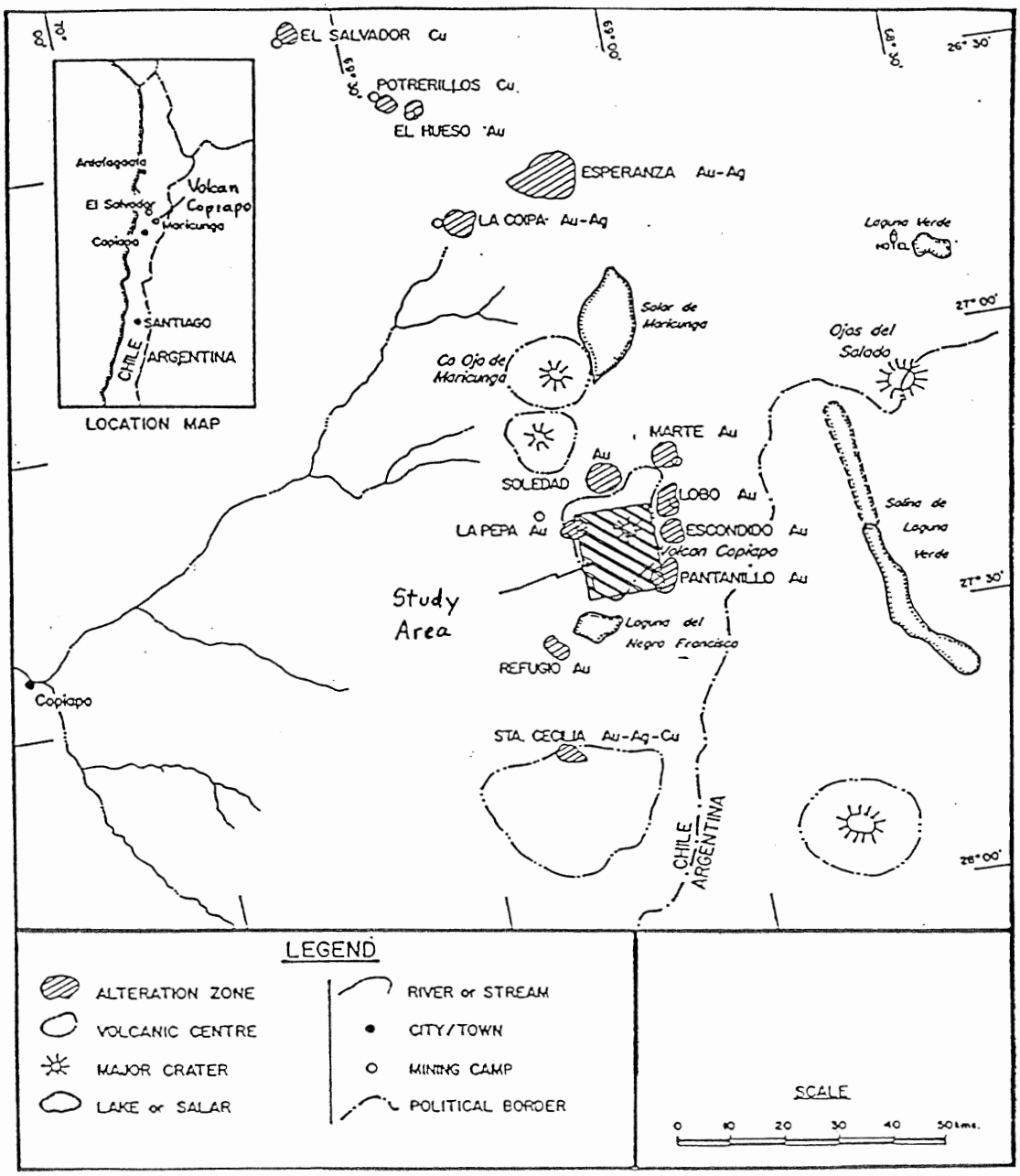

Figure 1.1 Location Map of the study area. Note the presence of gold deposits in alteration zones around study area (after Zentilli 1990).

tonnes (Mella, in Cousino 1951); the smallest reserve determination is 4.7 million tonnes of 40% sulphur (Godoy and Cuadra 1988). Zentilli (1990) assumes that the latter estimate applies only to the northern part of the Volcan Copiapo Complex. Although there have been many attempts to estimate sulphur reserves, existing reports contain insufficient geological information.

A 1:30,000 geological map of the area by Mercado (1982) is one of the few published. Walker et al. (1985), and Mulja (1986) conducted preliminary geological studies in the area on the argillic alteration and host rock type, but did not describe the sulphur deposits.

Geological studies of the sulphur deposits are based on cursory examination of field relations, hand sample description, and semi-quantitative geochemistry for S, Au, Ag, Hg, Ba, As, W, Cu, Mo, Pb, Zn and Sb (Zentilli 1990). This thesis serves as a follow-up to that report.

1.5 Methods

The methods used to investigate the mineralogy of the sulphur deposits are: thin section petrography, X-ray diffraction analysis, microprobe analysis, semiquantitative chemistry, and hand sample determination. The chemical and physical environments of sulphur-forming hydrothermal fluids are studied on the basis of mineral associations and sulphur isotopes. The geological history of the Copiapo Volcanic Complex (CVC), is modified through K-Ar and ^{40}Ar-^{39}Ar

geochronology with emphasis on the emplacement of the native sulphur deposits.

1.6 Organization of the Thesis

Chapter 2 discusses: 1) the role of caldera resurgence in epithermal mineralization; 2) the proposed acid-sulphate epithermal exploration model with emphasis on sulphur and gold; and 3) the possible evolution of sulphur from a magma to near surface or surficial deposits. Chapter 3 describes the tectonic environment, Maricunga metallogenic belt geology, Copiapo Volcanic Complex. Chapter 4 is the detailed geology and mineralogy of the altered volcanics at Volcan Copiapo, with emphasis on the native sulphur deposits. Chapter 5 describes the chemical and physical environments responsible for the formation of native sulphur deposits and acid-sulphate alteration at Volcan Copiapo. This is done by sample description and interpretation of sulphur isotopes. Chapter 6 introduces new K-Ar and $^{40}Ar/^{39}Ar$ age dates for the Volcan Copiapo region. These dates are used to modify the Copiapo Volcanic Complex geology. Chapter 7 presents conclusions, unsolved problems, and recommendations for further work for Volcan Copiapo.

1.7 Scope and Limitations

The conclusions in this study are limited to Volcan Copiapo. However, some of the findings may help to confirm, refine, or propose features or processes which allow

extrapolation to acid-sulphate hydrothermal alteration in other similar areas elsewhere.

CHAPTER 2: BACKGROUND OF EPITHERMAL VOLCANIC SYSTEMS

2.1 Introduction

It has long been known by many authors that shallow epithermal ore deposits are related to volcanism (e.g. Lindgren 1933). But only recently have geologists discovered a close spatial and possibly genetic relationship between these ore deposits and geothermal systems in volcanic settings (e.g. White 1981). This chapter gives an overview of the relations between epithermal precious and base-metals associated with calc-alkaline volcanism and places the distribution of sulphur in this context.

2.1 Volcanoes of Precious and Base-Metal Deposits

Most volcanic hydrothermal ore deposits form at the waning stages or promptly after a pause in volcanic activity and appear to be comagmatic with intrusive activity (Peterson et al. 1977; Sillitoe et al. 1983; Sillitoe 1988).

Four types of volcanoes are known to be associated with precious and base-metal deposits. These are large central vent volcanoes (mainly stratovolcanoes), flow dome complexes, calderas, and maars (Sillitoe and Bonham 1984). More than one type may be present at the same locality (Fig. 2.1). A relationship between the presence of native sulphur deposits and these types of volcanoes is observed by many authors (e.g. Sillitoe and Bonham 1984). In some cases the volcanic landform is preserved, but the paleosurface (including native

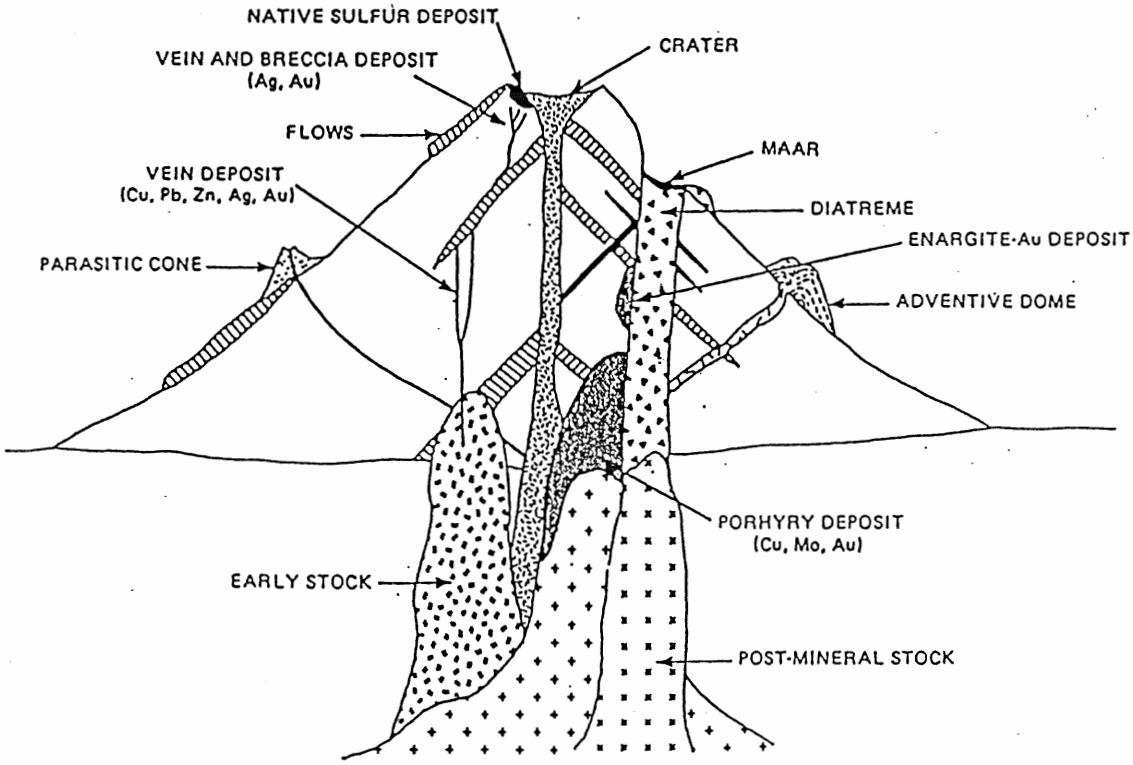

Figure 2.1 Idealized model of the possible ore types related to a stratovolcano. Note the presence of the native sulphur deposit and its association with gold mineralization (from Sillitoe and Bonham 1984).

sulphur deposits) is commonly removed by erosion. The type of volcano may still be recognized by the volcanic products present (Sillitoe 1973; Sillitoe and Bonham 1984; Sillitoe 1988).

Thick sequences of andesitic to dacitic volcanics dominated by pyroclastics and more distal epiclastic rocks (especially laharic breccias) suggest central vent stratovolcanoes (Fig. 2.2).

Voluminous rhyolitic to dacitic welded ignimbrites may be transitional to landslide (collapse) megabreccias and provide an indication of large ash-flow (Valles-type) calderas (Fig. 2.3). Ash-flow or Valles-type calderas, typically 10 to 40 km in diameter, are formed during the resurgent stage of a caldera (Sillitoe and Bonham 1984; Sillitoe 1988).

Dacitic to rhyolitic flow dome complexes (Fig. 2.4) commonly act as hosts to veins, stockwork, or breccia pipes in epithermal deposits. These domes usually represent the final post-explosion activity of a volcano (Sillitoe et al 1984; Silberman and Noble 1977). Mineralized domes may be unrelated to other types of volcanoes, but are commonly found in combination with calderas and maar volcanoes (Fig 2.1). The volcanic products associated with flow dome complexes and maar volcanoes are much less voluminous than other types of volcanoes, making preservation less likely in areas of erosion (Sillitoe and Bonham 1984).

Diatremes are conducive to the localization of precious and base-metal deposits (Fig 2.1) This localization occurs in

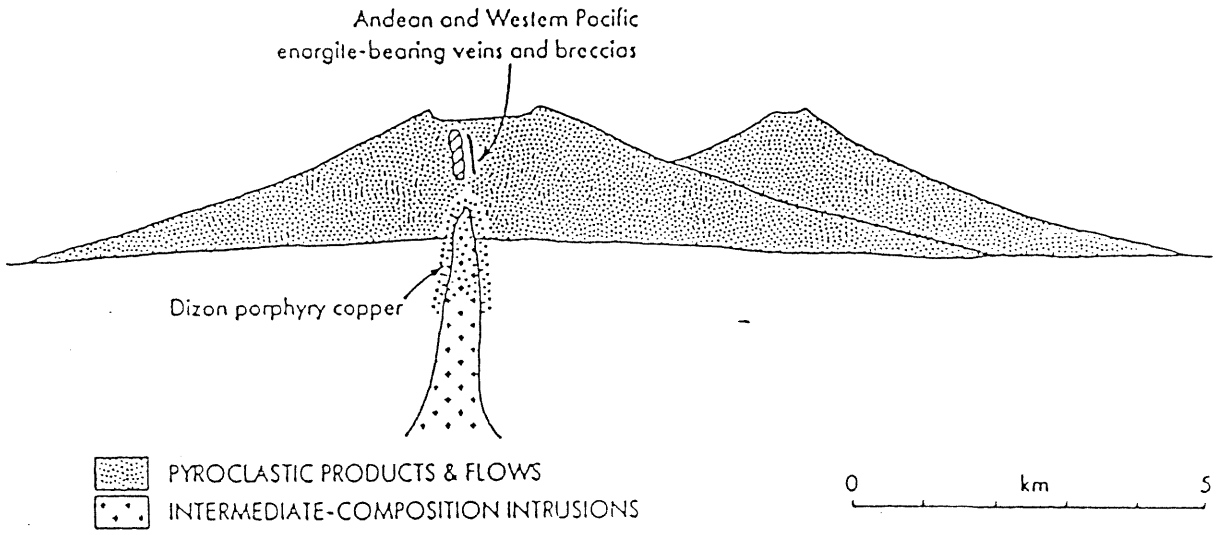

Figure 2.2 Example of mineralization associated with compound stratovolcanoes, including a summit caldera (from Sillitoe 1988).

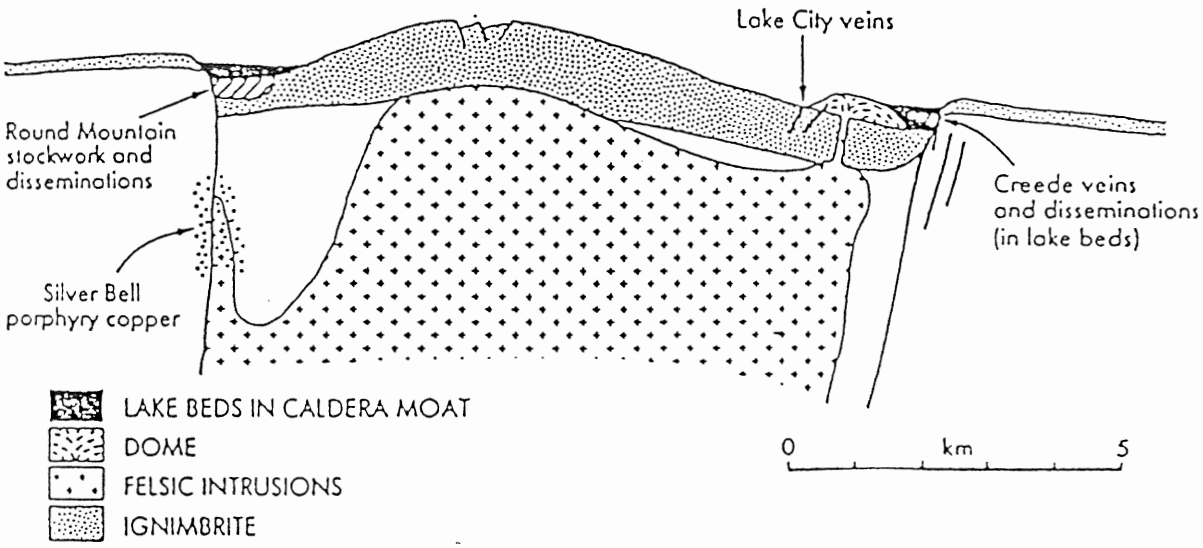

Figure 2.3 Example of mineralization associated with resurgent ash-flow (Valles-type) caldera from Round Mountain, Nevada and Creede, Colorado. The intra-caldera consists of exceptionally thick ignimbrite (>400m). Note that the ore is confined to the ring fracture zone. Ore may also be present in keystone graben faults in the centre of the Valles-type caldera (from Sillitoe 1988).

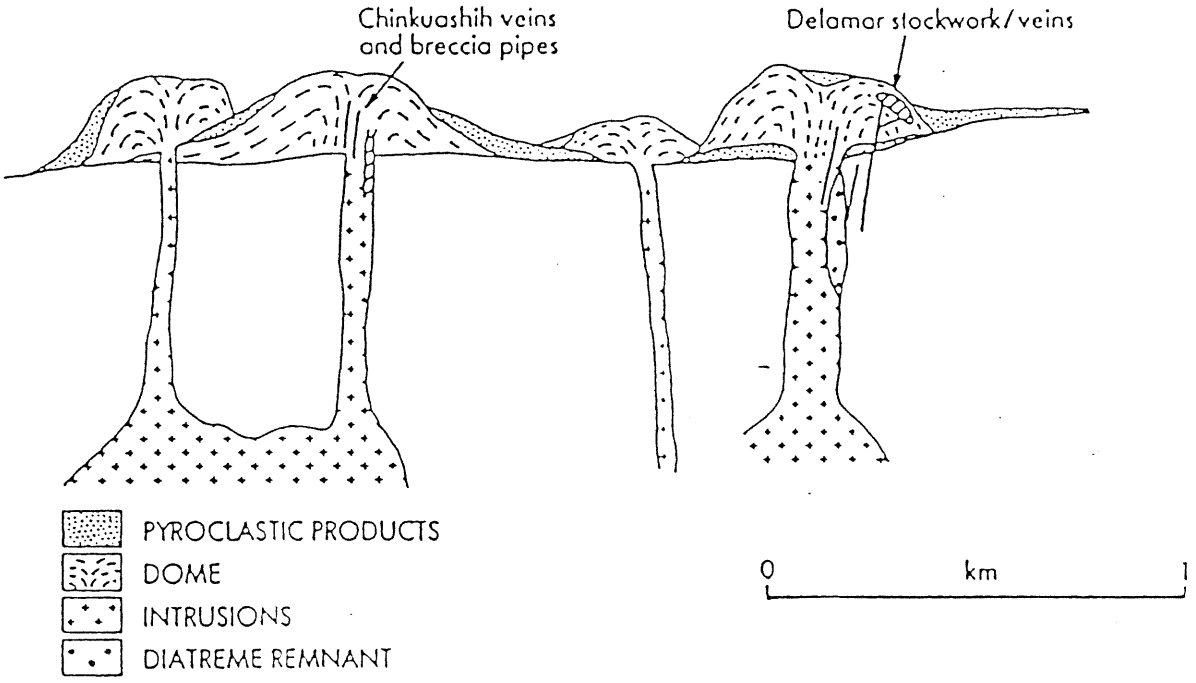

Figure 2.4 Examples of mineralization associated with flow-dome complexes from Chinkuashih, Taiwan (from Sillitoe 1988).

a hydrothermal breccia, stockwork, veins, or as a massive silica-pyrite replacement (e.g. Sillitoe et al. 1984; Sillitoe et al. 1985; Sillitoe and Bonham 1984; Thompson et al. 1985).

2.2.1 Structural Relations of Ore Forming Volcanoes

Structural control on the emplacement of intrusions near the surface is an integral part of the development of a volcano. These structures may be ring, radial, low-angle gravity, and keystone graben faults, or fractures associated with resurgent calderas (Fig. 2.3). Regional faults may also be reactivated during volcanic development and resurgence (Sillitoe 1988).

The major ore control is typically a ring-fracture zone along which caldera collapse took place. Caldera ring fractures may localize ore-related domes and provide a suitable structural site for the localization of younger magmatic hydrothermal activity (Sillitoe 1988). Precious and/or base-metal vein deposits may occur on or towards ring fractures, where reactivated graben faults are mineralized (Hayba et al. 1985).

Intersections of faults or fractures and juxtaposition of faults and permeable lithologies (e.g. pyroclastic rocks and pre-volcanic carbonates) are ideal sites for mineralization (Sillitoe 1988).

2.3 Epithermal Volcanic-Hosted Deposit Models:

Epithermal deposits are defined as the products of

volcanism-related hydrothermal activity at shallow depths and low temperatures, usually less than 1 km depth and at temperatures between 50 to 300°C (Gilbert and Park 1986). Three main types of epithermal, volcanic-hosted, deposits are distinguished by alteration mineralogy, major and trace metal content, and associated rock type (Bonham 1988; Sillitoe 1988).

A high-sulphur model, also called high-sulphidation or acid-sulphate type alteration, produces deposits characterized by the presence of enargite and advanced argillic alteration with high total sulphur content (enough sulphur to make native sulphur, sulphides, and sulphates the main minerals). This kind of alteration has a spatial, temporal, and possibly genetic relationship to calc-alkaline igneous rocks (e.g. Hayba et al. 1985; Sillitoe 1988; Bonham 1988).

A low-sulphur model, also named low-sulphidation type, is characterized by quartz-adularia-carbonate-sericite type alteration with a low total sulphur content and a high silver/gold ratio (e.g. Bonham 1988; Hayba et al. 1985; Sillitoe 1988).

An alkalic model is typified by quartz-fluorite-carbonate-adularia-roscoelite alteration with gold commonly occurring as tellurides displaying a low silver/gold ratio. A genetic relationship between this kind of alteration and alkaline igneous rocks exists (e.g. Bonham 1986; Bonham 1988; Sillitoe 1988).

Shallow porphyritic intrusions commonly imply that heat

engines drive the meteoric-hydrothermal systems responsible for deposition of ore (e.g. Sillitoe 1988). Estimates of the amount of magmatic water in epithermal deposits ranges from none to significant quantities (e.g. Sawkins 1986).

2.4 High-Sulphur Model:

It appears most appropriate to consider Volcan Copaipo in terms of the high-sulphur model because of the abundance of native sulphur. High-sulphur epithermal deposits have high total sulphur content (enough sulphur to make native sulphur, sulphides, and sulphates the main minerals), argillic to advanced argillic alteration, and commonly contain enargite-group minerals ($Cu_3(As,Sb)S_4$) in the ore zone (Bonham 1988; Sillitoe 1988). Enargite-group mineralization is not known in low-sulphur or alkaline epithermal precious metal systems (Heald-Wetlaufer 1983; Bonham 1988).

High-sulphur precious metal deposits are typically hosted in calc-alkaline andesite, dacite, rhyodacite, and rarely low-silica rhyolite. The intermediate volcanics associated temporally and spatially with these deposits are porphyritic with plagioclase, orthoclase, hornblende, biotite, and pyroxene being the typical phenocrysts (Ashley 1982). These intermediate, porphyritic volcanics commonly form flow-dome complexes (Fig. 2.3 & 2.4) (Ashley 1982; Sillitoe and Bonham 1984; Sillitoe 1988).

These deposits are almost always confined to silicified breccias and veins or as massive sulphide replacement

(Sillitoe 1983; Sillitoe 1985). "Multiple event" hydrothermal breccias are characteristic features of the silicified zones, and quartz veins in these deposits usually show multiple episodes of brecciation and healing. Gold-sulphide deposition in these deposits is usually present in open spaces in the breccia and is an important factor in the localization of high-grade ore in these deposits (Sillitoe 1988).

The alteration in such deposits is characterized by argillic quartz-kaolinite-K-mica, quartz-illite-montmorillonite or quartz-kaolinite assemblages (Bonham 1988). Advanced argillic assemblages commonly occur within the in and adjacent to the main feeder conduits for hydrothermal fluids (Ashley 1982). Advanced argillic alteration assemblages consist of: quartz-alunite +/- kaolinite (alunite = $(K,Na)Al_3(SO_4)_2(OH)_6$), quartz-alunite-native sulphur, quartz-diaspore, quartz-pyrophyllite-diaspore, quartz-alunite-pyrophyllite-diaspore and quartz-alunite-sericite (Ashley 1982). Advanced argillic alteration in these districts may contain all or only a few of these assemblages. Figure 2.5 is a cross section of a high-sulphur epithermal deposit with its typical advanced argillic to argillic zonation.

Surficial argillic zones are typically barren of ore minerals although pyrite may be present. Large volumes of propylitized volcanics with up to several percent pyrite is common in such districts. Oxidation of this pyrite can produce large areas of surface bleaching and iron oxide staining in arid and semi-arid environments, commonly referred

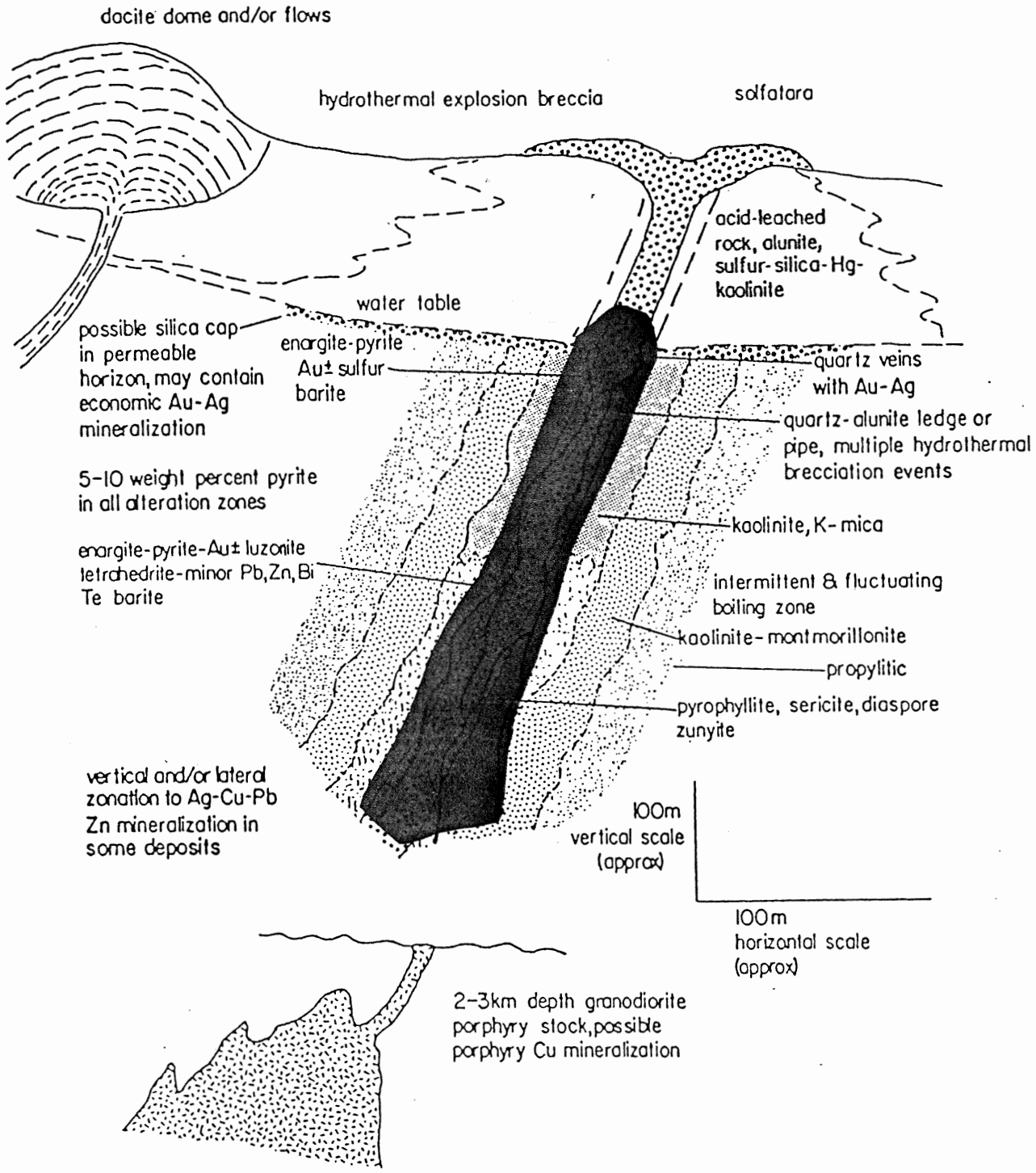

Figure 2.5 Schematic cross section of epithermal enargite/precious metal or high-sulphur-type deposits associated with granodiorite-dacite magmatism. Note: 1.) The surficial acid-leached rock with alunite, sulphur, silica, and Hg. 2.) The silica cap in permeable horizon (From Bonham 1988).

to as "red-thumb" type outcrops (Bonham 1988).

The typical ore minerals in these deposits are mercury and antimony sulphides, enargite-luzonite group minerals, tennantite-tetrahedrite group minerals, covellite, native gold and/or electrum, silver sulphide and sulfosalts, bismuthinite (Bi2S3), base metal sulphides, and tellurides (including Au Ag tellurides) (Ashley 1982; Bonham 1988).

Vertical and/or lateral zoning in such deposits is commonly seen (Fig. 2.5). Near the surface a zone may be present containing Sb and Hg (commonly seen as stibnite and cinnabar). This grades downwards into a central zone of enargite-luzonite (Fig 2.5). This central zone may grade vertically and laterally into tetrahedrite-tennantite, chalcopyrite, and bismuthinite. Gold, when present in significant amounts, is usually found in the enargite-luzonite zone, although gold is sometimes seen in the cinnabar zone (Bonham, 1988). Silver is most abundant in the tetrahedrite-tennantite zone, but also occurs in the enargite zone (Peterson et al. 1977).

2.4.1 Phase Relations of Acid-Sulphate Alteration

Stroffregen (1985) and Hayba et al. (1985) show the chemical environment for particular alteration features in acid-sulphate alteration based on theoretical thermodynamic calculations. They conclude that high-sulphur advanced-argillic alteration occurs at low pH and high oxygen fugacity (Fig 2.6). The highest argillic alteration is formed at a pH

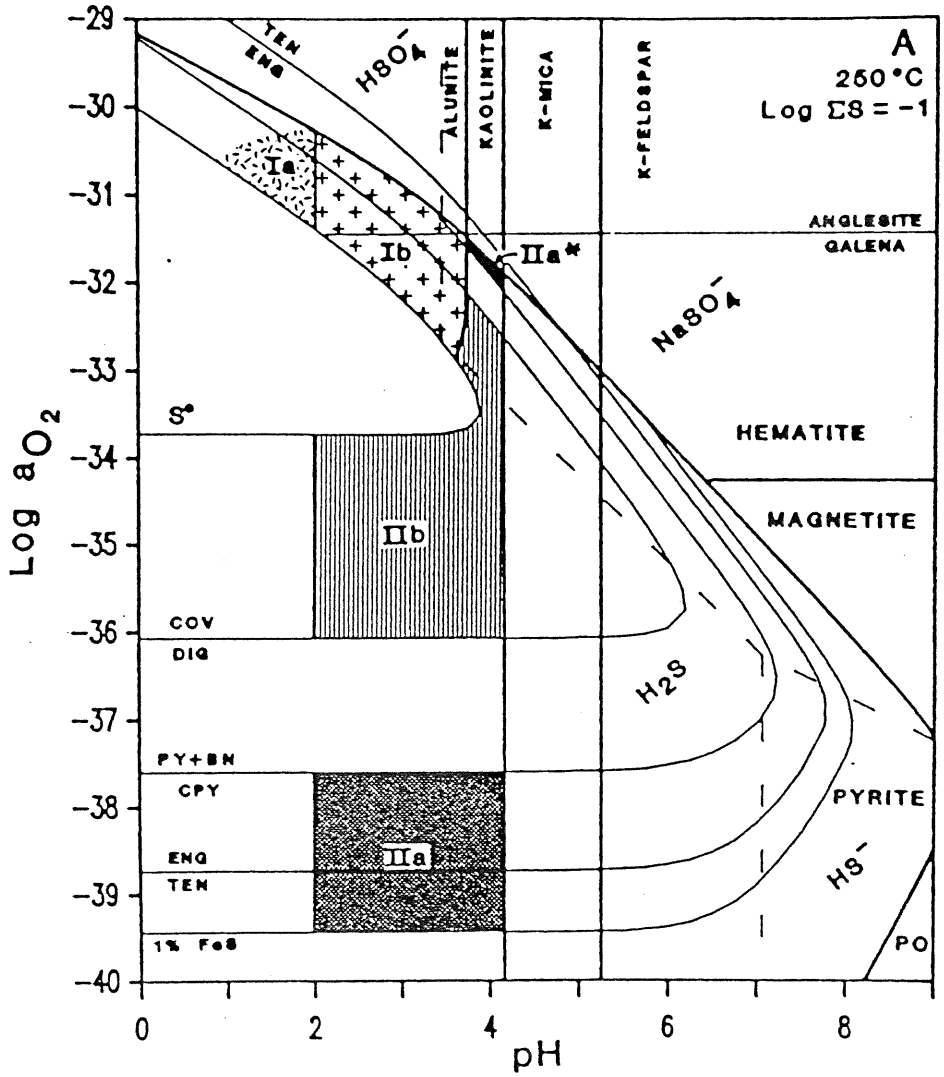

Figure 2.6 A log (a_{O2}-pH) diagram constructed at 250°C at a log total sulphur= -1. The salinity is 1 molal with a Na^+/K^+=10. Notation for the different mineral assemblages: (Ia) vuggy silica, (Ib) quartz-alunite-pyrite, (IIa) low fS_2 (chalcopyrite-bearing) ore assemblage, (IIb) high fS_2 (covellite dominated) assemblage. Abbreviations: ten= tennantite, eng= enargite, cov= covellite, dig= digenite, py= pyrite, bn= bornite, cpy= chalcopyrite, po= pyrrhotite, S°= native sulphur (after Hayba et al. 1985).

of less than 3 and contains vuggy silica, quartz-alunite, and native sulphur. This assemblage is commonly found near surface in the epithermal high-sulphur model (Fig 5.5).

2.4.2 Source of Sulphur in High-Sulphur Model

A magmatic input has been proposed for ore-forming fluids in high-sulphidation type alteration (eg. Hayba et al. 1985; Sillitoe et al. 1883). Many authors suggest there is a close genetic link between porphyry copper-molybdenum systems and high-sulphur epithermal systems. High-sulphur epithermal systems may represent the upper portions of porphyry copper-molybdenum systems (e.g. Wallace 1979; Ashley 1982; Sillitoe 1983; Sillitoe 1988).

CHAPTER 3: GEOLOGICAL SETTING

3.1 Introduction

The native sulphur deposits of Volcan Copiapo are situated in the Miocene age Copiapo Volcanic Complex. This complex is in the centre of the Maricunga Metallogenic Belt in the southernmost part of the Central Volcanic Zone in the Andean Cordillera.

3.2 Tectonic Setting

The Andean Cordillera is the result of convergence between the oceanic Nazca Plate and continental South America. Such a tectonic environment is characterized by seismicity, diastrophism, and magmatism in the continental plate. Andean magmatism may be produced by melting of the subducted oceanic Nazca Plate, partial melting of the continental lithosphere, and contamination/fractionation processes in the continental crust (Wilson 1989; Thorpe et al. 1984).

Active volcanism within the Andes occurred episodically since the Mesozoic and is divided into three zones (Fig 3.1) as follows: a northern volcanic zone (NVZ) extending from 5°N to 2°S in Ecuador and Colombia; a central volcanic zone (CVZ) extending from 16°S to 28°S in southern Peru, Bolivia, northern Chile, and Argentina; and a southern volcanic zone (SVZ) in southern Chile and Argentina (Thorpe et al. 1982; Wilson 1989). Separating these volcanic zones are gaps where active volcanism is absent (Fig 3.1). Uplift and erosion

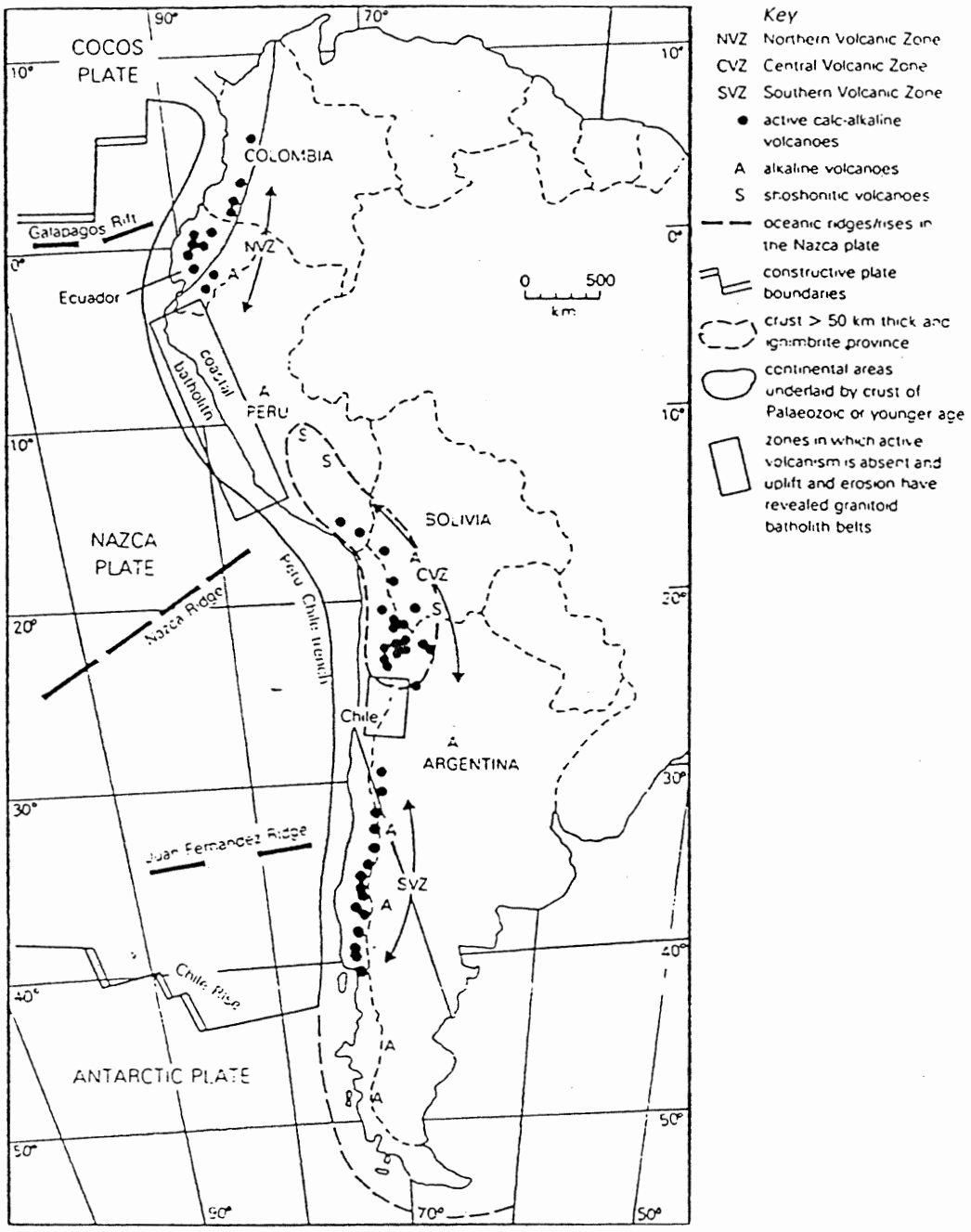

Figure 3.1 Distribution of active volcanoes along the Andean Cordillera of South America (from Wilson 1989).

reveal granitoid batholith belts in these inactive volcanic regions (Thorpe et al. 1982; Wilson 1989). This indicates that the present distribution of volcanicity has not been continuous. The active volcanic segments coincide with areas of steep subduction (c.a. 30°) whereas the gaps are underlain by shallow dipping subduction (c.a <10°) (Harmon et al. 1984; Thorpe et al. 1982).

Although the Copiapo Volcanic Complex (CVC) is of Miocene age, it is generally accepted that the present volcanic patterns were established in the early Miocene (Kay et al. in press). This means that the tectonic setting during the formation of the CVC can be considered to be similar to that of the present day.

3.2.1 Geology of the Central Volcanic Zone

The CVZ volcanism generally produces moderate to high-K lavas and pyroclastics that range in composition from basalt to rhyolite. Lavas of the CVZ are intermediate to acid in composition and grade eastward from calc-alkaline to shoshonitic. The basement consists of late Precambrian to Paleozoic metamorphic and granitoid rocks (Wilson 1989; Thorpe et al. 1984).

The CVZ is interpreted as a Mesozoic to Cenozoic eastward-migrating magmatic arc built over a Paleozoic to Precambrian basement. This arc formed along a subduction system active at least since Paleozoic times (Davidson and Mpodozis in press)

The CVZ has abundant Neogene hydrothermal alteration zones and native sulphur deposits associated with composite volcanoes, collapse calderas, subvolcanic intrusions, and active geothermal fields superimposed upon the Miocene volcanic belts. These deposits depict very shallow, little-eroded to essentially uneroded, epithermal systems (Davidson and Mpodozis in press). Such is the case for the native sulphur deposits at Volcan Copiapo.

3.3 Southern Central Volcanic Zone Discontinuity

Seismicity studies of the Andean convergent margin by many authors show a seismic discontinuity (Fig. 3.2) around 27°S in the Central Andes. This is attributed to a change in the angle of the subducted Nazca Plate in this area (e.g. Barazangi and Isacks 1976).

The CVZ abruptly terminates around 27°S and corresponds with this significant tectonic discontinuity. South of 27°S the dip of the underthrusting Nazca plate shallows to about 10°. North of 27°S the plate steepens gradually to about 30° (Barazangi and Isacks 1976; Araujo and Suarez 1986).

Other geological features noticed around 27°S are the "Easter Hot Line" submarine volcanic chain in the Nazca Plate (Bonatti et al. 1977); a cessation in Pleistocene-Recent volcanism south of 27°S; and more abundant upper Cenozoic siliceous volcanism north of 27° (Zentilli 1974, Allmendinger et al. 1983; Jordan et al. 1983; Gonzalez-Ferran et al. 1985).

The Copiapo Volcanic Complex has developed astride this

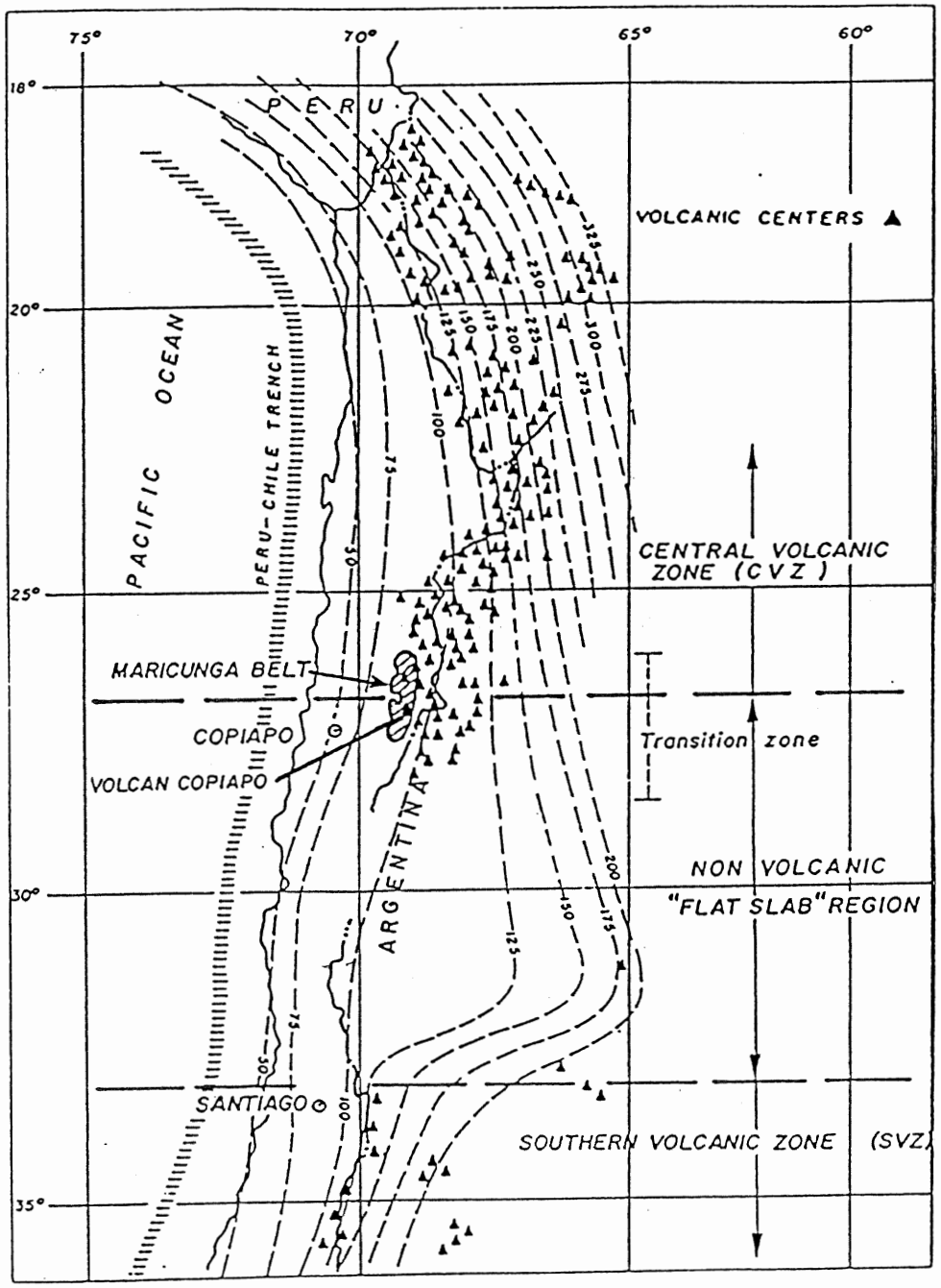

Figure 3.2 Map of the Andes (18-37o S) showing the distribution of magmatism relative to the modern seismic zone and the location of the Maricunga metallogenic belt within the modern "flat-slab" non-volcanic region. Generalized depth contours (in km) to the Wadati-Benioff zone from Cahill (1990). (after Davidson and Mpodozis in press).

27°S discontinuity.

3.4 Maricunga Metallogenic Belt

The CVC is located in the Maricunga metallogenic belt in the southern CVZ in northern Chile (Fig. 3.3) and is in the transition zone between the flat slab region and the more steeply dipping zone of the CVC (Fig. 3.2). This belt is defined by the presence of two main types of ore-producing hydrothermal alteration hosted by volcanics with intruded stocks (Sillitoe et al. in press; Vila and Sillitoe in press).

The first comprises porphyry-type mineralization which produces gold/gold-copper deposits or showings. The second type comprises acid-sulfate to high-sulphidation epithermal mineralization which produces epithermal gold and/or silver, base metal, and sulphur deposits or showings (Vila and Sillitoe in press; Sillitoe et al. in press).

The CVC is part of this belt which formed during the Miocene and consists of strato-volcanoes, calderas with associated ignimbrite sheets, and felsic domes. The overall composition of these Miocene volcanics ranges from andesite to rhyolite (Sillitoe et al. in press; Thorpe et al. 1982).

3.4.1 Sub-Belts of The Maricunga Metallogenic Belt

The Maricunga belt is subdivided into two N5°E-trending, but partially overlapping longitudinal sub-belts. The western La Coipa-Maricunga volcanic chain is early to middle Miocene in age (23-15.7 Ma) and is andesitic to dacitic in

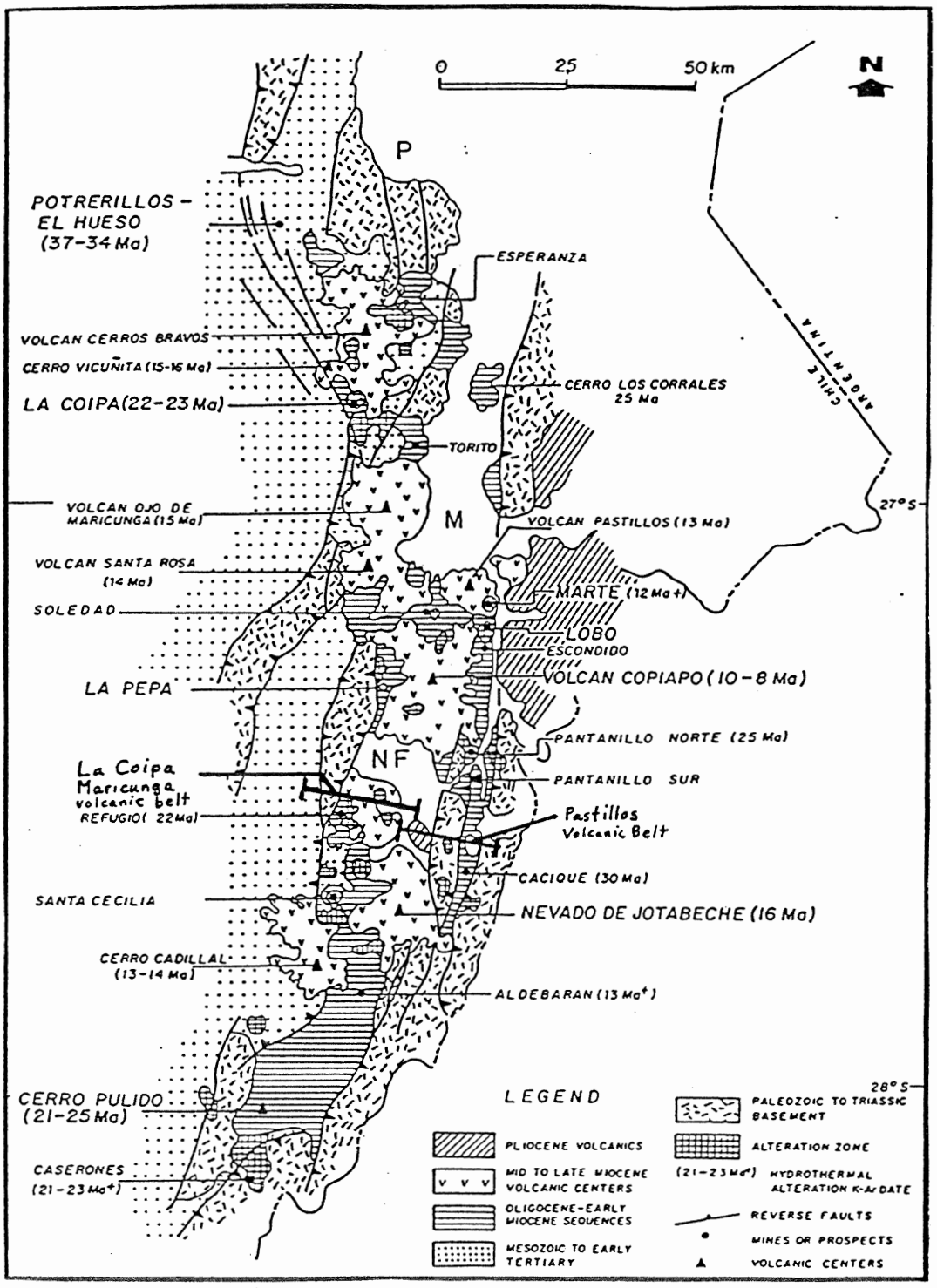

Figure 3.3 A geologic map of the Maricunga metallogenic belt with the determined ages of volcanic and alteration centres (after Davidson and Mpodozis, in press).

composition. This sub-belt consists of stratovolcanoes, domes, small calderas, unwelded ash flows and associated sub-volcanic bodies. The eastern Pastillitos volcanic chain is of middle Miocene age (13.9-12.9 Ma) and is mostly andesitic. It contains cones and stratovolcanoes confined to longitudinal grabens (Davidson and Mpodozis in press).

Sillitoe et al. (in press) show, through K-Ar geochronology, that the timing of Maricunga alteration-mineralization is transferable to the the timing of the western and eastern sub-belts (Fig. 3.3). They conclude that the Maricunga belt is a product of two discrete epochs of alteration-mineralization.

This is further supported through field relations. The eastern Pastillitos volcanic chain alteration centres show little erosion while the western La Coipa-Maricunga volcanic chain alteration centres are significantly eroded. Some alteration centres in the La Coipa-Maricunga volcanic chain are truncated by high-angle reverse faults while Pastillitos volcanic chain alteration centres obscure these reverse faults. La Coipa-Maricunga alteration centres are commonly found beneath volcanics from middle Miocene stratovolcanoes (Sillitoe et al. in press).

The two metallogenic epochs of alteration are indistinguishable with the exception of their difference in age (c.a. 6 M.Y.). Even dioritic hypabbysal intrusive rocks are the same in both locations (Vila and Sillitoe in press).

The migration of the locus of magmatism from the western

to the eastern sub-belt, some 15-20 km away, is attributed to the shallowing of the subduction zone that was initiated 18 to 16 Ma ago. (Sillitoe et al. in press; Kay et al. in press). This migration is part of a larger scale post-Triassic eastward migration throughout the Central Andes (Farrar et al. 1970; Zentilli 1974; Clark et al. 1976; Walker et al. 1987).

3.4.2 Maricunga Basement and Structural Geology

The Maricunga belt is underlain by a basement of Mesozoic sedimentary sequences which overlie Paleozoic granitic plutons and coeval felsic volcanics (Mercado 1982; Davidson and Mpdozis in press).

The belt is transected by NNE striking high-angle reverse faults. It is thought that these faults were activated since the early Miocene as a result of the flattening of the subduction zone (Davidson and Mpodzis in press; Mpodozis and Ramos in press).

3.5 Copiapo Volcanic Complex Geology

Tertiary rocks in the southern part of the Maricunga metallogenic belt cover a large area and are constrained in the west by pre-Tertiary formations while the north and south are partly covered by Quaternary fluvial, aeolian, and lacustrine sediments (Fig. 3.4) (Mercado 1982). These Tertiary rocks contain several major volcanic cones, Volcan Copiapo being the dominant one with 6052 m elevation; hence the name Copiapo Volcanic Complex.

Q	Quaternary Sediments
Cva	Volcan Sierra del Azufre
Cvvs	Caldera de Sierra Villalobos y Sierra de la Sol
Cvsr	Volcan San Roman
Cvc	Volcan Copiapo
Cvp	Volcan Pastillos
Cvsp	Volcan de Sierra Pastillitos y Cerro Las Cluecas
Cvl	Volcan Langunillas
Cvr	Volcan Santa Rosa
Cvm	Volcan Maricunga
PMz	Pre Mesozoic Basement

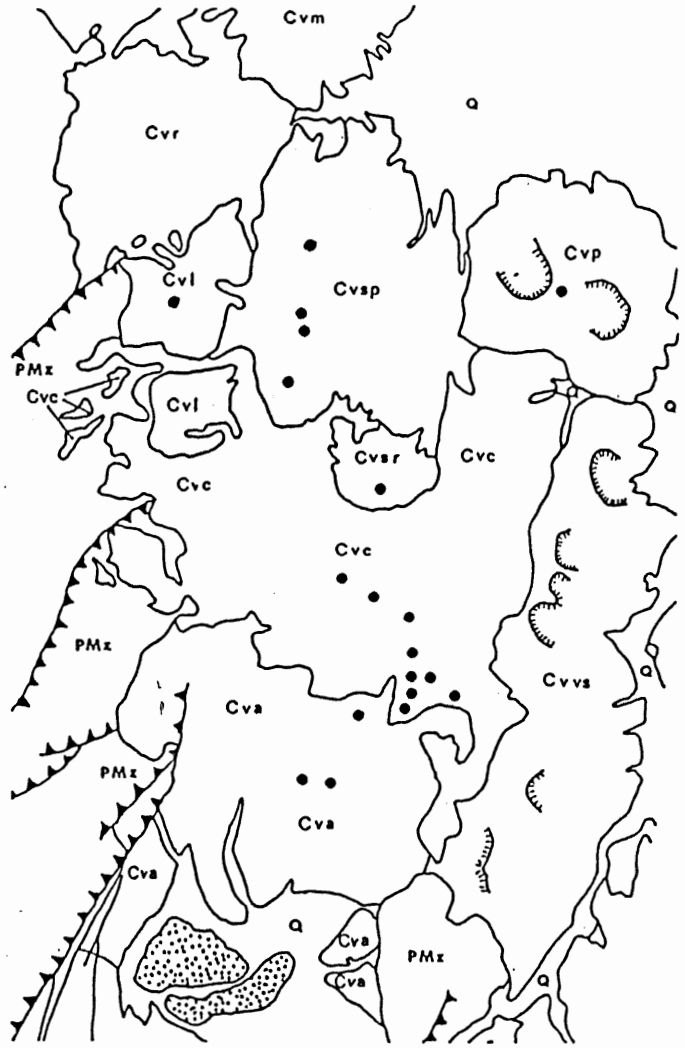

Figure 3.4 A map of the Volcan Copiapo geology. Volcan Copiapo is constrained in the west by basement formations and in the north and south by Quaternary sediments (After Mercado 1982).

3.5.1 Copiapo Volcanic Complex Basement Geology

The Paleozoic-Mesozoic basement, which outcrops in the west, unconformably underlies the Tertiary volcanics of the CVC (Fig. 3.4) (Mercado 1982).

According to Mercado (1982), the oldest unit is the early Paleozoic Chinches Formation which comprises arenites, pelites and limestones. The Pircas Formation contains late Mesozoic arenites and is the youngest basement around Volcan Copiapo. During the time of deposition of the Pircas Formation, the early Mesozoic El Hielo Batholith monzogranites, granodiorites and tonalites were emplaced (Fig. 3.4).

This basement is regionally folded and faulted with a strike direction parallel to the overall NNE-SSW trend of the Central Andes (Mercado 1982). The highest regional metamorphic grade, acquired by the Tertiary volcanics appears to be lowest greenschist (Zentilli 1974).

3.5.2 The Geology of Volcan Copiapo

The Volcan Copiapo proper is a large Miocene stratovolcano (called Volcan Copiapo or Cerro Azufre) of the Volcan Copiapo Complex. This stratovolcano contains more than a dozen discernable vents and summit calderas (Zentilli et al. 1991). Preliminary ^{40}Ar-^{39}Ar geochronology indicates that volcanic activity persisted for almost 5 Ma (Walker et al. 1991). The oldest units (14-12 Ma) of Volcan Copiapo outcrop along the outer perimeter while final volcanic activity (10-8.6 Ma) occurred around the composite cone Azufre (Mulja 1986;

Zentilli et al. 1986). However, there is much uncertainty on the detailed stratigraphy of the complex.

The Copiapo or Azufre cone fills a pre-existing caldera formed in a moderate eruption which emplaced pyroclastic flows to the southeast, northwest, and north-northeast. This caldera-forming eruption followed explosive activity and is associated with hydrothermal activity . The infilling of the caldera from erupted lava and the growth of the Azufre cone governed final volcanic activity (Zentilli et al. 1986).

Andesites and dacites constitute a large part of the CVC and are moderately to highly porphyritic (Walker et al. 1991). The predominant phenocrysts in these andesites are plagioclase and hornblende (+/- biotite) (Walker et al. 1991; Mulja 1986; Zentilli et al. 1986). Significant amounts of poorly welded, sorted to unsorted pyroclastics of andesitic to dacitic nature are also common (Mulja 1986; Mercado 1982).

Gonzalez-Ferran et al. (1985) stated that many of the lavas on Copiapo are very glassy. Mulja (1986) showed that the fresh glassy volcanics of Volcan Copiapo have high background values of gold (c.a. 10-20 ppb). Local hydrothermal alteration of these glassy volcanic rocks could lead to the concentration of this gold (Mulja 1986; Zentilli et al. 1986).

Volcan Copiapo contains native sulphur deposits, zones containing advanced argillic alteration, silicification, and iron oxides which are discernable from air photos on Volcan Copiapo. Over 50 of these alteration zones are discernable

from air photos of Volcan Copiapo. Their total area is estimated to be over 6 km^2 with sulphur outcropping over 1.3 km^2. Many of these alteration zones are partly overlain by andesitic flows, this reduces the number and total area of alteration zones that can be observed at surface (Zentilli 1990).

3.6 Summary

Volcan Copiapo is situated in the heart of the Miocene age Maricunga District in the southernmost Chilean CVC. The Maricunga District is subdivided into two partially overlapping N5°E-trending volcanic sub-belts. The western La Coipa-Maricunga belt is early to middle Miocene in age, while the eastern Pastillitos belt is middle Miocene in age. Both volcanic sub-belts are andesitic to dacitic and contain numerous alteration zones. Many of these alteration zones contain abundant native sulphur (Zentilli 1990; Mercado 1982; Sillitoe et al. in press).

CHAPTER 4: THE GEOLOGY OF THE VOLCAN COPIAPO SULPHUR DEPOSITS

4.1 Introduction

At Volcan Copiapo, native sulphur deposits occur with advanced argillic, silicic, and oxide alteration assemblages. Some surface exposures of these alteration zones are hundreds of metres in diameter. The native sulphur deposits are porous bodies which contain hydrothermal breccia vents, silica caps, and silica sinter. Figure 4.1 shows the location of samples from the sulphur deposits.

4.2 Sulphur Deposit Geology at Volcan Copiapo

At Volcan Copiapo the native sulphur deposits consist of sub-horizontal to surface-parallel, blanket-like bodies called "mantos" (Plate 1a & b). Besides native sulphur, sulphate minerals and silica constitute the majority of these mantos. Silica is often present in these deposits as a silica sinter. A hydrothermal breccia vent is present in one of the mantos in this study (Plate 2a &b). This vent is believed to be one of many in the area and is the source of the sulphur-rich fluids which formed the mantos. These mantos are partially covered by dacitic and andesitic flows (Plate 1a & b). Mantos exposed to surface are leached of sulphur, resulting in a hardening (called "caliche") of such alteration zones (Zentilli, 1990).

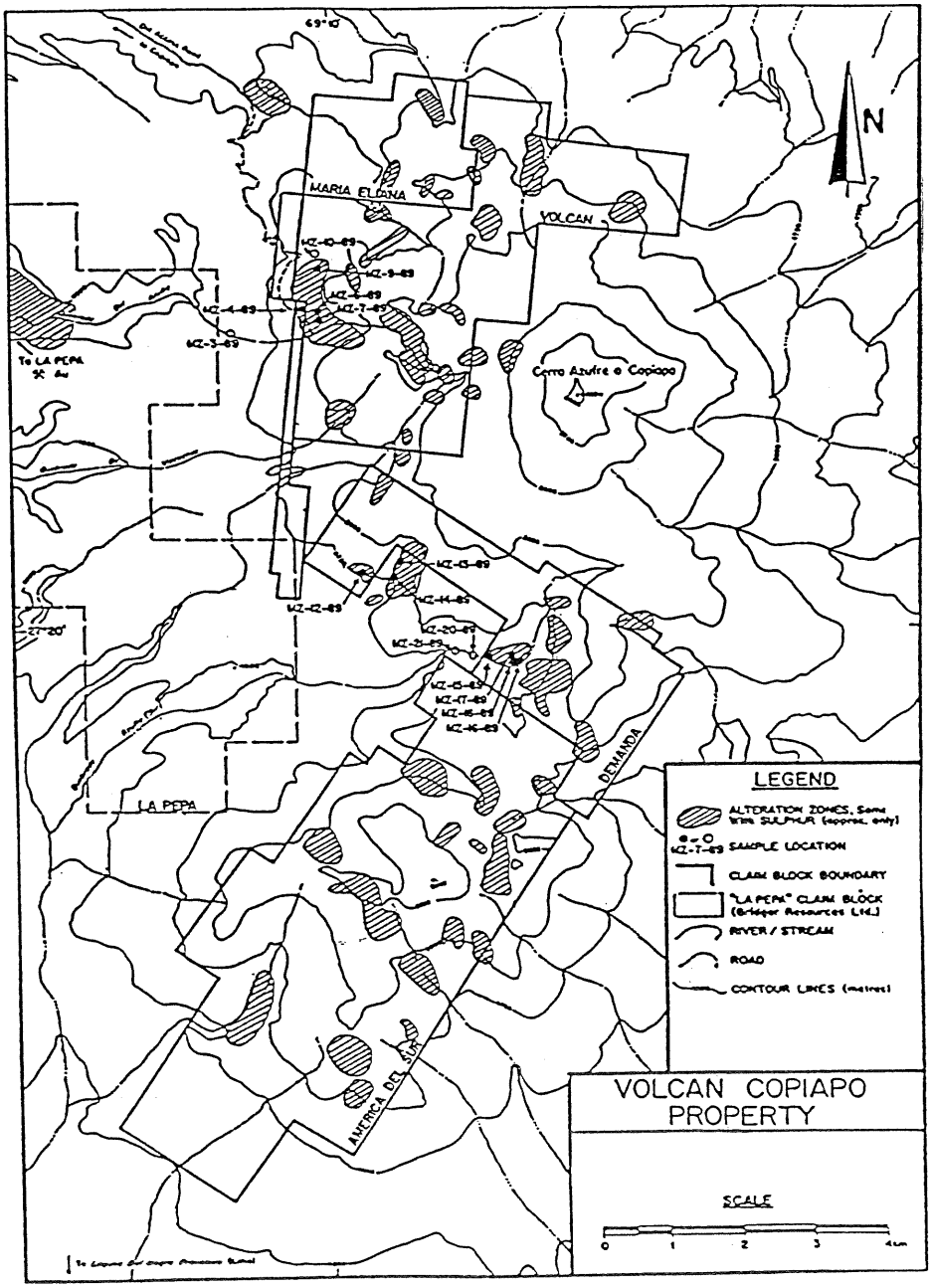

Figure 4.1 Volcan Copiapo alteration assemblage sample locations (from Zentilli, 1990).

4.2.1 Hydrothermal Vent at Quebrada Azufre Sur

In the manto at Quebrada Azufre Sur, south of the Volcan Copiapo proper, a hydrothermal vent with sulphur-rich advanced argillic alteration is present (Plate 2a & b). This vent is approximately 30 m in diameter and contains chaotic, irregular, hydrothermal explosion breccias and silicified, milled, pebble breccias (Plate 3a & b). The hydrothermal explosion breccia is made of angular fragments of porous to banded silica (Plate 3b and 4). These breccias are cemented with native sulphur and a yellow earthy alteration product of alunite and silica.

Banded silica exhibits a chalcedonic texture in hand sample and thin section (Plate 4). The porous silica in MZ-16a-89 is made from the total replacement of andesites, dacites, and pyroclastics with silica. The holes in the porous silica are made from the removal of plagioclase in host rocks.

The banded quartz in the hydrothermal breccia is similar in texture to that from the silica cap around the vent. Therefore, the banded quartz in the hydrothermal vent probably represents the partial destruction of the silica cap present around the vent (Plate 2b) or the destruction of earlier formed silica caps.

The porous hydrothermal breccia quartz represents host rocks which were altered and totally replaced by quartz. The voids of this quartz are generally empty, with the exception of minor amounts of native sulphur.

4.2.2 Silica Sinter

Silica sinter is abundant in the mantos around the hydrothermal vent in and forms a silica cap. (Plate 2b). In hand sample, quartz has a granular to cherty, massive to vuggy porous texture. A sample of silica cap sinter (MZ-15-89) contains massive quartz-rich alunite (verified by XRD).

Silica sinter is also locally present in the mantos away from the vent as cherty massive quartz (e.g. MZ-7-89 & MZ-9-89).

4.3 Sulphur-Intruded Host-Rocks at Volcan Copiapo

Sulphur impregnation from vents affects all host-volcanics at Volcan Copiapo, predominantly in the more permeable pyroclastics. However, some impregnation of sulphur does occur in less permeable andesites and dacites.

Samples MZ-17-89 and MZ-18-89 have been totally replaced with sulphur, alunite, and poorly crystallized tridymite. However, well preserved primary relics in the altered rocks resemble that of a hornblende andesite to dacite. Relics of zoned plagioclase and hornblende, with cleavage patterns, are easily recognizable (Plate 5 & 6 & 7). Small soft white pods, less than 5mm, are present in these alunitized samples and are identified by XRD as poorly crystallized tridymite (Plate 5).

In and near the vent, sulphur has migrated as pure native sulphur into layers and veins (Plate 8). In many places sulphur impregnated pyroclastics are cemented by sulphur; when indurated they are referred to as "caliche". The vent is

therefore surrounded by layers of sulphur-impregnated alunitized lapilli tuffs.

4.4 Mineralogy of Volcan Copiapo Sulphur Deposits

The mineralogy of samples from the sulphur deposits was studied by hand sample determination, thin section description, XRD analysis, and microprobe analysis. Table 4.1 shows the mineralogy of the alteration with respect to a geologic feature.

The sulphur mantos contain native sulphur, alunite, gypsum, minimiite, tridymite, quartz, and cinnabar (Table 4.1). The quartz is commonly found as silica sinter in these mantos or as a breccia in the hydrothermal vent. Cinnabar (<2 mm in size) is present near the hydrothermal vent with alunite but is absent elsewhere (Plate 9).

4.5 Semi-Quantitative Geochemistry

Minor amounts of cinnabar are visible in hand sample as specks up to 2 mm in size in the alunite-rich parts of samples in and near the vent. Whole rock geochemistry for Hg on these samples show that the vent area is anomalous with respect to the other sampled alteration zones. Near and in the vent area Hg values are 22960 to 10960 ppb while the rest of the alteration has 540 to 43 ppb Hg (Appendix D). In comparison with other alteration zones, the vent area is also enriched in Sb by an order of magnitude. Around the vent Sb values are 27-22 ppm while the rest of the alteration is <3 ppm (Appendix

Table 4.1 Mineralogy of the Volcan Copiapo Sulphur Deposits

Geologic Feature	Sample #	Mineralogy and Description	Methods of I.D.[1]
Sulphur Manto	MZ-4-89	Massive, porous, cryptocrystalline native sulphur with minor amounts of powdery white to light-brown silica (poorly crystallized)	XRD and HS.
Sulphur Manto	MZ-5-89	Massive gypsum[3] and minor tridymite impregnated with sulphur. Native sulphur[4] is also in mm sized pockets and veins.	XRD, TS, and HS.
Sulphur Manto	MZ-6-89	Massive, porous, poorly crystallized powdery tridymite impregnated by native sulphur[1]. Native sulphur also forms mm size veins.	XRD, TS, and HS.
Silica Sinter in Manto	MZ-7-89	Massive milky cryptocrystalline quartz encrusted by gypsum[3].	XRD, TS, and HS.
Silica Sinter in Manto	MZ-9-89	Massive cherty cryptocrystalline quartz with iron oxide staining.	XRD, TS, and HS.
Silica Rich Alteration Zone	MZ-13-89	Silica rich albitization alteration.	XRD, MP, TS, and HS.
Silica Rich Alteration Zone	MZ-14-89	Silica rich albitization and massive porous alunite[1].	XRD, MP, TS, and HS.
Silica Cap from Manto Near Hydrothermal Vent	MZ-15-89	Massive cryptocrystalline quartz with well formed massive alunite[1].	XRD, MP, and HS.
Hydrothermal Breccia Vent	MZ-16a-89	Porous and banded cherty cryptocrystalline quartz cemented by porous native sulphur[4] and porous alunite[1]. Traces of visible cinnabar[5].	XRD, MP, TS, and HS.
"Caliche". Sulphur cemented pyroclastic	MZ-16b-89	Quartz pebbles cemented by porous native sulphur[4].	XRD and HS.
Manto Near Vent	MZ-17-89	Porous sulphur impregnated massive alunite[1] and minimiite[2] with minor poorly crystallized tridymite. Sulphur veins mm size. Traces of visible cinnabar[5].	XRD, TS, and HS.
Manto Near Vent	MZ-18-89	Porous sulphur impregnated massive alunite[1] with poorly crystallized powdery tridymite. Sulphur veins mm size. Traces of visible cinnabar[5].	XRD, MP, TS, and HS.

[1] XRD= X-ray diffraction analyses (Appendix B).
MP= Microprobe analyses (Appendix F).
TS= Thin Section determination (Appendix C).
HS= Hand Sample determination (Appendix C).

Chemical Formula of Sulphur Bearing Minerals:

[1]Alunite = $(K,Na)Al_3(SO_4)_2(OH)_6$
[2]Minimiite = $(Na,K)Al_3(SO_4)_2(OH)_6$
[3]Gypsum = $CaSO_4\ 2H_2O$
[4]Native Sulphur = S_8

D). Geochemical analysis shows that all of the samples are anomalously low in metals with the exception of two Au values of 11 and 18 ppb.

4.6 Volcan Copiapo Sulphur Deposit Formation

The sulphur mantos at Volcan Copiapo are overlain by andesitic flows which are interpreted to be younger than the native sulphur deposits (Figure 4.2) (M. Zentilli pers. comm. 1991). This is confirmed by geochronology in Chapter 6.

However, this could also come from the fact that the overlying andesite flow is unaltered. One would expect that the gaseous acidic fluids, which formed the sulphur deposit, would alter all overlying rocks to at least a small degree. The deposit-forming fluids were not only confined to permeable layers at Volcan Copiapo. This is evident from sulphur-impregnated samples with relict phenocrysts of plagioclase and hornblende that resemble former andesites or dacites. This shows that sulphur impregnation is not only limited to permeable layers in the mantos. Therefore, total preservation of overlying flows is unlikely and the overlying volcanics are interpreted as younger than the sulphur deposit.

4.7 Comparison of Sulphur Deposits to the High-Sulphur Ore Model

The hydrothermal breccia vent with an abundant silica cap in the mantos of Volcan Copiapo is similar to that predicted by the high-sulphur epithermal model (Fig 2.5). The mineralogy and texture of samples near the hydrothermal vent

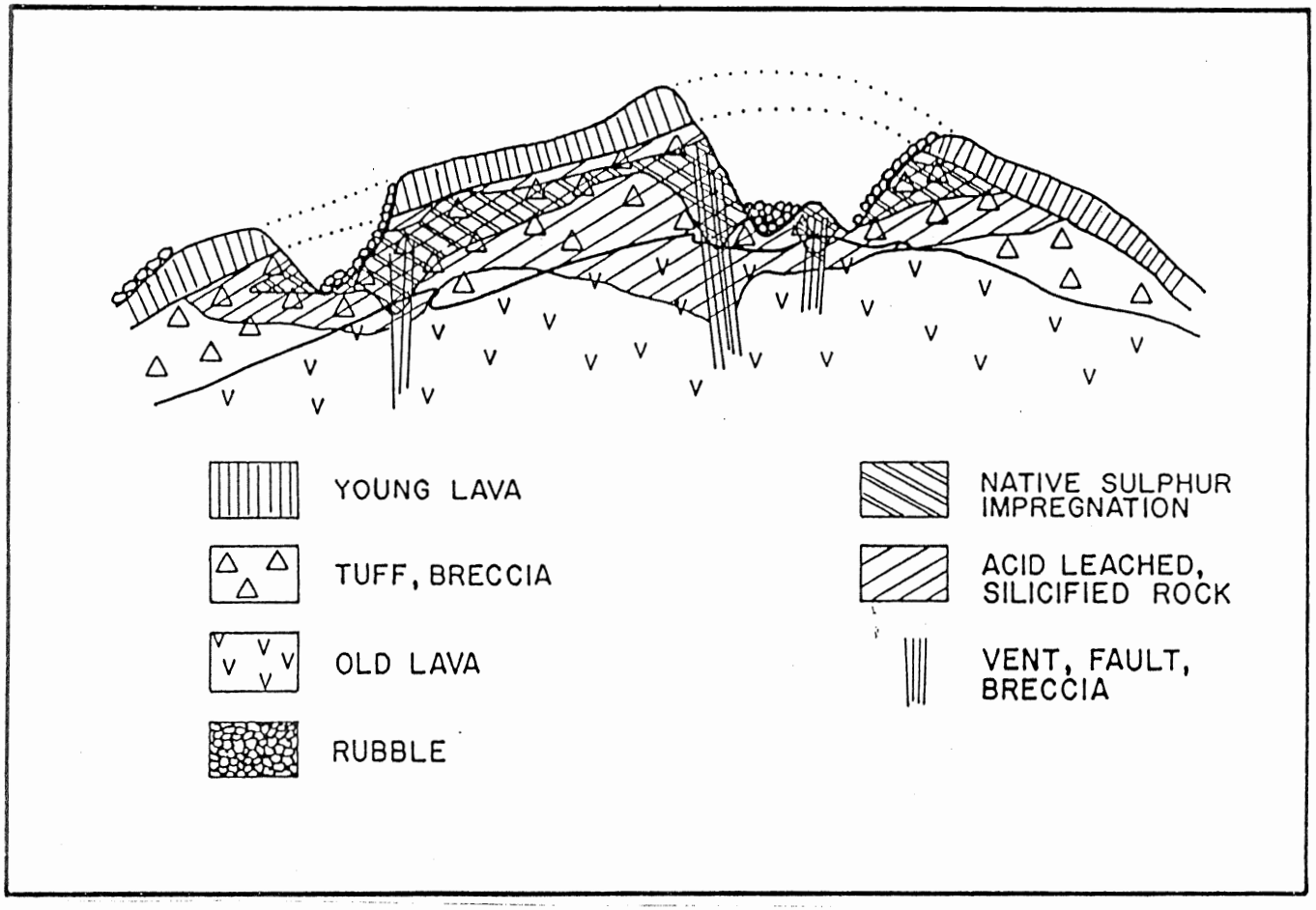

Figure 4.2 Schematic diagram showing the relationship between a sulphur manto and hydrothermal vents at Volcan Copiapo. Native sulphur impregnates permeable tuffs, breccias, and fractured zones. Younger lavas partially cover these mantos. Erosion exposes the mantos, but rubble partially covers them (from Zentilli 1990).

is identical to the surficial features seen in Figure 2.5. The vent mineralogy at Volcan Copiapo consists of native sulphur +/- alunite +/- minimiite (Na alunite) + tridymite +/- cinnabar. Hg and Sb are anomalously high around the vent at Volcan Copiapo. This is also commonly observed in high-sulphur epithermal deposits elsewhere. Therefore, based on the mineralogy and geologic features within the sulphur deposits at Volcan Copiapo, these sulphur deposits appear to be the equivalent of surficial features of acid-sulphate alteration. This is preserved by the younger lava flows previously mentioned.

CHAPTER 5: THE GENESIS OF THE SULPHUR DEPOSITS

5.1 Introduction

Acid-sulphate alteration can occur in three chemical environments: 1) Hypogene, which consists of fluids derived from depth with a direct magmatic input; 2) Primary Supergene, which is a surficial alteration resulting from descending fluids during hydrothermal activity; and 3) Secondary Supergene, which is surficial alteration due to weathering after hydrothermal activity has ceased (Hayba et al. 1985). Most authors believe that hypogene processes are most important in forming acid-sulphate epithermal deposits. (e.g. Hayba et al. 1985).

Pattern recognition and/or textural evidence may distinguish between environments, but misidentification of the origin of acid-sulphate alteration is common. The observed patterns range from stockworks of veins to massive alteration. In most cases light-stable isotope analysis can make correct identification of chemical environment (Hayba et al. 1985). Stable isotopes are used at Volcan Copiapo to discover the environments involved in the formation of both acid-sulphate alteration and native sulphur deposits.

5.2 Volcan Copiapo $\delta^{34}S$ Samples

Table 5.1 shows ten sulphur isotope analyses from native sulphur and sulphate minerals on Volcan Copiapo.

Sulphur isotope samples were hand picked whenever

Table 5.1. Sulphur Isotope Samples From Volcan Copiapo.

Sample #	Krueger Lab #	Description	$\delta^{34}S$ °/oo
MZ-4-89	SR-65043	Native Sulphur (S_8)	- 7.1
MZ-7-89	SR-65045	Gypsum (Massive) ($CaSO_4$ $2H_2O$)	- 1.6
MZ-16A-89	SR-65041	Native Sulphur (S_8)	- 13.5
MZ-17-89S	SR-65042	Native Sulphur (S_8)	- 15.4
MZ-17-89	SR-65050	Minimiite (Massive) (Na rich Alunite) ($(Na,K)Al_3(SO_4)_2(OH)_6$) Chemically Treated	- 9.6
MZ-18-89S	SR-65044	Native Sulphur (S_8)	- 12.0
MZ-18-89	SR-65046	Alunite (Massive) ($(K,Na)Al_3(SO_4)_2(OH)_6$) Chemically Treated	- 10.0
WZ-118-84	SR-65047	Alunite (Vein) ($(K,Na)Al_3(SO_4)_2(OH)_6$)	+ 4.1
WZ-120-84	SR-65048	Alunite (Vein) ($(K,Na)Al_3(SO_4)_2(OH)_6$)	+ 15.3
WZ-120-84T	SR-65049	Alunite (Vein) ($(K,Na)Al_3(SO_4)_2(OH)_6$) Chemically Treated Standard	+ 14.9

Where $^{34}S/^{32}S$ standard is Canyon Diablo Troilite= 0.0450045

$\delta^{34}S$ sample °/oo =[(($^{34}S/^{32}S$ sample)/($^{34}S/^{32}S$ standard))-1]*1000

possible. However, physical separation of MZ-17-89 and MZ-18-89 could not remove all native sulphur from the sulphate mineral. These samples are chemically treated with carbon disulphide (CS_2) to remove native sulphur. Tests on chemically treated sulphates show no structural or chemical change (Appendix A).

The samples have a large range in $\delta^{34}S$ (Table 5.1) for native sulphur and sulphate minerals (+15.3 to -15.4) (Fig. 5.1). Native sulphur has a smaller range of -7.1 to -15.4 $^{0}/_{00}$ (Table 5.1) and all samples of native sulphur are depleted in ^{34}S with respect to magmatic sulphur (Fig. 5.1). This suggests that the native sulphur deposits at Volcan Copiapo did not form directly from magmatic sulphur. The observed sulphur isotopic values for the native sulphur at Volcan Copiapo is explained by hypogene processes in which H_2S is depleted in ^{34}S forms native sulphur. A wide range in isotopic composition of -10.0 to +15.3 (Table 5.1) is present for the sulphate minerals of Volcan Copiapo (Fig. 5.1). These sulphates can be divided into those enriched in ^{34}S and sulphates depleted in ^{34}S, representing different chemical environments of sulphate formation. The sulphates high in ^{34}S are found in quartz-rich veins and are interpreted as a product of hypogene alteration. The sulphates poor in ^{34}S are massive and are interpreted as the products of supergene alteration.

A review of parameters responsible for influencing the rate of exchange and fractionation of sulphur isotopes at

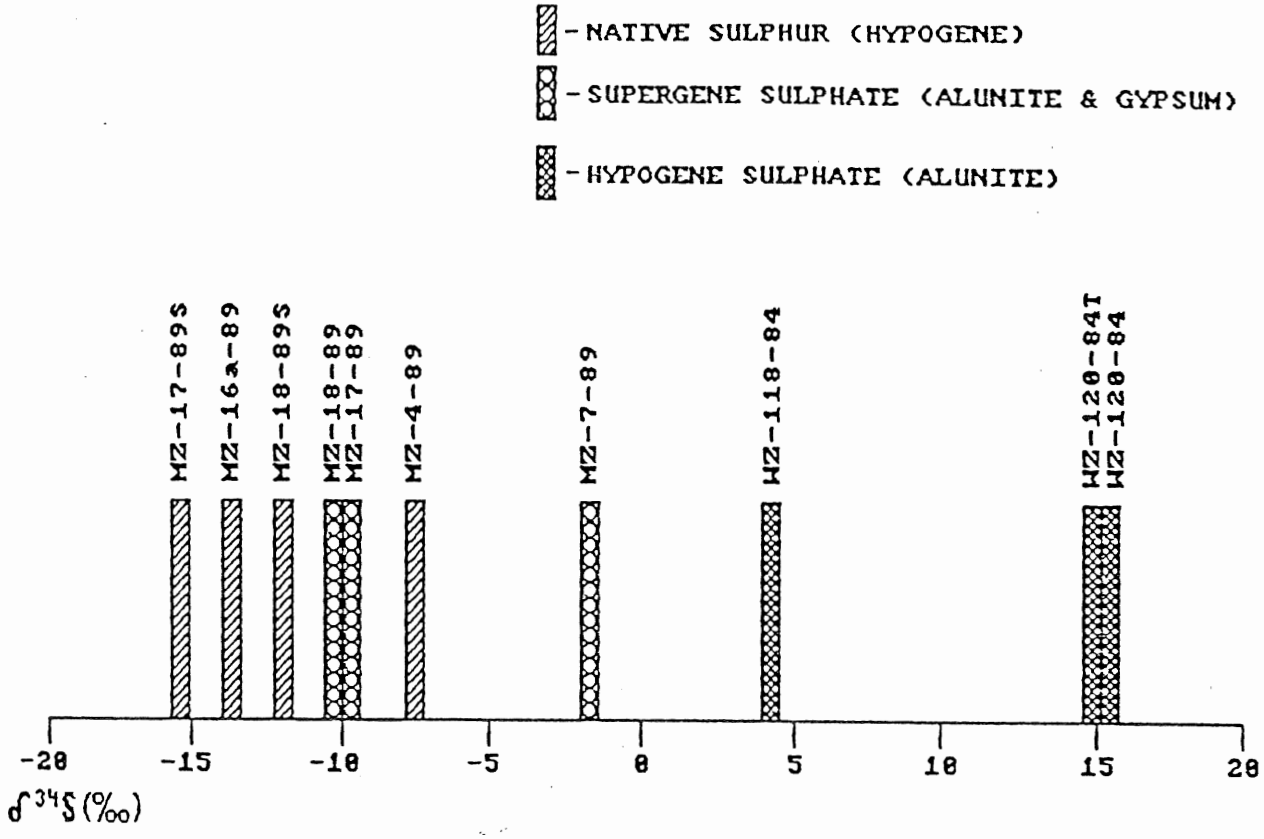

Figure 5.1 $\delta^{34}S$ histogram for Volcan Copiapo sulphur bearing minerals. Each bar represents one sample and the width corresponds to an analytical error of +/-0.2 per mil. The native sulphur is depleted in ^{34}S and is interpreted as being derived from hypogene processes (probably secondary hypogene, see text for explanation). The sulphate minerals enriched in ^{34}S are interpreted as being derived from hypogene processes, while the depleted sulphates are derived from supergene processes (probably primary supergene, see text for explanation). For a description of each isotopic sample and value refer to Table 4.1.

Volcan Copiapo precedes the reasoning for the interpretations.

5.3 Review of Sulphur Isotopes in Hydrothermal Environments

Sulphur isotopes can yield information about the chemical and physical processes involved in the formation of hydrothermal minerals. The following parameters control the isotopic composition of sulphur in hydrothermal minerals: 1) temperature, which determines fractionation between sulphur-bearing minerals; 2) fluid pH, which controls the rate of isotopic exchange; 3) the proportions of oxidized and reduced sulphur species in solution, which controls the amount of fractionation between ^{32}S and ^{34}S; 4) isotopic value of total sulphur, which can determine source; and 5) the concentration of sulphur in solution, which controls the rate of isotopic exchange (Rye and Ohmoto 1974; Hoefs 1987; Ohmoto and Lasaga 1982). The following points are discussed below.

5.3.1 Sulphur Isotope Geothermometry

Temperature determines the degree of sulphur isotope fractionation between coexisting sulphur-bearing phases. Mineral pairs in equilibrium at high temperature have small differences in isotopic composition. Lower temperatures favour mineral pairs in equilibrium with larger differences in isotopic composition. The smaller difference at higher temperature is from a higher rate of isotopic exchange (Rye and Ohmoto 1974).

If the isotopic composition is known for sulphur-bearing

mineral pairs formed at equilibrium, the temperature of hydrothermal formation can be found through the difference in $\delta^{34}S$ in the mineral pairs. This difference will correspond to temperatures determined by experimental and theoretical methods (Hoefs 1987; Ohmoto and Rye 1979). However, in lower temperature systems (e.g. solfataras, fumaroles, or hot springs) equilibrium is seldom obtained (Ohmoto and Rye 1979). The native sulphur deposits at Volcan Copiapo are formed by solfataras, therefore this system probably did not achieve equilibrium and absolute temperature determination is not possible.

5.3.2 Effect of pH on Sulphur Isotopic Equilibrium Rate

The pH of the sulphur-bearing fluid affects the rate of isotopic exchange between SO_4^{2-} and S^{2-}. At a pH below 3 a decrease of one unit in pH increases the rate of isotopic exchange by one order of magnitude. Between a pH range of 4 to 7, the rate of isotopic exchange remains relatively constant. At a pH greater than 7 the rate of isotopic exchange decreases (Ohmoto and Lasaga 1982). The mineralogy in the Volcan Copiapo sulphur deposits suggests that they formed at a pH of less than 3 (Fig. 2.6). Therefore, pH increased the rate of isotopic exchange in these deposits by at least one order of magnitude.

5.3.3 Effect of Oxygen Fugacity on $\delta^{34}S$ Values

An increase in oxygen fugacity strongy affects the $\delta^{34}S$

value because of the large fractionation between sulphate and sulphide at moderate to high temperatures (Rye and Ohmoto 1974). When both ^{32}S and ^{34}S are in solution, oxygen preferentially bonds to ^{34}S for greater stability (Hoefs 1987). As a result, the proportions of oxidized and reduced sulphur species in solution controls the sulphur isotopic composition of hydrothermal minerals (Fig. 5.2) (Rye and Ohmoto 1974).

The mineralogy of the Volcan Copiapo sulphur deposits suggests that the oxygen fugacity during the time of formation was relatively high (Chapter 2); therefore, strong fractionation between ^{32}S and ^{34}S is expected.

5.3.4 Source of Sulphur

The source of sulphur in hydrothermal systems may be traced by the sulphur isotopic composition of total sulphur. As a general rule, sulphur isotope values are grouped into three major categories according to $^{34}S/^{32}S$ ratio: 1) $\delta^{34}S$ of ca. 0 per mil is probably magmatic; 2) $\delta^{34}S$ of ca. $20^{0}/_{00}$ may have derived sulphur from ocean water sulphate; 3) $\delta^{34}S$ between 5-$15^{0}/_{00}$ derive sulphur from country rocks or some combination of 1 and 2 (Hoefs 1987; Ohmoto and Rye 1979). In many cases sulphur isotopes can not be used to distinguish between source. The above mentioned grouping is not always consistent with actual observations and should therefore be used with caution.

Sections 5.2.1, 5.2.3, and 5.2.3 suggest that there may

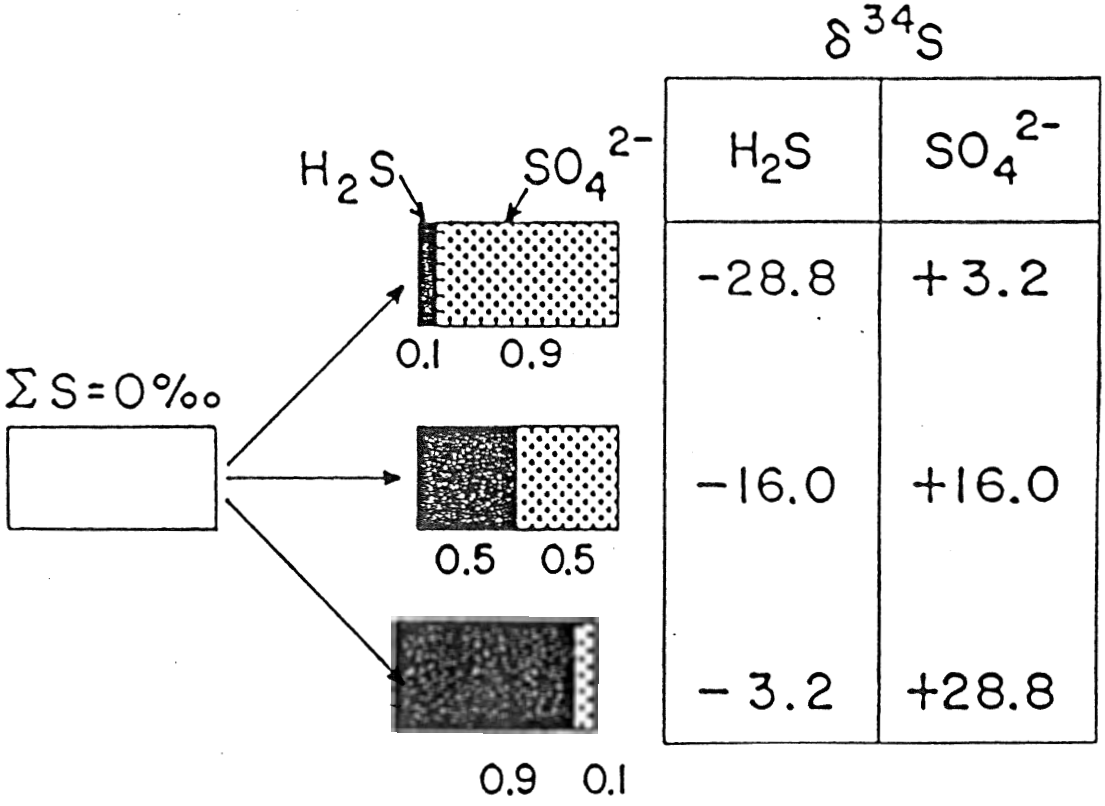

Figure 5.2 Variation of $\delta^{34}S$ of sulphate (ion or mineral) and H_2S with variation in H_2S/SO_4^{2-} of a hydrothermal solution at T= 200°C, Total Sulphur= 0 per mil (After Rye and Ohmoto, 1974).

be strong fractionation and disequilibrium of sulphur at Volcan Copiapo. This makes determination of source difficult without a quantitatively representative sample set throughout the hydrothermal system. The samples collected at Volcan Copiapo are of a reconnaissance nature only and are not a representative enough to determine source at this stage.

5.3.5 Sulphur Concentration

Cole and Ohmoto (1986) show that the time required to equilibrate sulphur isotopes depends partly on the concentration. High concentrations of sulphur take more time to equilibrate because there is a greater number of sulphur atoms to bring to equilibrium.

The concentration of the fluids that formed native sulphur deposits at Volcan Copiapo is not known. However, the volume of sulphur at Volcan Copiapo is on the order of millions of tonnes and suggests that the concentration must have been high. High concentration would slow the rate of equilibrium for sulphur isotopes.

5.3.6 Controlling Parameters for Volcan Copiapo $\delta^{34}S$

On the basis of the above review, it can be suggested that low-temperature sulphur-rich fluids, with a low pH and a high oxygen fugacity, formed the sulphur deposits at Volcan Copiapo (Sections 5.2.1, 5.2.2, 5.2.3, and 5.2.5). Such a fluid would show strong sulphur isotope fractionation and isotopic disequilibrium (Sections 5.2.1, and 5.2.3). The

proposed strong fractionation is in agreement with Volcan Copiapo data (Fig. 5.1).

The anticipated pH (Fig. 2.6) indicates that the rate of reaction of ^{34}S was fast (Section 5.2.2). A low temperature and high concentration imply that the rate of reaction is slow (Sections 5.2.1 and 5.2.5). Because isotopic equilibrium is not achieved, a slow rate of reaction is preferred.

5.4 Hypogene Acid-Sulphate Alteration at Volcan Copiapo

At Volcan Copiapo there are two different types of hypogene alteration. One type is called "primary hypogene" because the alteration is at or close to its source (Hayba et al. 1985). This type of hypogene alteration forms the alunite veins at the Marte deposit as described by Mulja (1986) (Fig. 5.1). The second type of alteration is called "secondary hypogene" because it is produced from some ascending primary hypogene fluids which is at or near the surface. This type of hypogene alteration formed the native sulphur deposits at Volcan Copiapo (Fig. 5.1).

5.4.1 Primary Hypogene Alunite Veins at Volcan Copiapo

The disproportionation (dissimilarity of ratios between two pairs of quantities) of magma-derived SO_2 gas at depth produces sulphuric acid (H_2SO_4) and H_2S gas at depth (Eqn. 5.1). This disproportionation produces a magmatic acid-sulphate fluid deep in the hydrothermal system. Sulphur isotope fractionation produces H_2SO_4 high in ^{34}S and H_2S

depleted in ^{34}S because of sulphate production (Fig. 5.2) (e.g. Ohmoto 1987; Hayba et al. 1985; Ohmoto and Rye 1979; Hoefs 1987).

(Eqn. 5.1) $4SO_2 + 4H_2O = 3H_2SO_4 + H_2S_{(g)}$ (Primary Hypogene)

This process appears valid for Volcan Copiapo because isotopic exchange and strong fractionation between sulphide and sulphate is seen. This process favours highly acidic, high oxygen fugacity fluids with moderate to high temperatures at depth (Ohmoto and Lasaga 1982; Ohmoto and Rye 1979; Hayba et al. 1985). Volcan Copiapo alunite samples WZ-120-84 and WZ-117-84 from Marte, are enriched in ^{34}S and are interpreted as primary hypogene alteration (Fig. 5.1). Hypogene alunite at Volcan Copiapo occurs in quartz veins of a granular texture.

5.4.2 Secondary Hypogene Sulphur Deposits at Volcan Copiapo

Native sulphur at surface is commonly associated with primary hypogene alteration processes at depth. Solfataric native sulphur is formed by ascending ^{34}S depleted $H_2S_{(g)}$ (Eqn. 5.2) (Hoefs 1987; Sakai et al. 1982). The source of $H_2S_{(g)}$ is the disproportionation of magmatic $SO_{2(g)}$ (Eqn. 5.1).

(Eqn. 5.2) $8H_2S_{(g)} = S_{8(s)} + 8H_{2(g)}$

At Volcan Copiapo all native sulphur samples from the native sulphur deposits are depleted in ^{34}S relative to ^{32}S (Fig. 5.1). This indicates that the sulphur deposit formed by secondary hypogene processes. The native sulphur deposits at Volcan Copiapo are, therefore, expected to be the surficial expression of primary hypogene processes at depth. Thus, the high-sulphur model (Fig. 2.5) predicts that alunite veins and sulphides should be found at depth under the native sulphur.

5.5 Supergene Acid Sulphate Alteration at Volcan Copiapo

Volcan Copiapo sulphate samples MZ-7-89, MZ-17-89, and MZ-18 are depleted in ^{34}S relative to ^{32}S (Fig. 5.1). The previously mentioned hypogene alteration mechanisms do not lead to sulfate minerals depleted in ^{34}S. Therefore, the depleted sulphates are thought to result from supergene alteration processes involving the oxidation of $H_2S_{(g)}$ or sulphide minerals produced from the disproportionation of $SO_{2(g)}$ in primary hypogene processes (Eqn 5.1).

The alteration mentioned above represents two surficial chemical environments in which acid-sulphate alteration can produce supergene alteration. The oxidizing of $H_2S_{(g)}$ is related to hydrothermal processes while the oxidizing of sulphide minerals is from weathering. Therefore, it is important to discriminate the two environments when studying hydrothermal systems (Hayba et al. 1985).

Sulphur isotopes alone can not distinguish between the two environments. However, texture relations in the samples

from Volcan Copiapo can discriminate between the two environments.

At Volcan Copiapo late stage native sulphur veins cut the alunitized rocks and cinnabar is found evenly distributed within alunite in these samples (MZ-17-89, MZ-18-89). This alunite must have formed in a hydrothermal environment since it contains native sulphur and cinnabar. Cinnabar and native sulphur are unstable and weather easily when exposed. Therefore, it is unlikely to produce alunite by weathering while preserving cinnabar and native sulphur. Hydrothermal activity is supported by the presence of the hydrothermal breccia vent at Quebrada Azufre Sur. Therefore, MZ-17-89 and MZ-18-89 have formed by "hydrothermal supergene" processes.

Zentilli (1990) describes a surficial weathering zone depleted in native sulphur. This zone is hardened and contains massive sulphates.

The following sections discuss the chemical reactions involved in supergene alteration from hydrothermal and weathering processes.

5.5.1 Primary Supergene Acid-Sulphate Alteration

Surficial alteration related to hydrothermal processes is referred to as "primary supergene" because it is an integral part of the hydrothermal system. This kind of supergene alteration is credited with the formation of massive sulphates in the native sulphur deposits at Volcan Copiapo.

Simple atmospheric oxidation of H_2S, from hypogene

processes, occurs when fluids rich in $H_2S_{(g)}$ come in contact with the atmosphere above the water table to form sulphuric acid. This newly formed sulphuric acid percolates into hydrothermally-heated ground waters to produce hot strongly-acidic fluids (Eqn. 5.3) (Kurasawa 1984; Hayba 1985; Bethke 1984). This oxidation of H_2S results in a very intense and extensive near-surface solfataric alteration extending to shallow depth (approximately 50m maximum). This alteration is usually not well preserved because it is soft and shallow (Henley 1985; Reed and Spycer 1985; Hayba et al. 1985).

(Eqn. 5.3) $H_2S + 2O_2 = H_2SO_4$ (Primary Supergene)

The near-surface oxidation of this H_2S (Eqn. 5.3) will produce H_2SO_4 depleted in ^{34}S to form primary supergene sulphates depleted in ^{34}S with respect to ^{32}S (Ohmoto and Rye 1979).

5.5.2 Secondary Supergene Acid-Sulphate Alteration

The term "secondary supergene" refers to alteration which post-dates the hydrothermal system. This type of alteration is commonly produced by simple weathering (Bonham 1988; Hayba et al. 1985). Secondary supergene alteration is seen on the surface of mantos at Volcan Copiapo as a hardened zone of massive sulphate poor in native sulphur. Also, red oxide staining is common in the volcanics around sulphur-rich alteration. None of this alteration was studied isotopically

because a weathering origin is obvious.

Oxidation alteration of sulphides and native sulphur can produce sulphuric acid which may produce secondary supergene acid-sulphate alteration (Eqn. 5.3 & 5.4) (Hayba et al. 1985; Znamenskiy and Nosik 1984).

(Eqn. 5.3) $2FeS_2 + 7H_2O + 15/2(O_2) = 2Fe_2O_3\ 3H_2O + 4H_2SO_4$
Secondary supergene alteration of pyrite

(Eqn. 5.4) $S_8 + 8H_2O = 6H_2S_{(g)} + 2H_2SO_{4\ (aq)}$
Secondary supergene alteration of native sulphur

In hydrothermal systems, pyrite and native sulphur both form primarily from H_2S produced by primary hypogene processes and, therefore, have low $\delta^{34}S$ values. A sulphate mineral formed by simple weathering of native sulphur or pyrite, should be isotopically similar.

Secondary supergene acid-sulphate alteration from pyrite produces large areas of surface bleaching and iron oxide staining is common in arid and semi-arid environments (Hayba 1985; Bonham 1988).

5.6 Summary on the Genesis of Alteration at Volcan Copiapo

Isotopic evidence from Volcan Copiapo suggests that the disproportionation of magmatic $SO_{2(g)}$ results in primary and secondary hypogene processes which form alunite quartz veins at depth ($\delta^{34}S$ +15.3 to +4.1 $^{o}/_{oo}$) and native sulphur deposits ($\delta^{34}S$ -15.4 to -7.1 $^{o}/_{oo}$) at surface.

Primary supergene processes, associated with the

hydrothermal emplacement of native sulphur, produce sulphuric acid to form sulphate minerals ($\delta^{34}S$ -10.0 to -1.6 $^{0}/_{00}$).

At Volcan Copiapo secondary supergene weathering of sulphides produces iron oxide staining in volcanics near sulphur-rich alteration. Also, the weathering of sulphur mantos produces a hard massive surficial zone of secondary supergene sulphate alteration (Zentilli 1990).

CHAPTER 6: GEOCHRONOLOGY

6.1 Introduction

Geochronology is important in the study of volcanogenic hydrothermal processes. Absolute age determination reveals relationships between volcanism and related hydrothermal processes. The previous chapters demonstrate that Volcan Copiapo native sulphur deposits are related to acid-sulphate-type hydrothermal processes. However, the timing of sulphur deposit emplacement relative to volcanism and ore-forming alteration mineralization is only speculative.

New K-Ar and $^{40}Ar/^{39}Ar$ age dates in and around the sulphur deposits are used to define a relationship between the formation of sulphur deposits and CVC volcanism. These dates together with $^{40}Ar/^{39}Ar$ and/or K-Ar age dates by Mulja (1986), Sillitoe et al. (in press), Gonzalez-Ferran et al. (1984), and Zentilli (1974), relate the timing of Volcan Copiapo native sulphur deposit emplacement to volcanism and acid-sulphate gold mineralization at Marte and Lobo.

6.2 Copiapo Volcanic Complex Geochronology Data

The results of three new K-Ar and two new $^{40}Ar/^{39}Ar$ age dates in and near the Volcan Copiapo native sulphur deposits are given, together with all known CVC K-Ar and $^{40}Ar/^{39}Ar$ dates (Table 6.1 & 6.2). The methods and raw data for age determination of the five new age dates are in Appendices H & I. Figure 6.1 shows the location of all known CVC age dates.

Table 6.1. K-Ar data in the Copiapo Volcanic Complex.

Event Dated	Sample Number	Locality and Material Dated	Age (M.Y.)
Post-Alteration Andesite Flow Over Native Sulphur Deposit	MZ-26-85	Volcan Copiapo. Hornblende	8.7 +/-0.5
Alteration From Silica Cap Near Volcanic Vent in Native Sulphur Deposit.	MZ-15b-89	Volcan Copiapo Sulphur Deposit. Alunite.	13.3 +/-0.5
Alteration From Sulphur Impregnated Host-Volcanics Near Volcanic Vent in Native Sulphur Deposit.	MZ-18-89	Volcan Copiapo Sulphur Deposit. Alunite.	37.3 +/-1.4
Alteration. Au Bearing Veins.	WZ-120-84[1]	Marte. Alunite.	12.0 +/-0.6
Andesite Flow.	Z-669[2]	North Side of Santa Rosa. Hornblende. Two Dates on Same Sample.	16.1 +/-0.8 16.2 +/-0.6
Andesite Flow.	Z-673[2]	North Side of Santa Rosa. Biotite. Two Dates on Same Sample.	13.7 +/-2.7 14.3 +/-1.6
Andesite Flow.	1652[3]	East Side, Volcan Santa Rosa. Volcanism.	13.8 +/-0.6
Andesite Flow.	1654[3]	North Side, Volcan Pastillito. Total Rock.	12.9 +/-0.5
Andesite Flow.	MAAC-86-8[4]	Marte. Hornblende.	13.6 +/-0.4
Au Alteration.	MAAC-86-6[4]	Marte. Alunite.	13.3 +/-0.4
Au Alteration.	MAAC-86-7[4]	Lobo. Alunite.	12.9 +/-0.4
Au Alteration.	MAAC-89-1[4]	La Pepa. Alunite.	23.0 +/-0.7
Au Alteration.	MAAC-89-1[4]	La Pepa. Alunite.	22.3+/-0.7

[1] From Mulja (1986).

[2] After Zentilli (1974). Corrected for Steiger and Jaeger (1977) constants.

[3] From Gonzalez-Ferran (1985).

[4] From Sillitoe et al. (in press).

Table 6.2 $^{40}Ar/^{39}Ar$ data in the Copiapo Volcanic Complex.

Event Dated	Sample Number	Locality and Material Dated	Age (M.Y)
Post Alteration. Younger Andesitic Flow Over Native Sulphur Deposits.	MZ-11-89	West Face of Volcan Copiapo Summit. Hornblende.	6.6+/-0.3
Post Alteration. Younger Andesitic Flow Over Native Sulphur Deposits.	MZ-11-89	West Face of Volcan Copiapo Summit. Biotite.	Excess Argon. Total Gas Age= 8.0
Young Dacitic Flow.	Z-68-78[1]	North-West Face Volcan Copiapo Summit. Biotite.	8.61+/-0.11
Young Andesitic Flow.	WZ-16-84[1]	Far North-West in Volcan Copiapo Proper. Hornblende.	8.59+/-0.09
Andesitic Flow.	WZ-23-84[1]	South-East Part of Volcan Copiapo Proper. Hornblende.	10.09+/-0.23
Andesite Flow.	WZ-107-84[1]	In Villalobos Caldera. Biotite.	13.29+/-0.05

[1] From Mulja (1986).

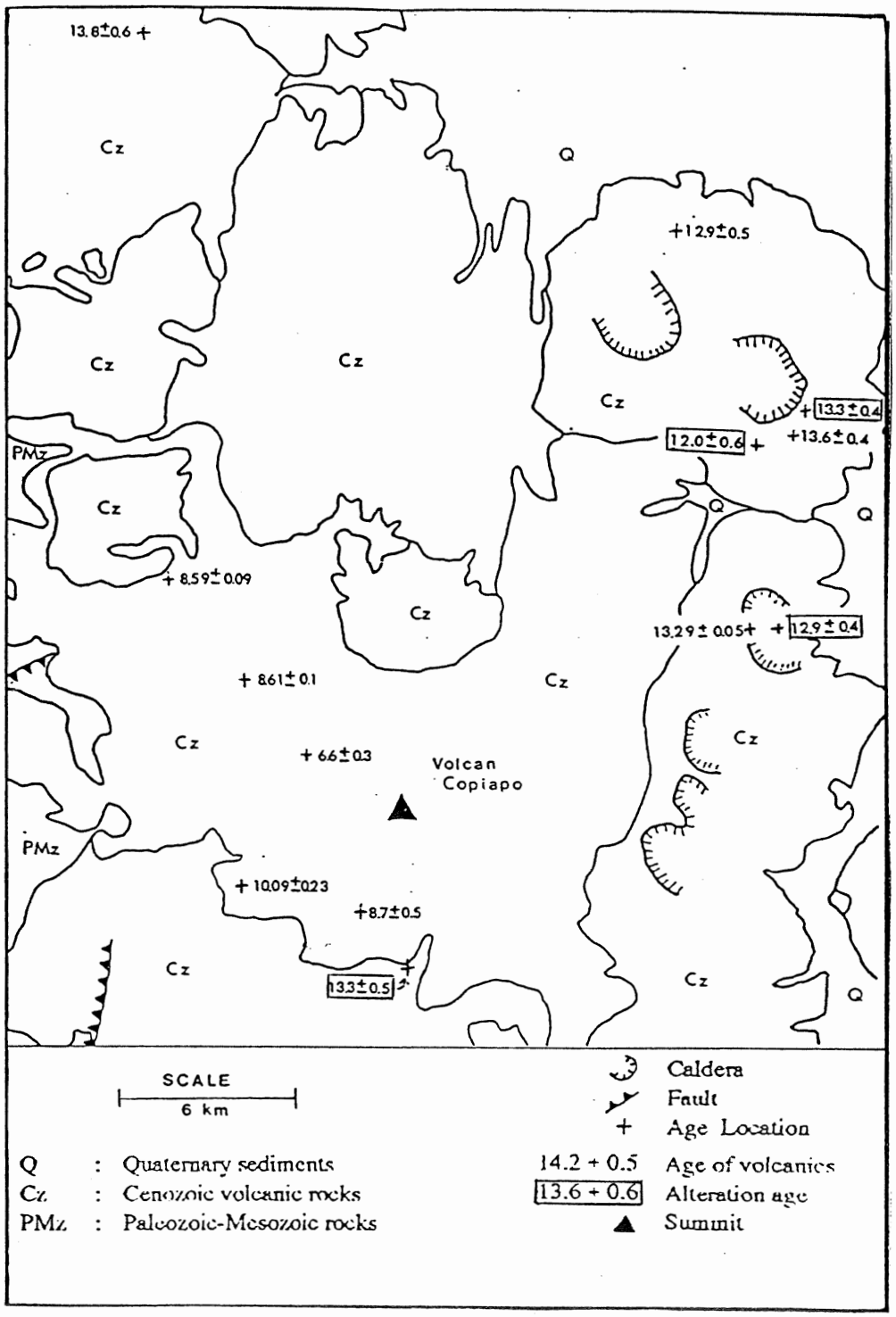

Figure 6.1 Location Map of all known age dates for the Copiapo Volcanic Complex.

6.2.1 New $^{40}Ar/^{39}Ar$ Copiapo Volcanic Complex Data

$^{40}Ar/^{39}Ar$ geochronology on hornblende and biotite from andesite sample MZ-11-89 was done at Dalhousie University on a new high sensitivity VG 3600 mass spectrometer. The relative age spectrum plots for both samples is in Figure 6.2, and a summary of the steps is in Appendix I.

The age spectrum for MZ-11-89 hornblende (Fig. 6.2) shows a plateau at 6.6 +/-0.3 M.Y., which is the interpreted age. Note that the spectrum for hornblende is saddle shaped. This is characteristic of hornblende with excess argon (Harrison and McDougall 1981). Often, excess argon in hornblende suggests that the plateau age of 6.6 +/-0.3 M.Y. is a maximum (Harrison and McDougall 1981). However, in this case the plateau age accounts for over 75% of the relative age spectrum plot and is probably correct (P.H. Reynolds pers. comm. 1991).

The age spectrum for MZ-11-89 biotite (Fig 6.2) shows an older age than that of the hornblende. P.H. Reynolds (pers. comm. 1991) states that hornblende generally gives better dates than biotite because excess argon has a greater effect on biotite. Because excess argon is present in the hornblende, the elevated age in biotite is attributed to excess argon. For biotite, one step in the apparent age spectrum plot is in agreement with the hornblende age and has a value of 6.4 +/-0.3 M.Y. (Fig. 6.2). However, this step is characteristic of an ^{39}Ar recoil artifact in chloritized biotite (Lo and Onstott 1989).

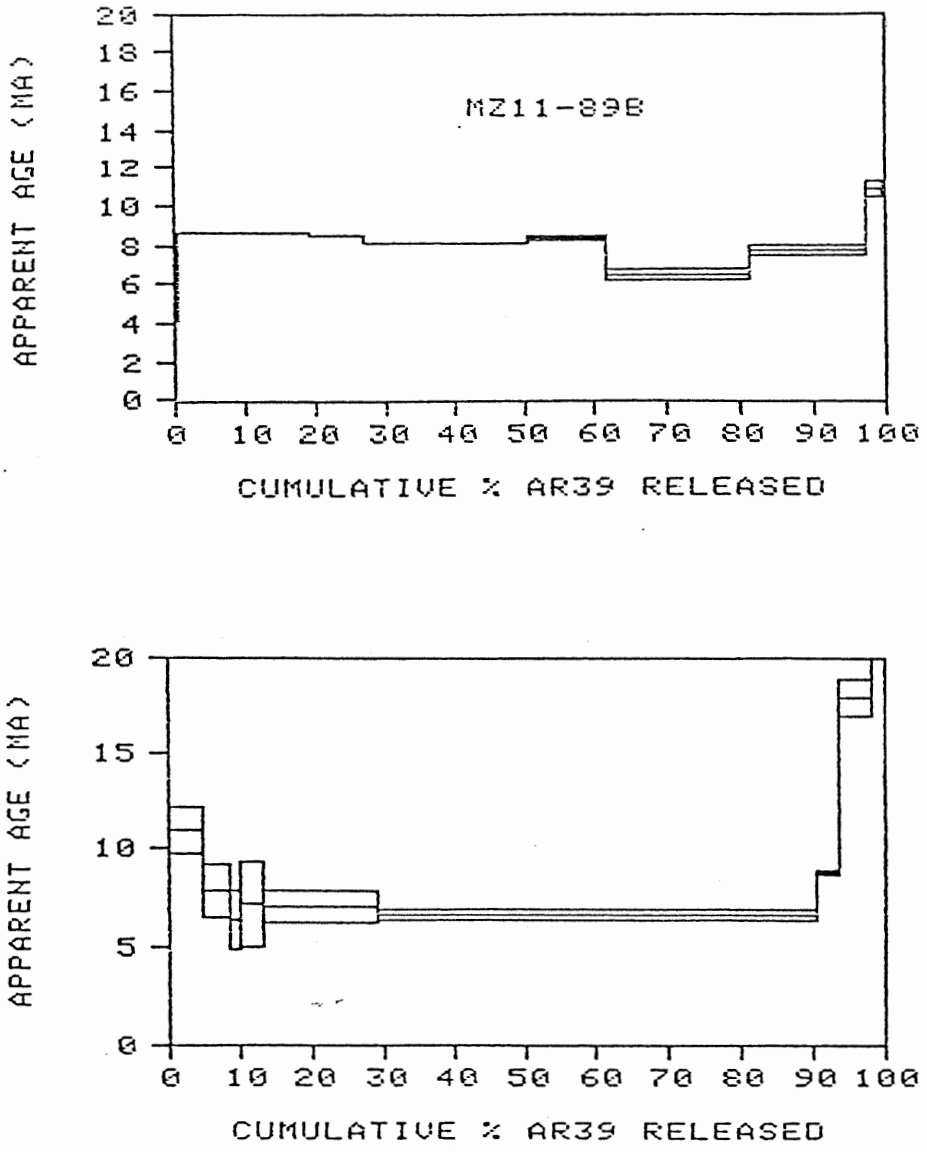

Figure 6.2 Absolute age-spectrum plots for sample MZ-11-89 biotite and hornblende. This sample is from an andesite flow near the summit of Volcan Copiapo which overlies the sulphur deposits. The plateau age of the hornblende is 6.6 +/-0.3 M.Y. Note that the spectrum plot for hornblende is saddle shaped. This is characteristic of hornblende containing excess argon. The biotite spectrum plot is artificially older than the hornblende because of excess argon. The heating steps for both spectrum plots are in Appendix H.

6.2.2 New K-Ar Data for Copiapo Volcanic Complex

Three new K-Ar age dates were done by Krueger Enterprises Inc. and are listed in Table 6.1 and Appendix H. Two of the samples (MZ-18-89 & MZ-15b-89) are the alteration mineral alunite, whereas the third sample is hornblende from a fresh andesite (MZ-26-85).

K-Ar dating differs from $^{40}Ar/^{39}Ar$ age dating in that there is only one heating step which releases all of the argon in a sample. This essentially gives an age which is theoretically equal to the area under the curve in $^{40}Ar/^{39}Ar$ dating or equal to the total gas age in Appendix I. For example, if a K-Ar analysis were done on the MZ-11-89 hornblende sample, it should yield a date equal to the $^{40}Ar/^{39}Ar$ gas age of 8 M.Y. instead of the $^{40}Ar/^{39}Ar$ date of 6.6 +/-0.3 defined by a plateau. Therefore, K-Ar is less reliable, especially in samples containing excess argon. This might be so for a number of existing K-Ar age dates in the Copiapo Volcanic Complex. Another limitation of conventional K-Ar dating is that an aliquot of the sample must be independently analyzed for potassium. Inhomogeneity of the sample may lead to additional error. However, K-Ar age dates are still useful with caution as a first approximation because they usually give dates which are relatively close to the more reliable $^{40}Ar/^{39}Ar$ dates. Unfortunately, only a few labs are able to do the step-heating $^{40}Ar/^{39}Ar$ dates, and many K-Ar dates are published despite their inherent deficiency.

In addition to the above difficulties, the volcanics at

Volcan Copiapo are young and often difficult to date because of their high content of atmospheric argon. This is seen and discussed below for samples MZ-18-89 and MZ-15b-89.

6.2.3 Atmospheric Contamination

In young volcanic rocks the contamination from atmospheric ^{40}Ar is commonly high and introduces significant errors in the determined age (York and Farquhar 1982). Such is the case for a volcanic hydrothermal alunite, MZ-18-89, which yielded a K-Ar date of 37.3 +/- 1.4 Ma (Table 6.1 & Appendix H). This apparent age is clearly wrong because it is significantly older than the host volcanics.

In K-Ar geochronology the total amount of ^{40}Ar measured is from: radiogenic argon expelled from a mineral (alunite); argon present in the rock when formed; and any contaminating atmospheric argon introduced during the experiment. Atmospheric argon contains ^{40}Ar, ^{38}Ar, and ^{36}Ar of which the relative proportions are known ($^{40}Ar/^{36}Ar$=295.5) (McDougall and Harrison 1988; York and Farquhar 1972).

The presence of atmospheric ^{40}Ar is measured by observing the amount of ^{36}Ar and assuming that all of ^{36}Ar is atmospheric (McDougall and Harrison 1988). The uncertainty in measuring this peak height is clearly seen in Figure 6.3 (York and Farquhar 1972).

Figure 6.3 shows the error in radiogenic argon determination for given errors in the ^{40}Ar, ^{38}Ar, and ^{36}Ar peak height measurement. If the contamination exceeds 90%,

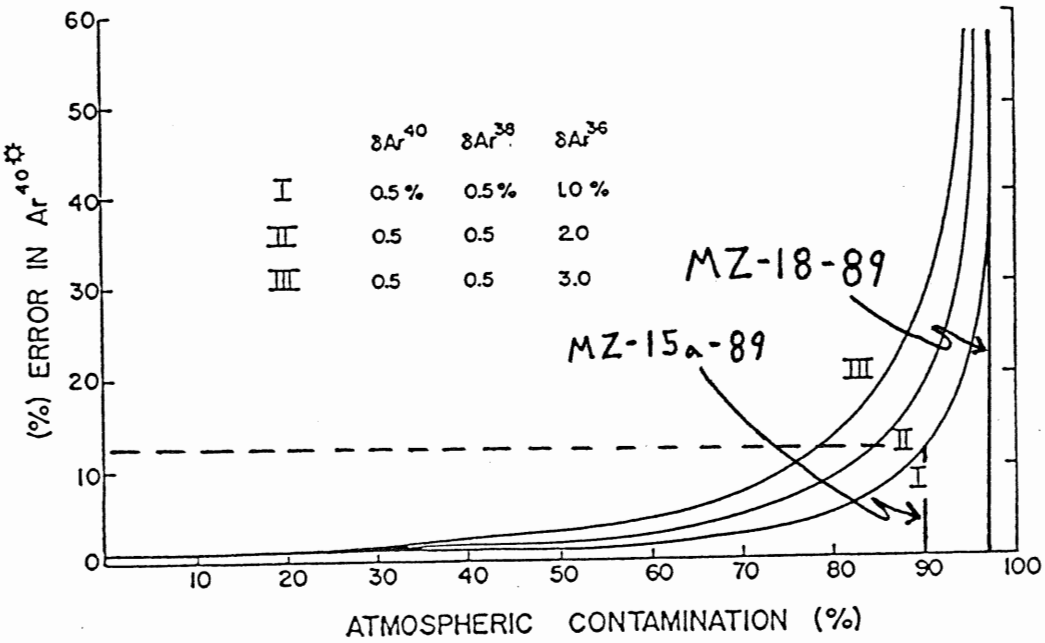

Figure 6.3 Error in radiogenic Ar as a function of atmospheric argon contamination. K-Ar dates from Krueger correspond approximately to curve I above. MZ-18-89 contains 96.65% atmospheric argon which allows for a large error in the percent of measured radiogenic Ar. MZ-15a-89 contains 90.85% atmospheric argon which corresponds to an error of +/-14% in radiogenic argon. This increases the amount of error in the K-Ar date to +/-14% (from York and Ferquhar 1972).

accurate values for the radiogenic argon volume can only be found when the peak heights are measured with greater accuracies than 0.5%. T. Bills, K-Ar Laboratory Manager of Krueger enterprises (pers. comm. 1991) estimates the errors in radiogenic argon to be slightly better than the lowest errors in Figure 6.3 (curve 1). An error for Krueger radiogenic argon determination can therefore be approximated by this curve. It should also be noted that the ^{36}Ar peak is usually several orders of magnitude smaller than the ^{40}Ar peak and is therefore more difficult to measure accurately (York and Farquhar 1972).

MZ-18-89 has an atmospheric contamination of 96.65%, which represents a significant amount of error in the amount of radiogenic argon determined (Fig. 6.3). The amount of error is so great that the determined age is highly suspect.

MZ-18-89 was chemically treated with carbon disulphide (CS_2) to dissolve native sulphur from the sample (Appendix A). Calculations (Appendix G) indicate that the amount of K put in solution by the treatment is at least three orders of magnitude less than that detectable using conventional flame spectophometer analysis for K-Ar geochronology. Therefore this chemical treatment has no effect on the K measurement for K-Ar age dating. Another possibility is that chemical treatment could reduce the amount of argon in the sample (P.H. Reynolds, pers. comm. 1991). If this had been the case the date for MZ-18-98 would be younger than expected, instead of older.

Sample MZ-15b-89 is also an alunite sample and contains 90.85% atmospheric argon. According to Figure 6.3, the amount of analytical error attributed to atmospheric argon is +/- 14%. In young volcanics, time is directly proportional to the amount of radiogenic argon (P.H. Reynolds, pers. comm. 1991). This corresponds to an error of about 1.6 M.Y. in the date.

6.2.4 Grouping of CVC Dates

For interpretation, all of the age dates of the CVC fall into four groups as follows: acid-sulphate mineralization between 23.0 +/-0.7 and 22.3 +/-0.7 M.Y.; volcanism older than 12.9 +/-0.5 M.Y.; acid-sulphate mineralization from 12.0 +/- 0.6 to 13.6 +/-0.4 M.Y.; and volcanism between 10.09 +/-0.23 to 6.6 +/-0.3 M.Y. All dates fit this grouping with the exception of the highly suspect alunite date from sample MZ-18-89. All acceptable dates are plotted with respect to age (Fig. 6.4) and are used in the following interpretations of CVC geology.

6.3 Age of Volcan Copiapo Native Sulphur Deposits

K-Ar geochronology in the sulphur deposits at Quebrada Azufre Sur hydrothermal vent, on a silica cap bearing alunite (MZ-15b-89), gives an age of 13.3 +/-0.5 M.Y. This sample contains a large amount of atmospheric argon and is bordering on suspect (Fig 6.3).

A reliable K-Ar age date on an unaltered andesite hornblende (MZ-26-85), from a flow that partially covers the

native sulphur deposits, gives an age of 8.7 +/-0.5 M.Y. Zentilli (1990), from field observations, states that this andesitic flow appears to be younger than the native sulphur deposits. This is also supported by the lack of alteration in these overlying andesites. If the native sulphur deposits were emplaced later than the andesite flows, these should have experienced some alteration. Therefore, the sulphur deposits are older than 8.7 +/-0.5 M.Y. and are probably 13.3 +/- 0.5 M.Y. However, there is a possibility that the overlying andesites remobilized the potassium in the sulphur deposit.

Sillitoe et al. (in press) and Mulja (1986) show by K-Ar dating of alunite that acid-sulphate gold mineralization at the Lobo and Marte deposits occurred between 12.0 +/-0.6 and 13.6 +/-0.6 M.Y. This coincides with the probable 13.3 +/-0.5 M.Y. age in the native sulphur deposits of Volcan Copiapo. Therefore, it is possible that the formation of these important sulphur deposits are coeval with acid-sulphate gold mineralization at Lobo and Marte.

6.4 Evolution of the Copiapo Volcanic Complex

The dated volcanics on Volcan Copiapo are 6.6 +/-0.3 to 10.09 +/-0.23 M.Y and constitute the youngest volcanic activity in the CVC. These volcanics overlie acid-sulphate mineralization and volcanism of the La Coipa-Maricunga (25-20 M.Y.) (Zentilli 1974) and Pastillito (14-12.5 M.Y.) volcanic chains (Sillitoe et al. in press).

The Copiapo Volcanic Complex was dominated by explosive

volcanism and caldera formation until the early mid-Miocene (Mulja, 1986). This is supported by the large volume of pyroclastics in the CVC and the presence of early small mid-Miocene summit calderas and or explosive craters at Volcan Pastillos, Villalobos, and possibly Volcan Copiapo (Fig. 6.1 & 6.4).

At the waning stages of this volcanic activity, mid-Miocene acid-sulphate alteration produced the gold mineralization present at Marte and Lobo. As indicated above, the native sulphur deposits at Volcan Copiapo also formed at this time (Fig. 6.1 & 6.4).

Volcanism is apparently absent between the early mid-Miocene and the end of the late-Miocene. An interruption in volcanism is justified because a cessation in volcanism is observed after Pastillito volcanic belt volcanism.

After a quiet phase, explosive volcanic activity was reinitiated to produce large volumes of pyroclastics and lavas of andesite and dacite composition. This volcanism is dated at 6.6 +/-0.3 to 10.09 +/-0.23 M.Y, and covers a large area of earlier formed volcanics, acid-sulphate mineralization, and native sulphur deposits (Fig 6.1 & 6.4).

6.5 Conclusions

Geochronology indicates that the formation of the native sulphur deposits at Volcan Copiapo is coeval with mid-Miocene acid-sulphate economic gold deposits at Marte and Lobo. Previous chapters suggest that the native sulphur deposits at

Volcan Copiapo are the preserved surficial expression of acid-sulphate mineralization at depth. There is a high probability that a genetic link exists between these native sulphur deposits and acid-sulphate gold mineralization. Both formed at the same time and appear to have formed by the same geological process.

The new $^{40}Ar/^{39}Ar$ date on MZ-11-89 hornblende of 6.6 +/- 0.3 M.Y. from the summit of Volcan Copiapo represents the youngest known volcanism of the Volcan Copiapo Complex. New $^{40}Ar/^{39}Ar$ dating techniques are more accurate than K-Ar methods and may modify the age of the CVC.

CHAPTER 7: CONCLUSIONS

7.1 Conclusions

Many investigators (e.g. Bonham 1988; Sillitoe 1988) have proposed an epithermal high-sulphur model which describes acid-sulphate gold mineralization (Chapter 2). Native sulphur at surface is often mentioned but is not seriously used to find volcanic-hosted precious metal deposits. This preliminary study conclude that the geology and chemical environment of the sulphur deposits are similar to surficial acid-sulphate alteration in epithermal precious metal deposits.

The presence of a hydrothermal breccia vent and silica capping rock in the sulphur deposits at Volcan Copiapo suggests that they formed in an epithermal environment near a water table. The mineralogy and geochemistry of the Volcan Copiapo sulphur deposits is the same as the surficial mineralogy of epithermal high-sulphur precious metal deposit models with the exception of an anomalous amount of native sulphur (Chapter 2 & 4). These sulphur deposits therefore appear to be a sulphur-rich surficial expression of epithermal acid-sulphate alteration.

Sulphur isotopes suggest that native sulphur formed from $H_2S_{(g)}$ which was produced by the disproportionation of magmatic $SO_{2(g)}$. Two chemical environments are proposed for the formation of sulphate minerals. One environment produces alunite veins at depth from sulphuric acid which was produced

by the disproportionation of $SO_{2(g)}$. The other chemical environment produces the sulphates, alunite, gypsum, and minimiite from sulphuric acid made from the oxidation of $H_2S_{(g)}$ near surface.

Dating of the native sulphur deposits indicates that they are coeval with acid-sulphate gold mineralization in Marte and Lobo. This supports the idea that the native sulphur deposits at Volcan Copiapo represent the surficial expression of possible acid-sulphate deposits at depth. K-Ar dating shows that younger volcanism has covered a large portion sulphur rich alteration at Volcan Copiapo.

The pattern of volcanism at Volcan Copiapo is not in agreement with the regional eastward migration of magmatism proposed by many authors (e.g. Zentilli 1974; Sillitoe et al. in press; Davidson and Mpodozis in press). Instead of migrating, the CVC experienced at least three cycles of volcanism (c.a 22, c.a. 13, and c.a. 7 M.Y.) at essentially the same geographic location. A lava flow on the northwestern flank of Volcan Copiapo at 6.6 +/- 0.3 M.Y. is the youngest known volcanism of the Maricunga District and should overlie the older products of the La Coipa-Maricunga and Pastillos volcanic belts.

REFERENCES

Allmendinger (1983) Tectonic development, southeastern border of the Puna Plateau, northwestern Argentine Andes. Geol Soc Am Bull 97:1070-1082.

Ashley RP (1982) Occurrence model for enargite-gold deposits. US Geol Survey Open File report 82-795:144-147.

Barazangi JA, Isacks BL (1976) Spatial distribution of earthquakes and subduction of the Nazca plate beneath South America: Geology 32:139-154.

Bethke PM (1984) Controls on base- and precious metal mineralization in deeper epithermal environments: US Geol Survey Open File report 84-890, 40p.

Bonatti E, Harrison CGA, Fisher DE, Honnorez J, Schilling JG, Stipp JJ, Zentilli M (1977) Easter volcanic chain (southwest Pacific): a mantle hot line. J Geophys Res 82:2457-2478.

Bonham HF (1988) Models for volcanic hosted epithermal precious metal deposits. In: Bulk minable precious metal deposits of the western United States. Schafer RW, Cooper JJ, Vilkre PG (eds) Geol Soc Nevada, 259-271p.

Bonham HF (1984) Three major types of epithermal precious metal deposits (abs). Geol Soc Am Bull 16:449.

Cahill T (1990) Earthquakes and tectonics of the Central Andean Subduction Zone. PhD Thesis, Cornell University, Ithaca, NY, 225p.

Clark AJ, Farrar E, Caelles JC, Haynes SJ, Lortie RB, McBride SL (1976) Longitudinal variations in the metallogenetic evolution of the Central Andes: a progress report. Geol Assoc Can special paper 14:23-58.

Cole DR, Ohmoto H (1986) Kinetics of Isotopic Exchange at elevated temperatures and pressures. in Valley, J.W., H.P. Taylor, and J.R. O'Neil (eds.) Stable Isotopes in High Temperature Geological Processes., Rev. In Min 16:41-87.

Cousino A (1951) The world sulfur situation 1951-1955. Production and potential consumption. Unpublished student paper for course on research in manufacturing, Harvard Business School, Excerpt: 9p.

Davidson J, Mpodozis C (1991) Regional geologic setting of epithermal gold deposits, Chile. in press, 28p.

Farrar E, Clark AH, Haynes SJ, Quirt GS, Conn H, Zentilli M (1970) K-Ar evidence for the post Palaeozoic migration of

granitic intrusive foci in the Andes of northern Chile. Earth Planet Sci Lett 10:60-66.

Field CW, Fifarek RH (1985) Light Stable-Isotope Systematics in the Epithermal Environment. in Berger, B.R. and P.M. Bethke (eds.), Geology and Geochemistry of Epithermal Systems, Rev in Econ Geol 12:1-24.

Fournier RO (1985) The Behaviour of Silica in Hydrothermal Systems. in Berger, B.R. and P.M. Bethke (eds.), Geology and Geochemistry of Epithermal Systems, Rev in Econ Geol 12:45-72.

Godoy S, Cuadra C (1988) Como aprovechar las reservas de azufre?. Boletin Minero, Santiago, Chile 2-6p.

Gonzalez-Ferran O, Baker PE, Rex DC (1985) Tectonic- volcanic discontinuity at latitude 27o south Andean Range, associated with Nazca plate subduction. in K. Kobayashi and T.S. Sacks (eds.), Structures and Processes in Subduction Zones, Tectonophys 112:423-441.

Guerra JB (1901) Industria minera y metalurgica del departamento de Copiapo; Imprenta "El Amigo del Pais", Copiapo, 220p.

Harmon RS, Hoefs J (1984) Oxygen isotope ratios in Late Cenozoic Andean volcanics. In Andean magmatism: chemical and isotopic constraints. Harmon RS, Barreiro BA (eds) Shiva Publishing Ltd, Nantwich, U.K, 9-20p

Harrison TM, McDougall I (1981) Excess 40Ar in metamorphic rocks from Broken Hill, New South Wales: Implications for 40Ar/39Ar age spectra and the thermal history of the region. Earth Plan Sci Lett 55:123-149.

Hayba DO, Bethke PM, Heald P, Foley NK (1985) Geologic, Mineralogic, and Geochemical Characteristics of Volcanic-Hosted Epithermal Precious Metal Deposits in Berger, B.R. and P.M. Bethke (eds.) Geology and Geochemistry of Epithermal Systems, Rev Econ Geol 2:129-167.

Heard-Wetlaufer P, Hayba DO, Foley NK, Goss JA (1983) Comparative anatomy of epithermal precious- and base-metal districts in volcanic terranes (abs). Joint annual meeting of GAC/MAC/GCU Victoria BC.

Henley RW (1985) The Geothermal Framework of Epithermal Deposits in Berger, B.R. and P.M. Bethke (eds.), Geology and Geochemistry of Epithermal Systems, Rev Econ Geol 2:1-24.

Henley RW, Brown KL (1985) A Practical Guide to the Thermodynamics of Geothermal Fluids and Hydrothermal Ore Deposits in Berger, B.R. and P.M. Bethke (eds.), Geology and Geochemistry of Epithermal Systems, Rev Econ Geol 2:25-44.

Hoefs J (ed.) (1987) Stable Isotope Geochemistry (Minerals and Rocks 9), Springer-Verlag, Heidelberg, 241p.

Jordan TE, Isacks BL, Allmendinger RW, Brewer JA, Ramos VA, Ando CJ (1983) Andean tectonics related to geometry of subducted Nazca plate. Geol Soc Am Bull 94:341-361.

Kay SM, Maksaev V, Mpodozis C, Moscoso R, Nasi C (1987) Probing the Andean Lithosphere: Mid-Late Tertiary magmatism in Chile (29o-30.5oS) over the zone of subduction. Jour Geophys Res 92:6173-6189.

Lindgren W (1933) Mineral deposits (4 ed) McGraw-Hill, New York, 930p.

Lo CH, Onstott TC (1989) 39Ar recoil artifacts in chloritized biotite. Geochim Cosmochim Acta 53:2697-2711.

McDougall I, Harrison TM (1988) Geochronology and Thermochronology by the 40Ar/39Ar Method. Oxford Monographs on Geology and Geophysics, no. 9. Oxford University Press, N.Y.

Mella F (1933) Private report cited in Cousino (1951)

Mercado M (1982) Hoja Laguna del Negro Francisco. Carta Geologica de Chile 1:100,000, SERNAGEOMIN, Chile No56, 72p, 1 map.

Mpodozis C, Ramos V (in press) The Andes of Chile and Argentina. In: Geology of the Andes and its relationship to hydrocarbon and mineral resources, symposium, Santiago, Chile 1985.

Mulja T (1986) Hydrothermal alteration, gold distribution and geochronology of epithermal gold mineralization in the Copiapo volcanic complex, Chile. BSc thesis, Dalhousie University, Halifax, Nova Scotia, 145p.

Ohmoto H, Rye RO (1979) Isotopes of sulphur and carbon. In: Geochemistry of hydrothermal ore deposits, Barnes HL (ed) John Wiley and Sons, University Park, Penn, 798p.

Ohmoto H (1987) Stable isotope geochemistry of ore deposits. Rev Min 16:491-559.

Ohmoto H, Lasaga AC (1982) Kinetics of reactions between aqueous sulfates and sulfides in hydrothermal systems. Geochem Cosmochim Acta 46:1727-1746.

Peterson U, Noble DC, Arenas MJ, Goodel PC (1977) Geology of the Julcani mining district, Peru. Econ Geol 72:931-949.

Reed MH, Spycher NF (1985) Boiling, cooling, and oxidation in

epithermal systems: a numerical modelling approach. In: Geology and geochemistry of epithermal systems: Soc of Econ Geol, reviews in economic geology (v 2) Berger BR, Bethke PM (eds).

Rye RO, Ohmoto H (1974) Sulfur and Carbon Isotopes and Ore Genesis: A Review. Econ Geol 69:826-842.

Sakai H, Casadevall TJ, Moore JG (1982) Chemistry and isotope ratios of sulfur in basalts and volcanic gases at Kilauea Volcano, Hawaii. Geochim Cosmochim Acta 46:729-738.

Sayago C (1874) Historia de Copiapo, imprenta El Atacama, Copiapo, 452p.

Silberman ML, Noble DC (1977) Age of igneous activity and mineralization, Cerro de Pasco, central Peru. Econ Geol 72:925-930.

Sillitoe RH, McKee EH, Vila T (in press) Reconnaissance geochronlogy of the Maricunga gold-silver belt, northern Chile. Spec Vol Econ Geol.

Sillitoe RH (1988) Epochs of intrusion-related copper mineralization in the Andes. J South Am Earth Sci 1:89-108.

Sillitoe RH (1985) Ore-related breccias in volcanoplutonic arcs. Econ Geol 80:1467-1514.

Sillitoe RH, Baker M, Brook W (1984) Golds deposits and hydrothermal eruption breccias associated with a maar volcano at Wau. Papau, New Guinea. Econ Geol 79:638-655.

Sillitoe RH, Bonham HF Jr (1984) Volcanic landforms and ore deposits. Econ Geol 79:1286-1298.

Sillitoe R (1983) Enargite-bearing massive sulphide deposits high in porphyry copper systems. Econ Geol 78:348-352.

Sillitoe, R.H. (1976) Metallic mineralization affiliated to subaerial volcanism; a review. in Volcanic processes in ore genesis: The Institute of Mining and Metallurgy. The Geological Society of London, pp. 99 - 114.

Sillitoe RH (1973) The tops and bottoms of porphyry copper deposits. Econ Geol 68:799-815.

Steiger RH, Jager E (1977) Subcommision on geochronology: convention on the use of decay constants in geo- and cosmo-chronology. Earth Planet Sci Lett 36:359-362.

Thompson T, Trippal A, Dwelley P (1985) Mineralized veins and breccias of the Cripple Creek District, Colorado. Econ Geol 80:1669-1688.

Thorpe RS, Francis PW, O'Callaghan L (1984) Relative roles of source composition, fractional crystallization and crustal contamination in the petrogenesis of Andean volcanic rocks. R Soc London Phil Trans, A310:675-692.

Thorpe RS, Francis PW, Hammill M, Baker MCW (1982) The Andes. In: Andesites: orogenic andesites and related rocks, 724p.

Vila T and Sillitoe R (in press) Gold-rich porphyry systems in the Maricunga belt, northern Chile.

Walker J, Zentilli M (1984) Proposal for research grant, unpublished report, 14 pp.

Walker J, Moulds T, Zentilli M, Feigenson M (1991) Spatial and temporal variations in the Andean Central Volcanic Zone (26o-28oS). G.S.A. Special Vol. In Press.

Wallace AB (1979) Possible signatures of buried porphyry-copper deposits in middle to late Tertiary volcanic rocks of western Nevada. In: Proceedings of the fifth symposium of the international association on the genesis of ore deposits (v 2) Nevada bureau of mines report 33:69-76.

White DE (1981) Active geothermal systems and hydrothermal ore deposits. Econ Geol 75th anniversary volume pp 392-423.

Wilson M (1989) Igneous petrogenesis: a global tectonic approach. Unwin Hyman, 466p.

York D, Farguhar RM (1982) The Earth's age and geochronology. Jacobs JA, Wilson JT (eds) Pergamon Press, 178p.

Zentilli M (1990) The Volcan Copiapo Property, Maricunga District, Chile: Geology and mineral potential. Unpublished Cuesta Research Ltd. report, Dartmouth, Nova Scotia.

Zentilli M, Mulja T, Reynolds PH, Walker JA (1986) Gold mineralization related to the evolution of a Miocene volcanic complex in the southern central Andes (abs). Maritime Sed and Atlantic Geol 22:211.

Zentilli M (1974) Geological evolution and metallogenic relationships in the Andes of northern Chile between 26 and 29o south. Unpublished Ph.D. thesis, Queen's University, Kingston, Ont. 460 pp.

Znamenskiy VS, Nosik LP (1984) Isotopic composition of sulfur and genesis of volcanogenic sulfur deposits (southern Kuril islands). Jour Vol Geotherm Res 20:41-54.

PLATES

Plate 1a & b The western side of Volcan Copiapo summit, showing the sulphur deposits at Manto Volcan and Quebrada Azufre viewed from the La Pepa Gold Mine. For scale the manto is over 100 m thick Note: Sulphur Manto is overlain by little to unaltered andesites and dacites. Sulphur Manto is sub-parallel to the surface (from Zentilli 1990).

B

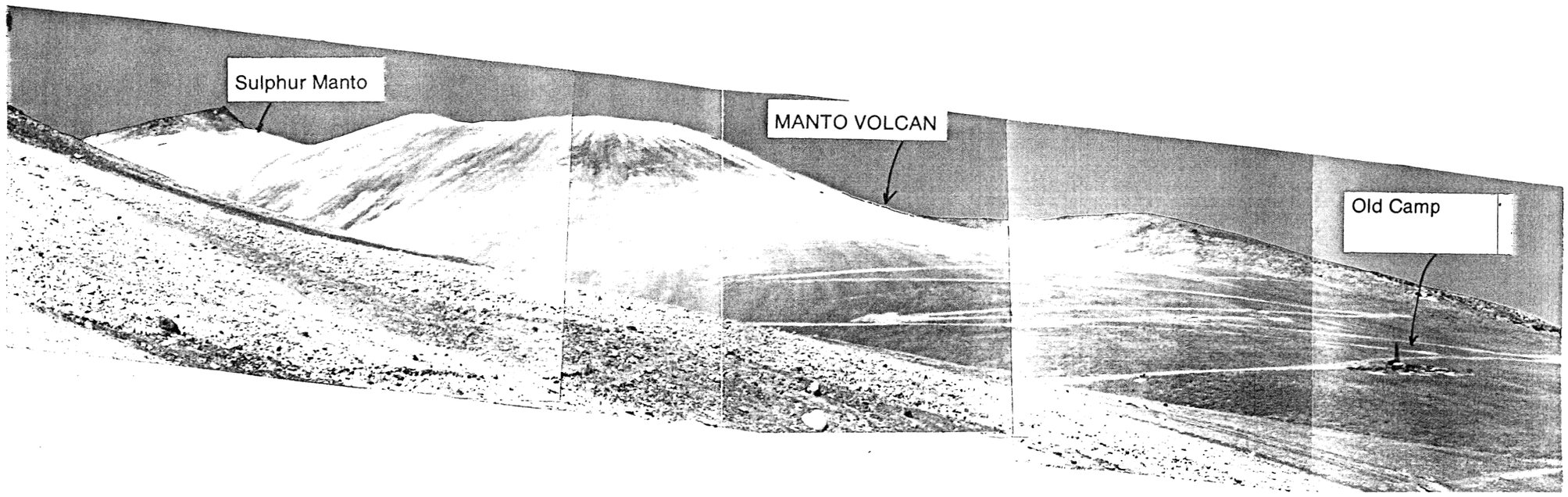

A

Plate 2b Quebrada Azufre Sur hydrothermal breccia vent (far right) in a much larger sulphur rich manto (from Zentilli 1990).

Plate 2a Close view of the hydrothermal breccia vent (c.a. 30m in diameter). Note the presence of a silica cap around the vent area. (from Zentilli 1990).

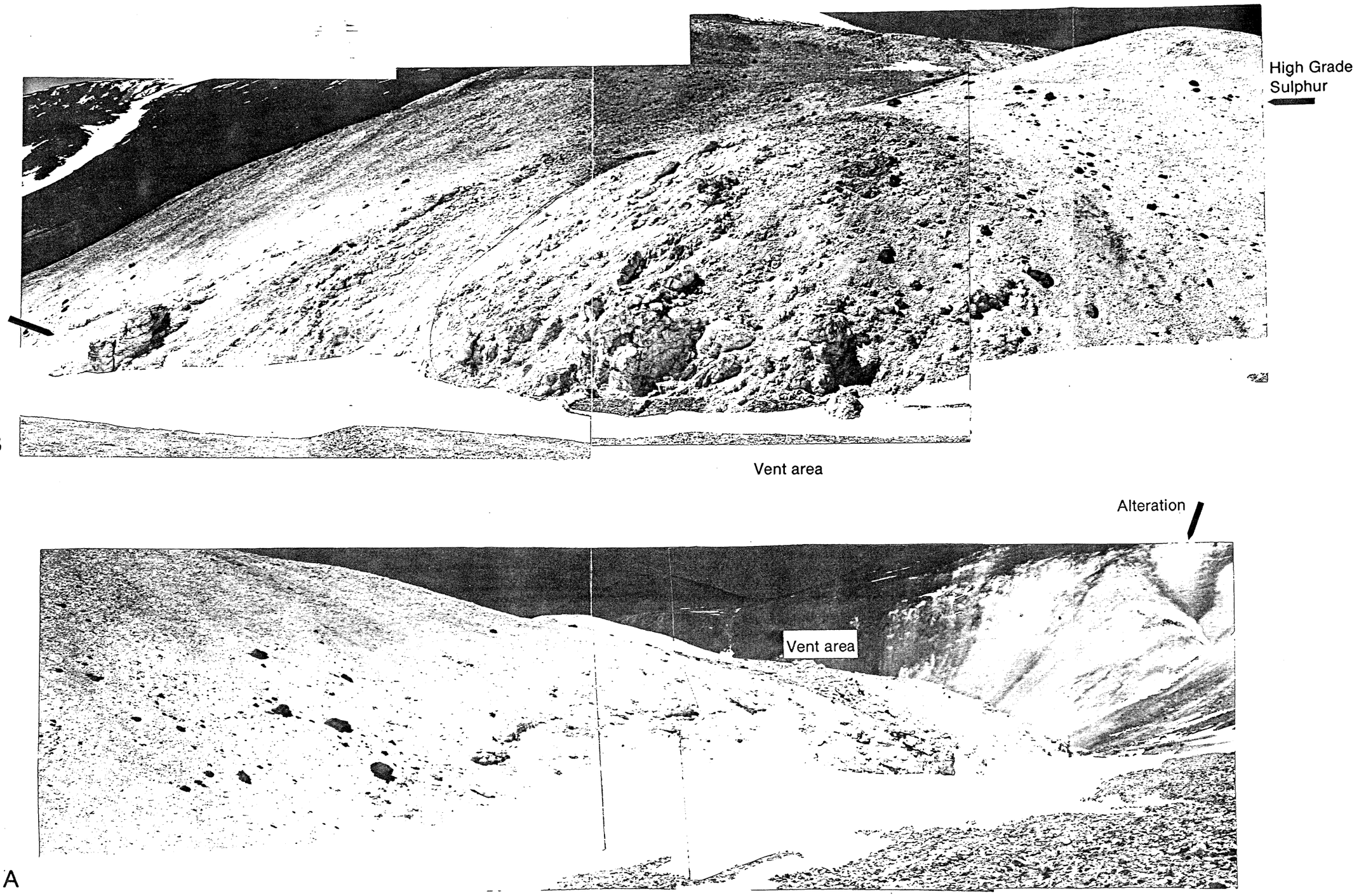
High Grade
Sulphur
"Silica Cap"
B
Vent area
Alteration
Vent area
A

Plate 3b A close view of the sulphur "manto" at Quebrada Azufre Sur. Note hammer for scale (from Zentilli 1990).

Plate 3a An outcrop view at the Quebrada Azufre Sur vent showing sulphur and alunite-cemented silica rich hydrothermal explosion breccia. Silica is present as in porous to banded angular fragments. MZ-16a-89 in plate 4 is a representative hand sample of this breccia. Note hammer for scale (from Zentilli 1990).

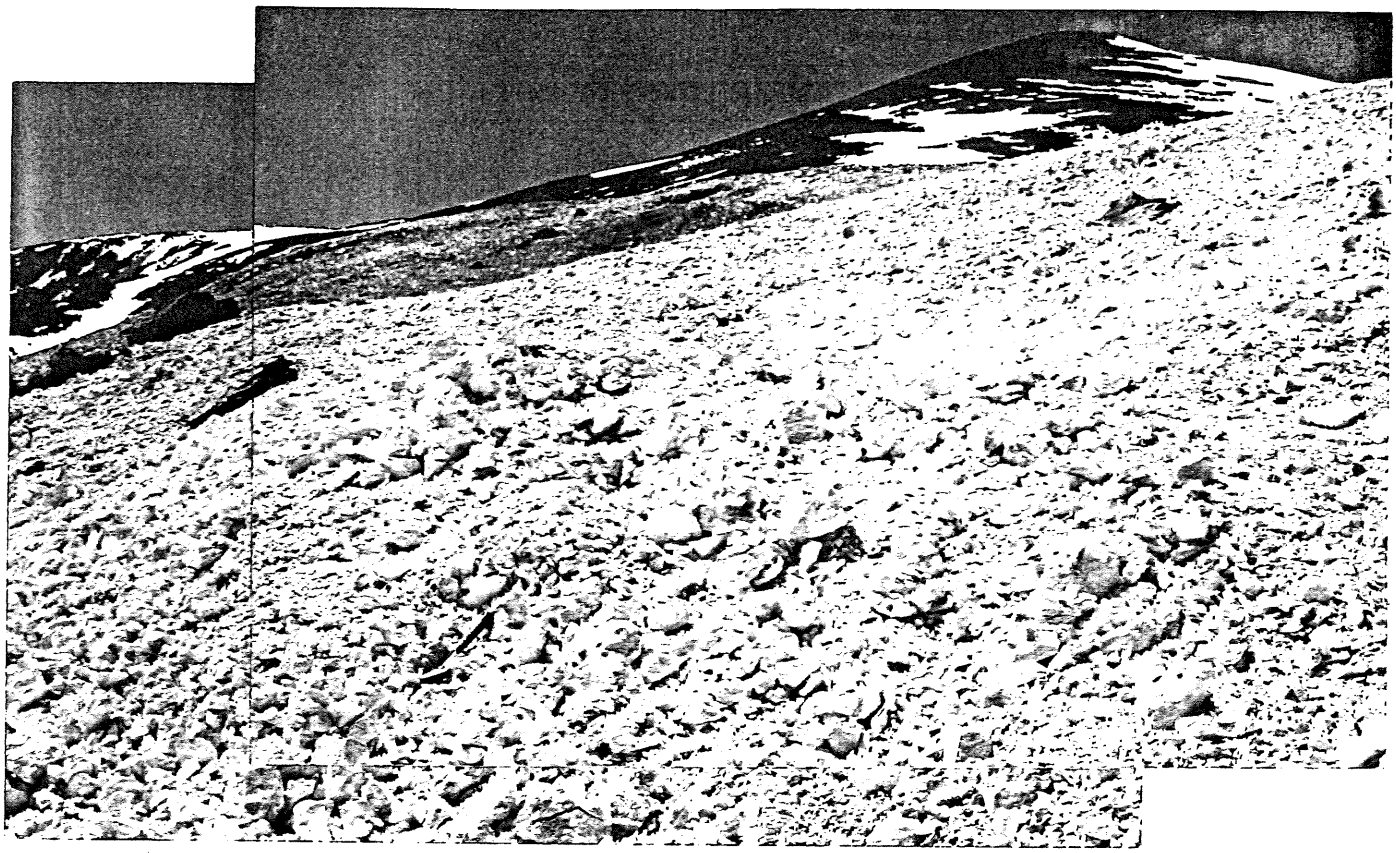

Plate 4 MZ-16a-89 hand sample from the hydrothermal explosion breccia vent at Quebrada Azure Sur. Silica is present as low quartz and chert in porous to banded angular fragments. Most of the banded silica displays a chalcedony texture. The pores in porous silica appear to be due to the removal of plagioclase from former andesites, dacites and pyroclastics. The breccia is cemented with sulphur and alunite. Small specs of cinnabar < 2mm are present in the cement where alunite is abundant. Black square 1 cm (from Zentilli 1990).

Plate 5 MZ-18-89 comes from outside the vent at Quebrada Azufre Sur. This sample is a sulphur impregnated alunitized rock with fine soft poorly crystallized tridymite, often seen as pods <5mm in diameter. Although this sample has undergone total replacement relics of zoned euhedral plagioclase and euhedral hornblende displaying cleavages are seen in thin section indicating that this rock is a former andesite or dacite. Black square 1 cm (from Zentilli 1990).


16

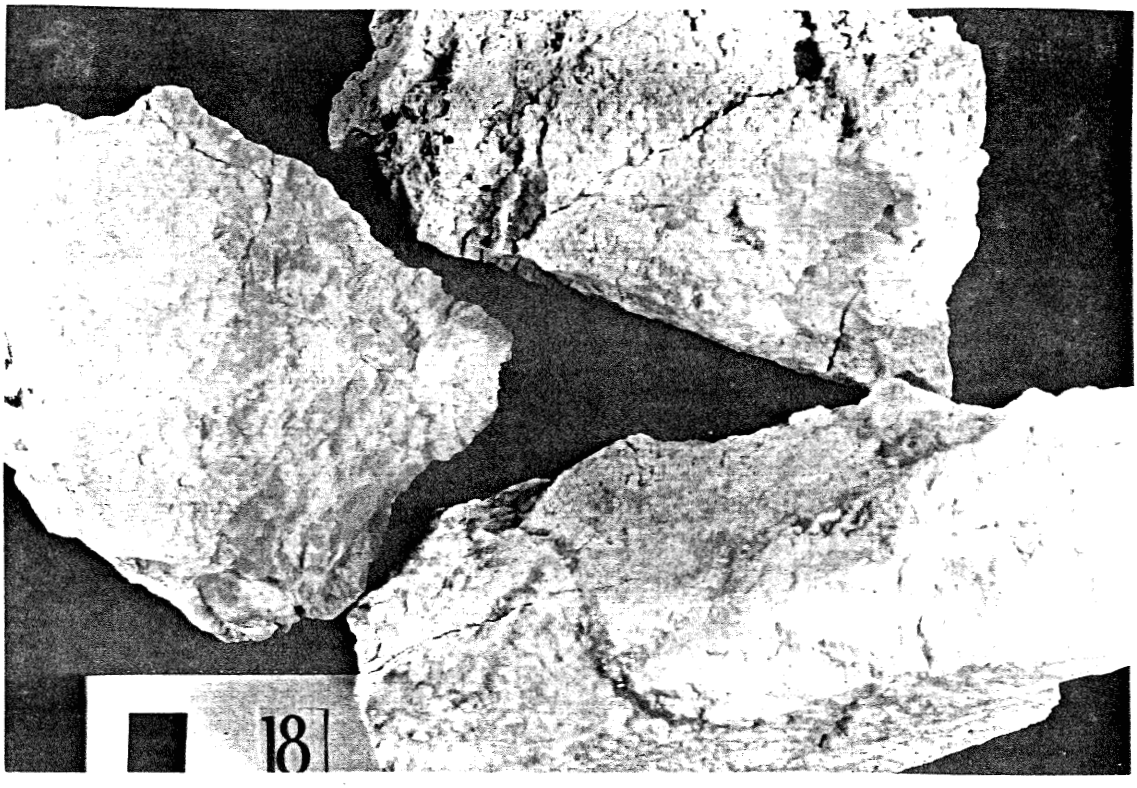
18

Plate 6 MZ-17-19 has relict phenocrysts of zoned plagioclace in a sulphur impregnated volcanic rock. XRD determination identifies this sample as being made of native sulphur, alunite, minimiite, and a small amount of tridymite. Because of the euhedral unbroken shapes of the relicts and the similarity to an unaltered andesite. This sample represents the almost total replacement of a former andesite or dacite. (field of view 3 cm).

Plate 7 MZ-18-89 relict phenocrysts of plagioclase are present in this sulphur impregnated sample. XRD determination identifies a mineralogy of native sulphur, alunite, and a small amount of tridymite. This sample has euhedral relicts of zoned plagioclase which are similar to unaltered an unaltered andesite. This sample represents an almost total replacement of a former andesite or dacite. (field of view is 3 cm).

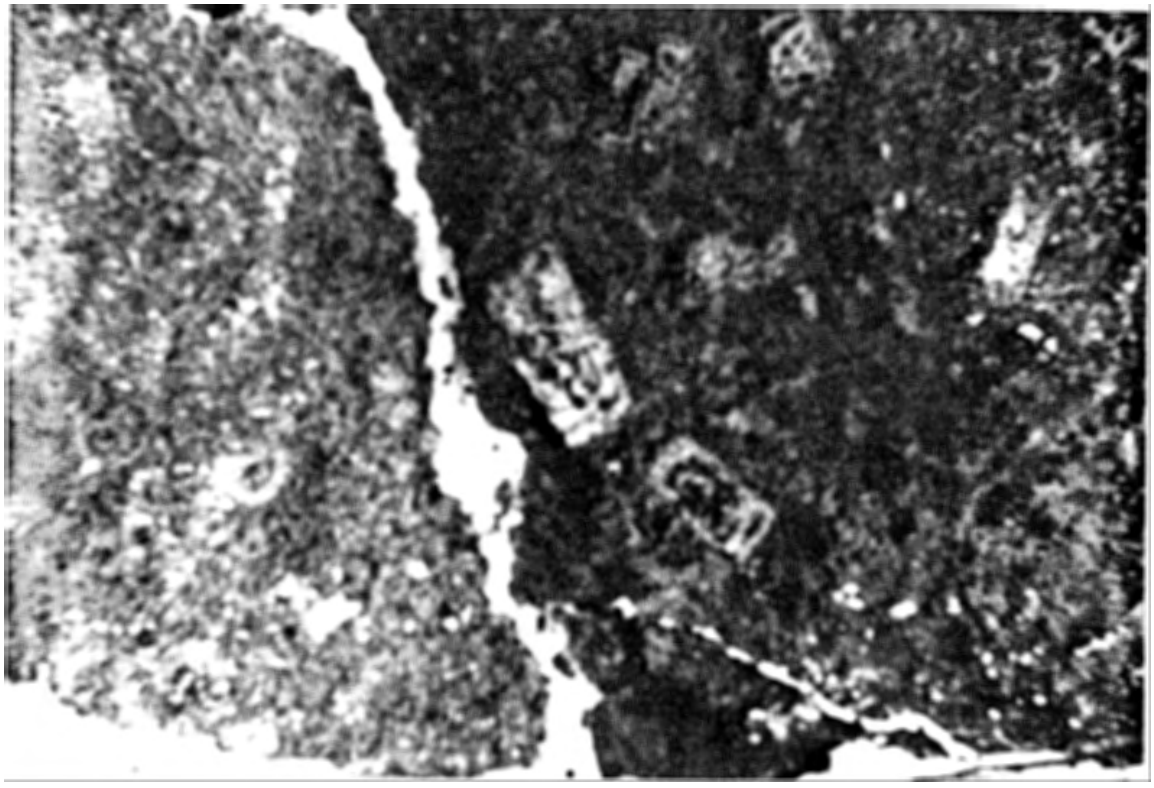

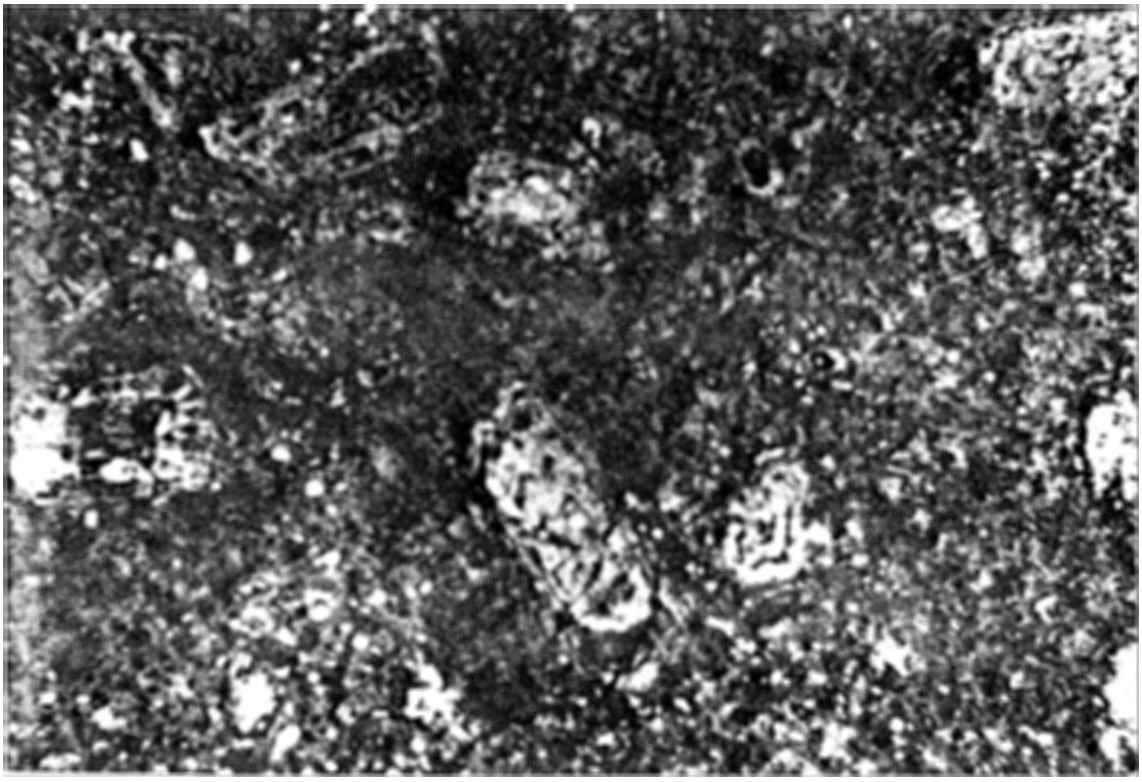

Plate 8 MZ-4-89 is high grade hand picked sulphur with minor amounts of fine soft amorphous silica (<15%) from Manto Volcan. Black square 1 cm(from Zentilli 1990).

Plate 9 MZ-16a-89 visible cinnabar in alunite from the hydrothermal breccia vent. (field of view 1.5 cm).

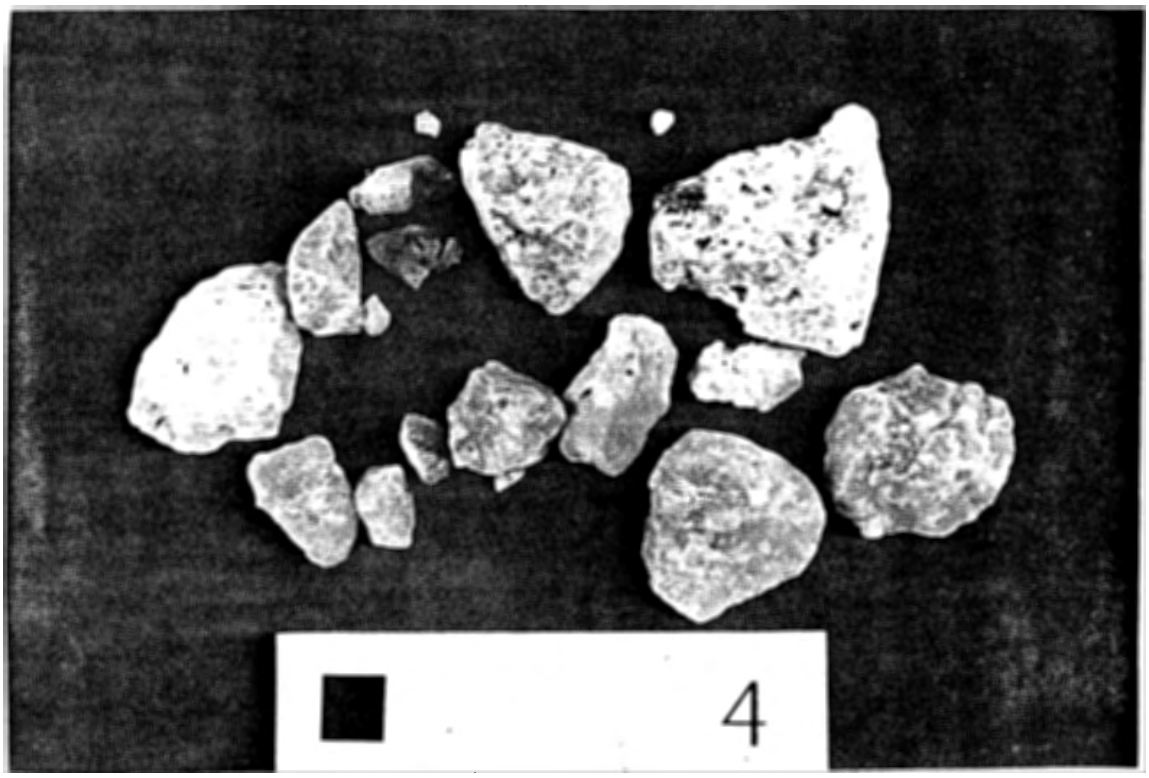
4

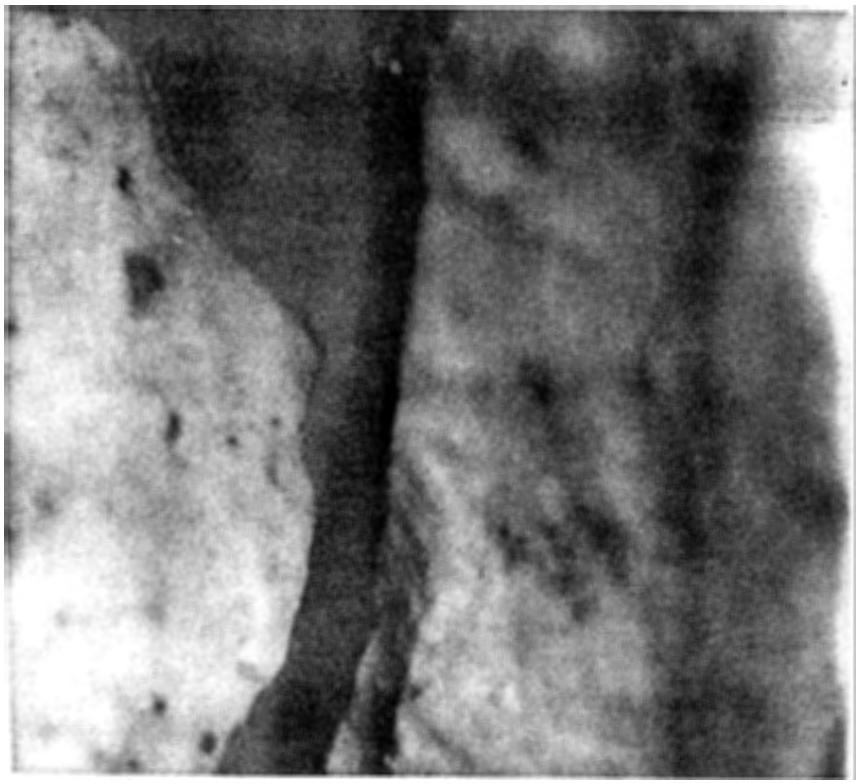

Appendix A:

Chemical Treatment of Samples With Carbon Disulphide to Remove Native Sulphur

Introduction

Chemical treatment of sulphur rich samples with carbon disulphide is a practical inexpensive method of separating native sulphur from other sulphur bearing minerals.

Chemistry

Carbon disulphide (CS_2) dissolves native sulphur while having no effect on sulphate minerals, salts, and silicates. Carbon disulphide (CS_2) has a high affinity for sulphur and is a symmetrical polyatomic molecule with an overall polarization of zero. Native sulphur (S_8) is a ring structure of S with no polarization. The laws of chemistry state that non-polar solids dissolve in non-polar solvents. Therefore non-polar solids (native sulphur) will dissolve in non-polar solvents (CS_2), especially if the solvent has a high affinity for the elements of the solid. Sulphate minerals and salts of sulphur are polar to ionic in nature and will not react with non-polar carbon disulphide.

Reasons For Using Carbon Disulphide

A. X-Ray Diffraction

Native sulphur contains 67 peaks between 2 and 72^0 on XRD. As a result native sulphur can make XRD determination of other

mineral phases difficult. Removal of native sulphur using CS_2 can unmask the peaks of other minerals. For example one of the major peaks of gypsum has the same location as one of the peaks of sulphur. Removal of native sulphur also increases the intensity of all other mineral peaks. As a result, minerals which make up a small percentage of the rock can be identified by XRD.

B. Stable Isotopes

Carbon disulphide can be used to separate fine native sulphur from sulphate minerals for stable isotope work. This method is used to separate the sulphate minerals in MZ-17-89 and MZ-18-89.

C. Geochronology

CS_2 can remove native sulphur from K-bearing sulphates with no effect on age determination. This method is used to separate alunite in MZ-18-89. This sample could not be sufficiently dated using K-Ar geochronology at Krueger Enterprises Inc., but chemical evidence suggests that this is not from the treatment of the sample with CS_2 (see discussion below).

Experimental Work on Treating Samples With Carbon Disulphide

A. X-Ray Diffraction

XRD analysis on numerous chemically treated sulphate and silicate minerals indicate that there is no change in structure. There is no shift in position of peaks and the only peaks removed

are those of native sulphur (Appendix B). Sulphur saturated carbon disulphide readily evaporates and as a result precipitates pure native sulphur (identified by XRD for MZ-16a-89a) (Appendix B).

B. Atomic Absorption Analysis

Atomic absorption analysis on CS_2 in contact with native sulphur and alunite for approximately one hour detect trace amounts of K (0.25 ppm). This amount of K could come from impurities in native sulphur or from the alunite. If one assumes that the K detected comes from alunite, calculations show that the K in solution is three orders of magnitude smaller than that detectable by conventional flame spectrophotometric analysis (McDougall and Harrison, 1988; York and Farquhar, 1982) (Appendix E).

C. Sulphur Isotope Analysis

Sample WZ-120-84 was used to test the effects of chemical treatment on sulphur isotopic values. Sample WZ-120-84 contains alunite veins with no visible native sulphur. Alunite from this sample is used to test the affects of chemical treatment on ^{34}S values. The alunite chemically treated for approximately two hours yields a ^{34}S value of +14.9 $^{0}/_{00}$ while the untreated sample is +15.3 $^{0}/_{00}$ (Table 4.1). This discrepancy could be due to sampling and analytical error. Ohmoto and Rye (1979) state that analytical error may be +/- 0.2$^{0}/_{00}$. The untreated alunite is mainly white with minor light yellow patches and chemical treatment makes alunite white. This light yellow colour is

suspected to be free sulphur and could therefore explain the rather insignificant change in ^{34}S.

Appendix B:

X-Ray Diffraction Patterns

Alteration mineral assemblages are identified by the writer using a Siemens Diffractometer 500 at the Bedford Institute of Oceanography, Bedford, Nova Scotia Canada. A JCPDS data base is used to search for a list of positive mineral identification and to overlay standard X-ray diffraction peaks over unknown samples.

The following parameters are used on the diffractometer:

Radiation: Copper alpha
Filter: Nickel
Kv/mA: 40/20
Scan Speed: 1 degree per minute
Parabolic Background Correction: Typical width = 0.15
STD above background = 3.00
Alpha-2 removal
Alpha-1 / alpha-2 ratio = 2.00
Calibration of 2-theta

JCPDS data base searches are based on the following parameters:

Error window 2-theta measurement: 0.15
Number of strongest standard lines: 1 to 3
Number of lines for a match: 3
Strongest number of lines searched: 15
No phase restrictions or chemistry restrictions
Exponential weighting factor for standard lines matched, unknown lines matched, intensity match, d-spacing match: 1.0, 1.0, 1.0, 1.0.

Note: All patterns which have the extension .CHEM are chemically treated with carbon disulphide to remove native sulphur.

The following XRD patterns constitute a representative set from a total of 58. All other XRD patterns are in a file and are available upon request from Dr. M. Zentilli.

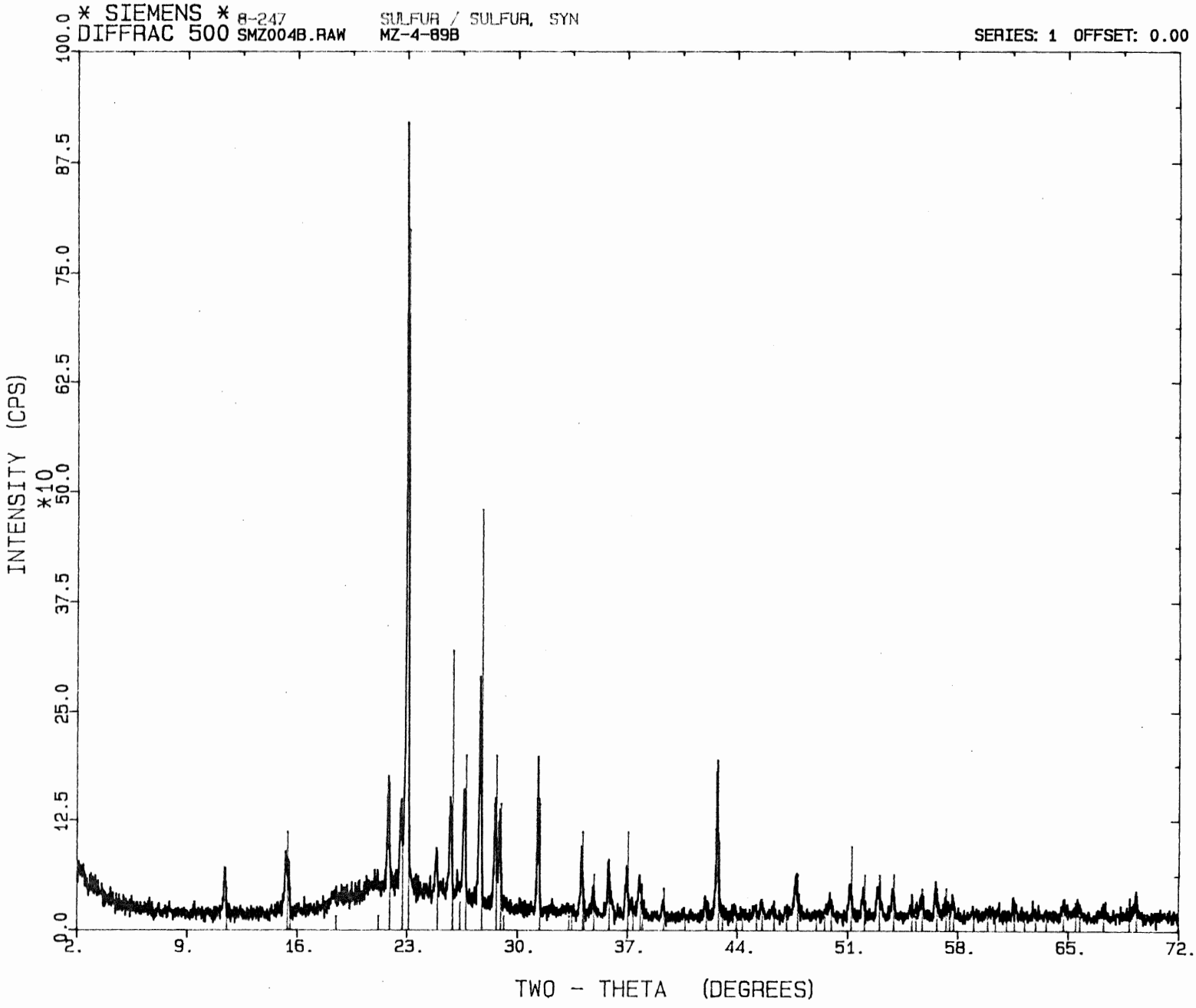
* SIEMENS * 8-247
DIFFRAC 500 SMZ004B.RAW
SULFUR / SULFUR, SYN
MZ-4-89B
SERIES: 1 OFFSET: 0.00
INTENSITY (CPS)
*10
100.0
87.5
75.0
62.5
50.0
37.5
25.0
12.5
0.0
2.
9.
16.
23.
30.
37.
44.
51.
58.
65.
72.
TWO - THETA (DEGREES)

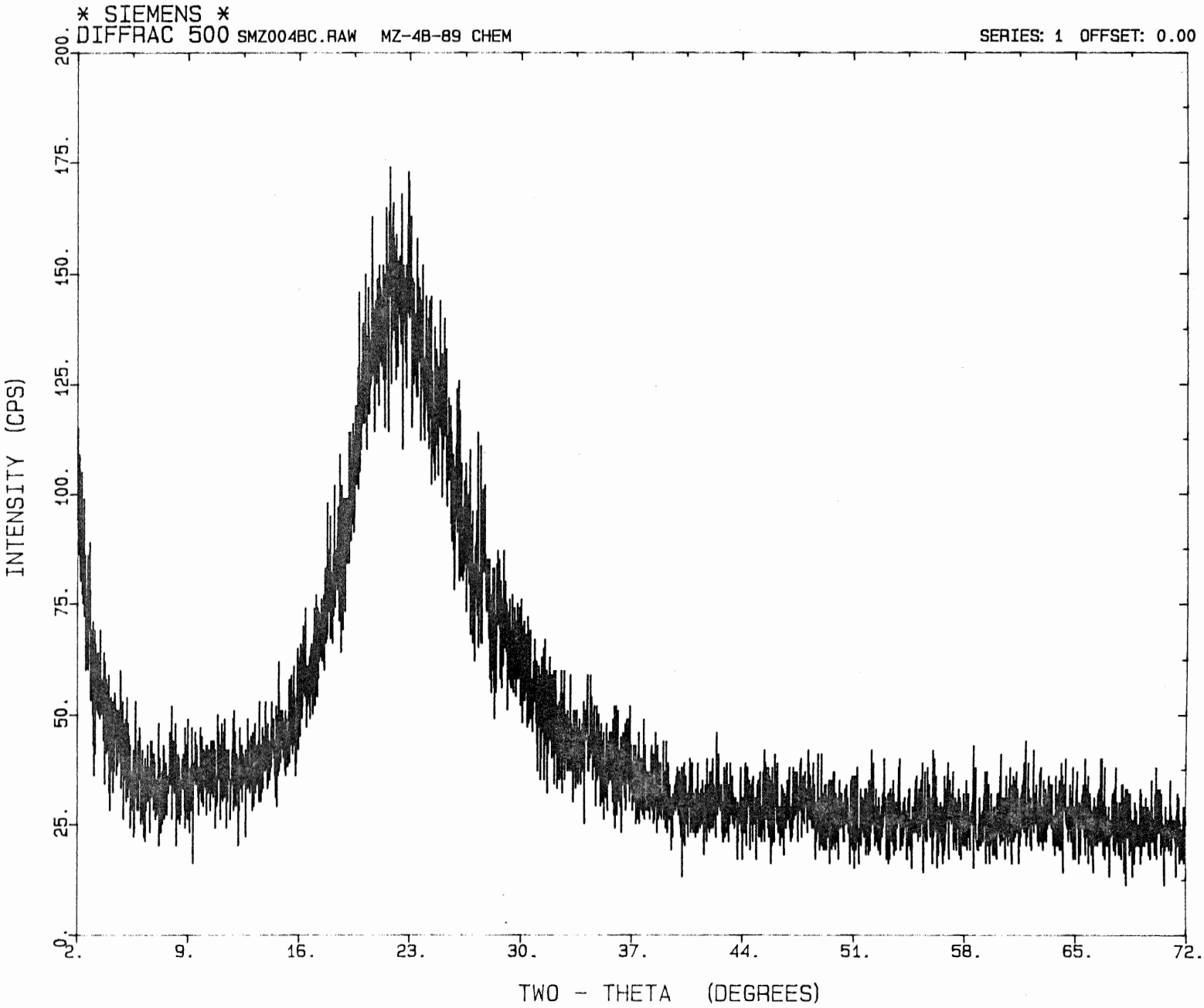
* SIEMENS *
DIFFRAC 500 SMZ004BC.RAW MZ-4B-89 CHEM
SERIES: 1 OFFSET: 0.00
INTENSITY (CPS)
0.
25.
50.
75.
100.
125.
150.
175.
200.
2.
9.
16.
23.
30.
37.
44.
51.
58.
65.
72.
TWO - THETA (DEGREES)

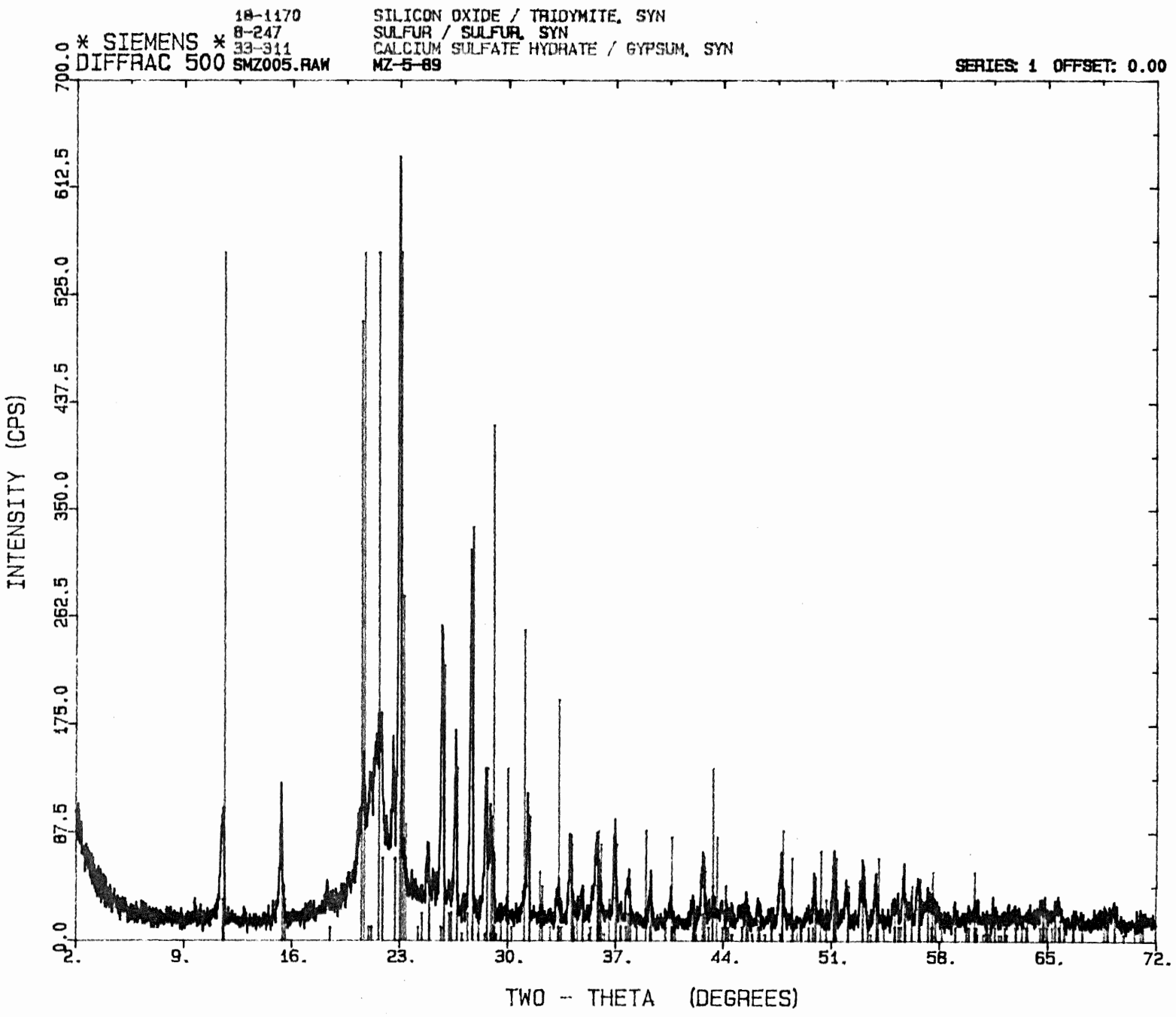
18-1170 SILICON OXIDE / TRIDYMITE, SYN
8-247 SULFUR / SULFUR, SYN
33-311 CALCIUM SULFATE HYDRATE / GYPSUM, SYN
* SIEMENS *
DIFFRAC 500
SMZ005.RAW
MZ-5-89
SERIES: 1 OFFSET: 0.00
INTENSITY (CPS)
700.0
612.5
525.0
437.5
350.0
262.5
175.0
87.5
0.0
2.
9.
16.
23.
30.
37.
44.
51.
58.
65.
72.
TWO - THETA (DEGREES)

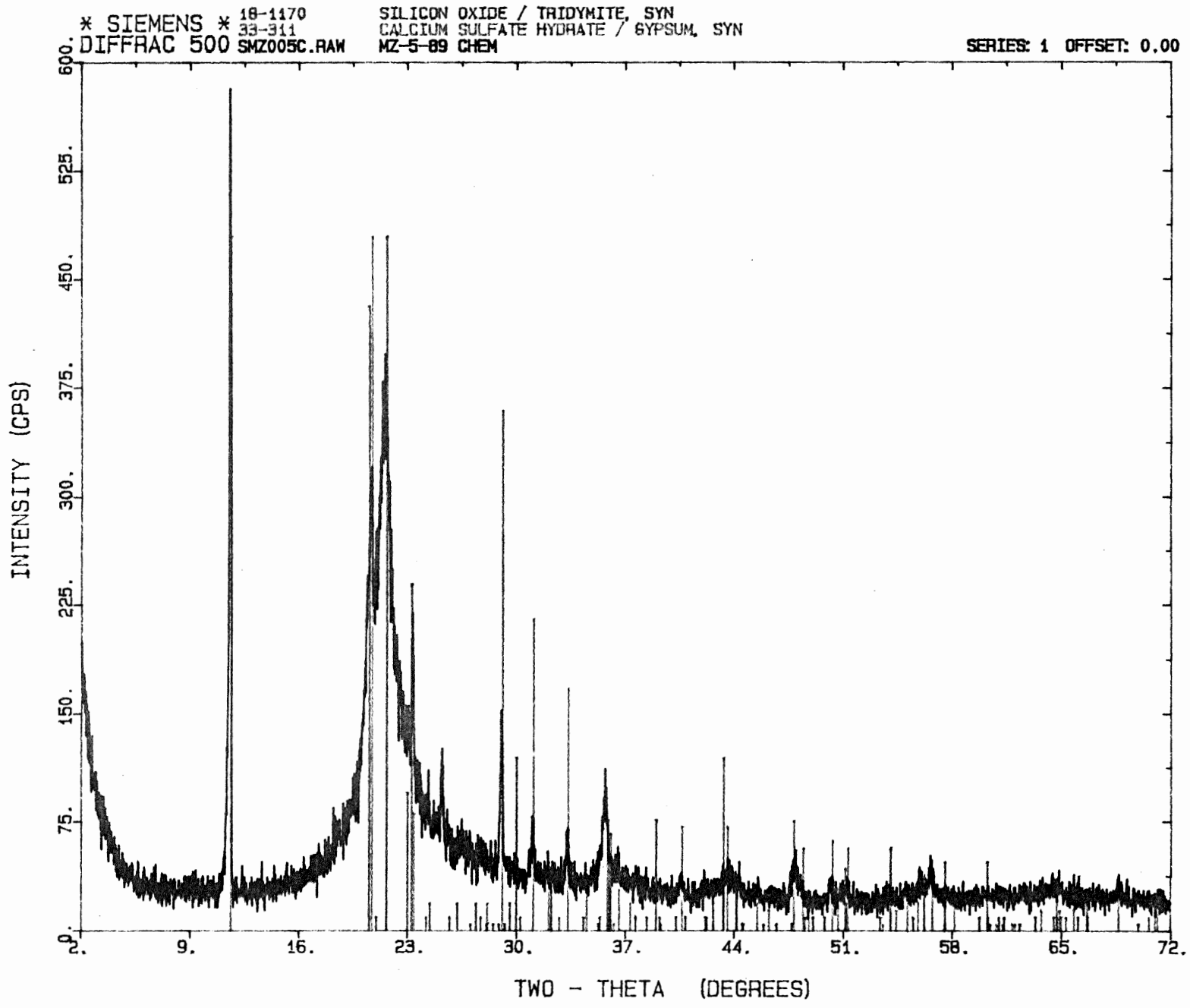
* SIEMENS * 18-1170
33-311
DIFFRAC 500 SMZ005C.RAW
SILICON OXIDE / TRIDYMITE, SYN
CALCIUM SULFATE HYDRATE / GYPSUM, SYN
MZ-5-89 CHEM
SERIES: 1 OFFSET: 0.00
INTENSITY (CPS)
600.
525.
450.
375.
300.
225.
150.
75.
0.
2.
9.
16.
23.
30.
37.
44.
51.
58.
65.
72.
TWO - THETA (DEGREES)

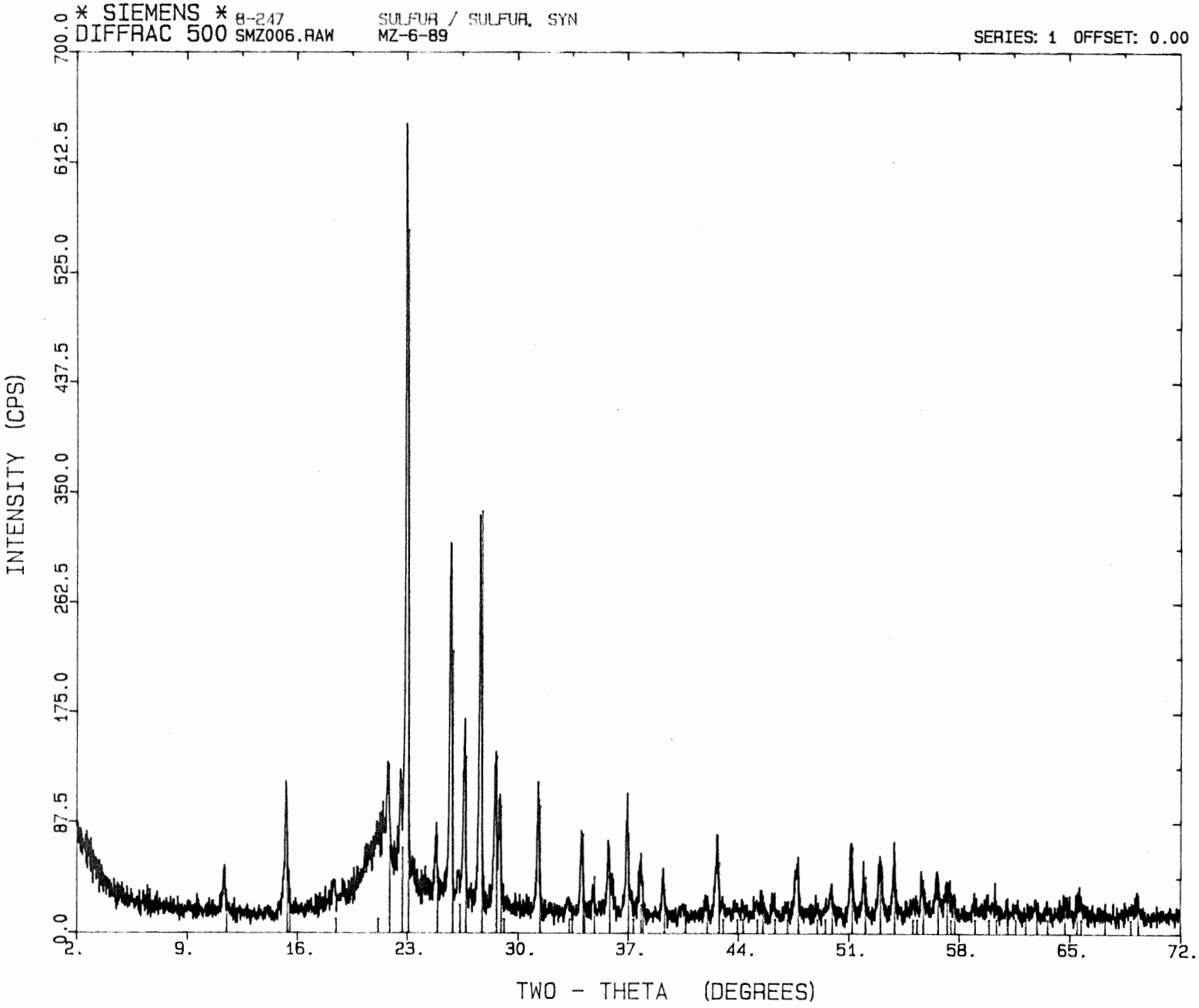
* SIEMENS * 8-247
DIFFRAC 500 SMZ006.RAW
SULFUR / SULFUR, SYN
MZ-6-89
SERIES: 1 OFFSET: 0.00
INTENSITY (CPS)
700.0
612.5
525.0
437.5
350.0
262.5
175.0
87.5
0.0
2.
9.
16.
23.
30.
37.
44.
51.
58.
65.
72.
TWO - THETA (DEGREES)

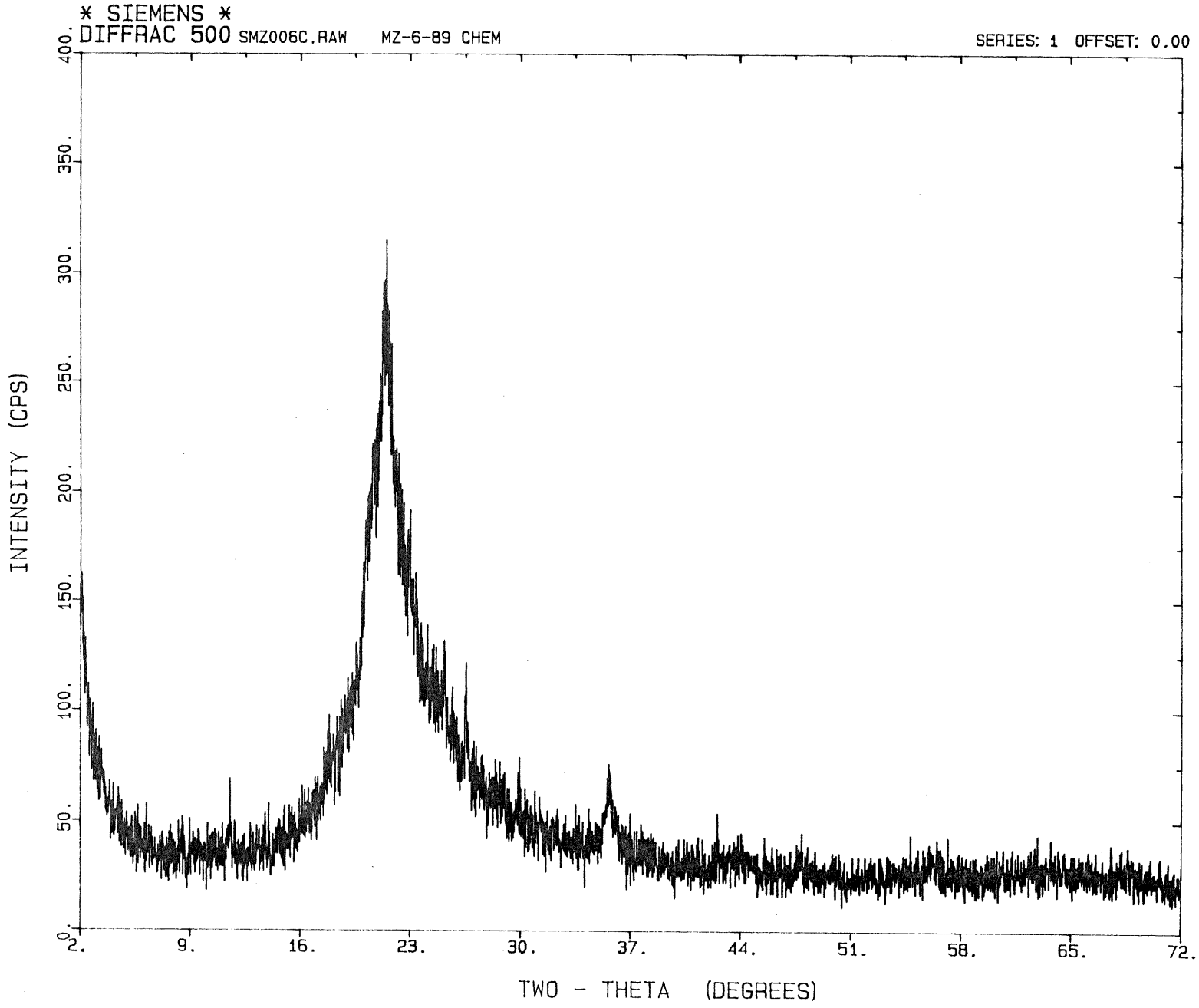
* SIEMENS *
DIFFRAC 500 SMZ006C.RAW MZ-6-89 CHEM
SERIES: 1 OFFSET: 0.00
INTENSITY (CPS)
0.
50.
100.
150.
200.
250.
300.
350.
400.
2.
9.
16.
23.
30.
37.
44.
51.
58.
65.
72.
TWO - THETA (DEGREES)

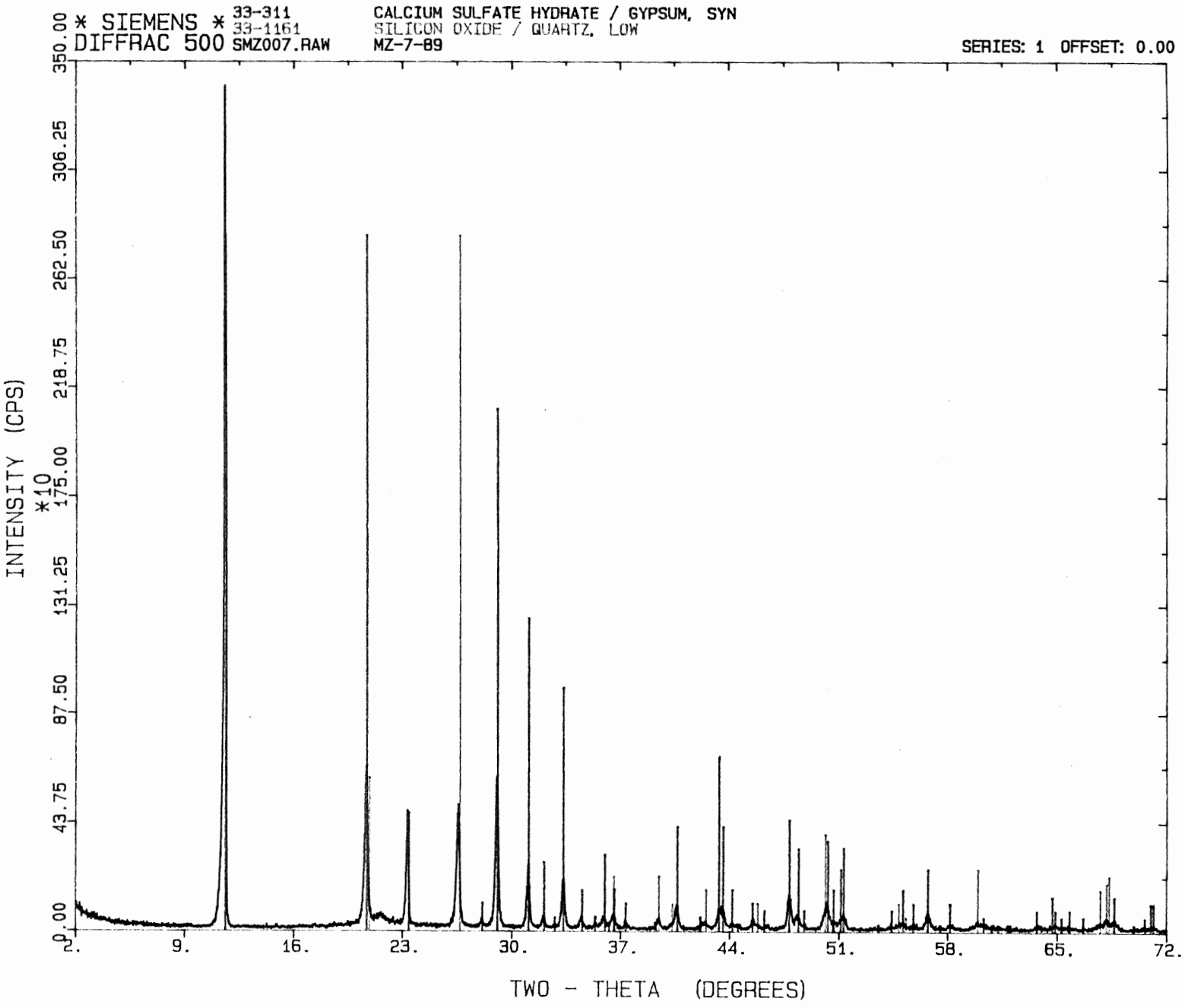
* SIEMENS * 33-311
DIFFRAC 500 33-1161
SMZ007.RAW
CALCIUM SULFATE HYDRATE / GYPSUM, SYN
SILICON OXIDE / QUARTZ, LOW
MZ-7-89
SERIES: 1 OFFSET: 0.00
INTENSITY (CPS)
*10
0.00
43.75
87.50
131.25
175.00
218.75
262.50
306.25
350.00
2.
9.
16.
23.
30.
37.
44.
51.
58.
65.
72.
TWO - THETA (DEGREES)

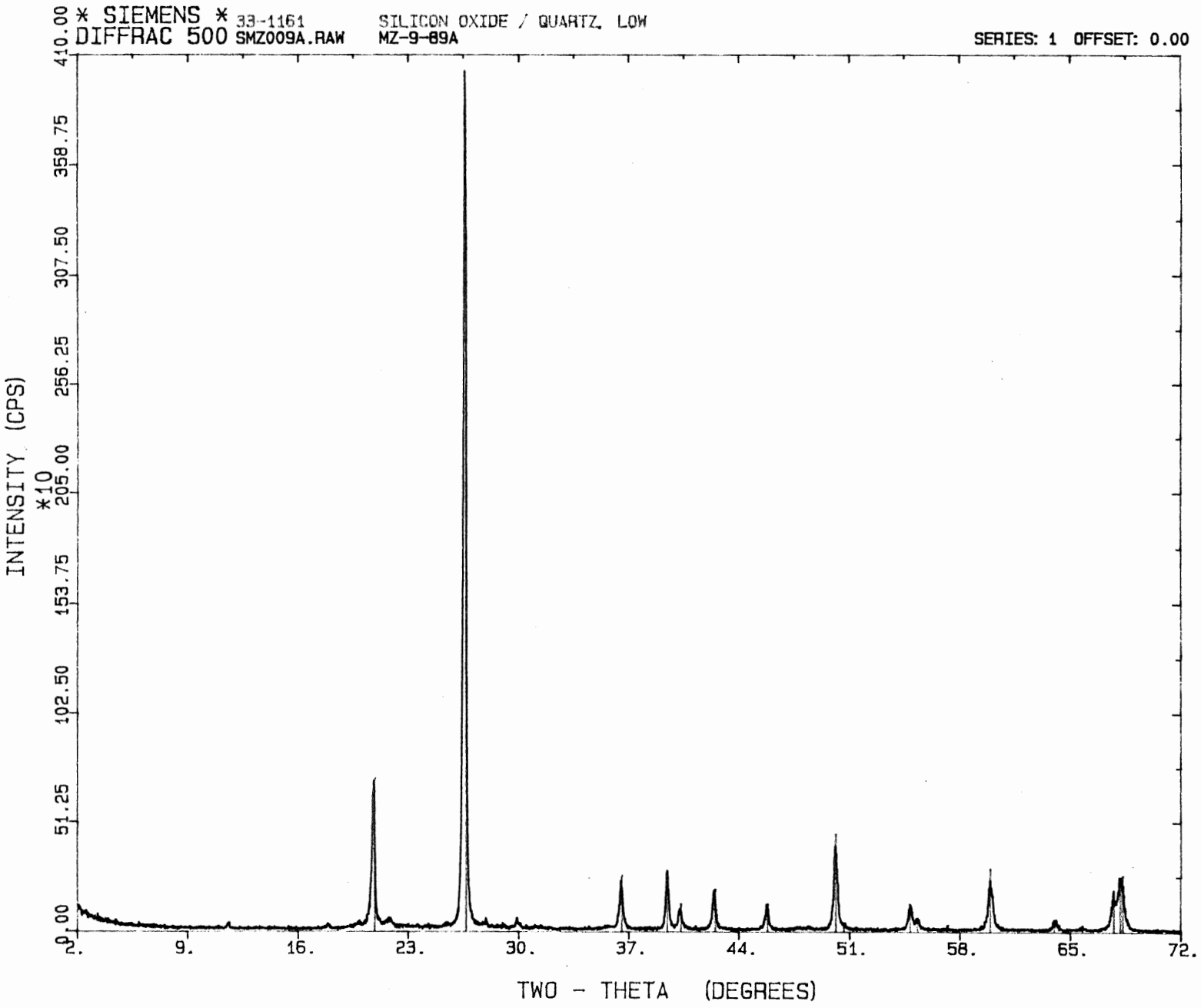
* SIEMENS * 33-1161
DIFFRAC 500 SMZ009A.RAW
SILICON OXIDE / QUARTZ, LOW
MZ-9-89A
SERIES: 1 OFFSET: 0.00
INTENSITY (CPS)
*10
410.00
358.75
307.50
256.25
205.00
153.75
102.50
51.25
0.00
2.
9.
16.
23.
30.
37.
44.
51.
58.
65.
72.
TWO - THETA (DEGREES)

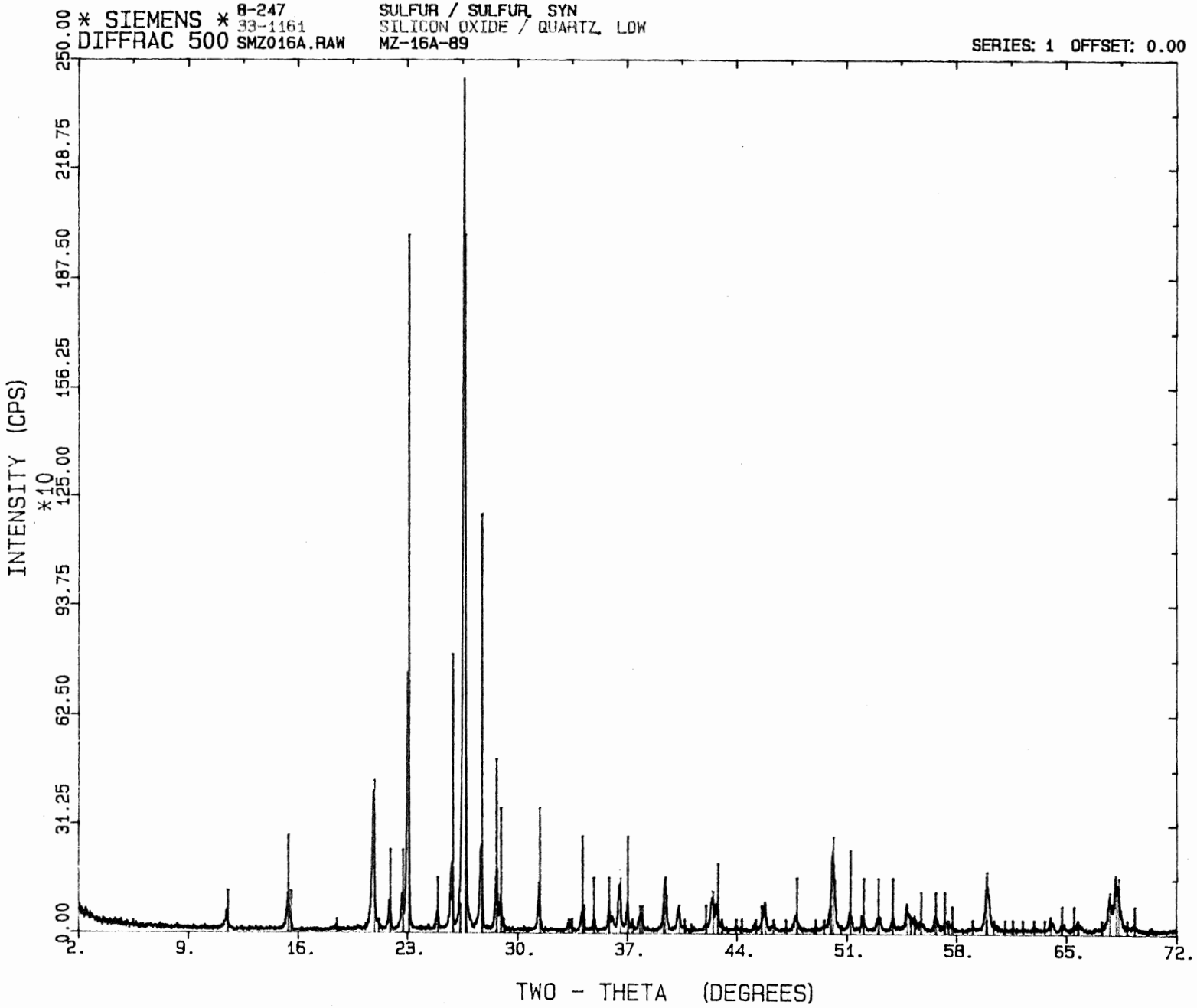
* SIEMENS *
DIFFRAC 500
8-247
33-1161
SMZ016A.RAW
SULFUR / SULFUR, SYN
SILICON OXIDE / QUARTZ, LOW
MZ-16A-89
SERIES: 1 OFFSET: 0.00
INTENSITY (CPS)
*10
250.00
218.75
187.50
156.25
125.00
93.75
62.50
31.25
0.00
2.
9.
16.
23.
30.
37.
44.
51.
58.
65.
72.
TWO - THETA (DEGREES)

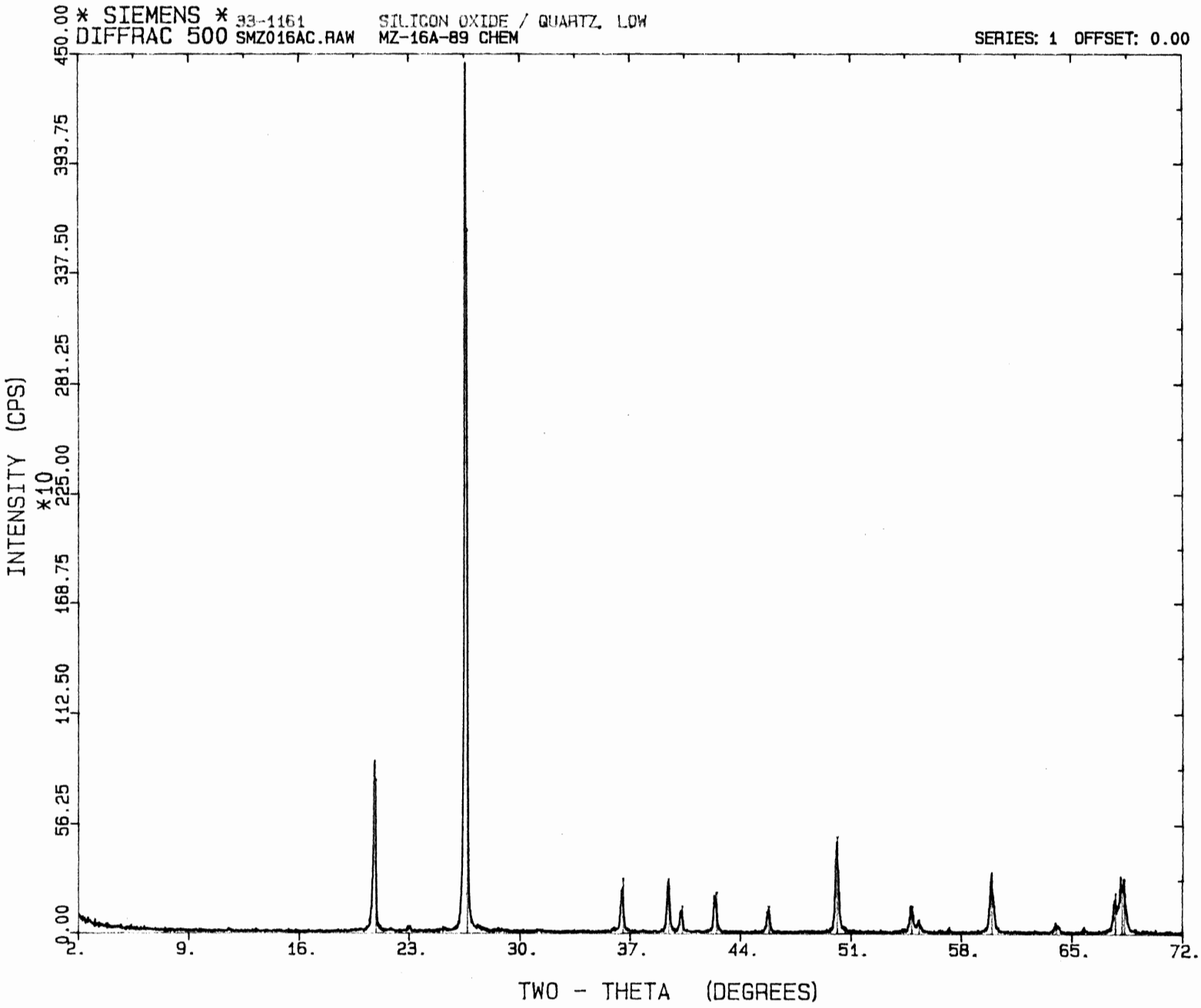
* SIEMENS * 33-1161 SILICON OXIDE / QUARTZ, LOW
DIFFRAC 500 SMZ016AC.RAW MZ-16A-89 CHEM
SERIES: 1 OFFSET: 0.00
INTENSITY (CPS)
*10
450.00
393.75
337.50
281.25
225.00
168.75
112.50
56.25
0.00
2.
9.
16.
23.
30.
37.
44.
51.
58.
65.
72.
TWO - THETA (DEGREES)

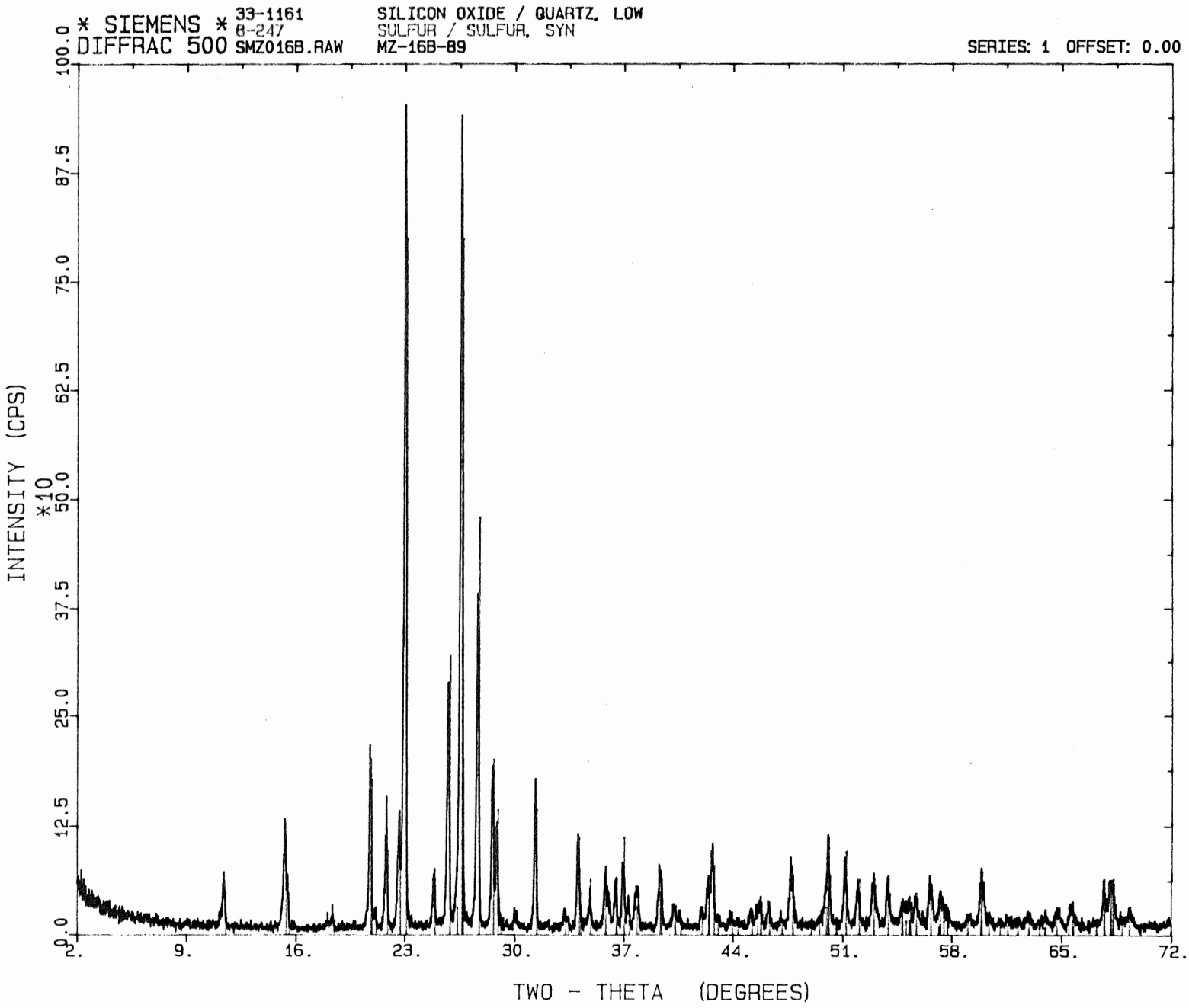
* SIEMENS * 33-1161
DIFFRAC 500 8-247 SMZ016B.RAW
SILICON OXIDE / QUARTZ, LOW
SULFUR / SULFUR, SYN
MZ-16B-89
SERIES: 1 OFFSET: 0.00
INTENSITY (CPS)
*10
100.0
87.5
75.0
62.5
50.0
37.5
25.0
12.5
0.0
2.
9.
16.
23.
30.
37.
44.
51.
58.
65.
72.
TWO - THETA (DEGREES)

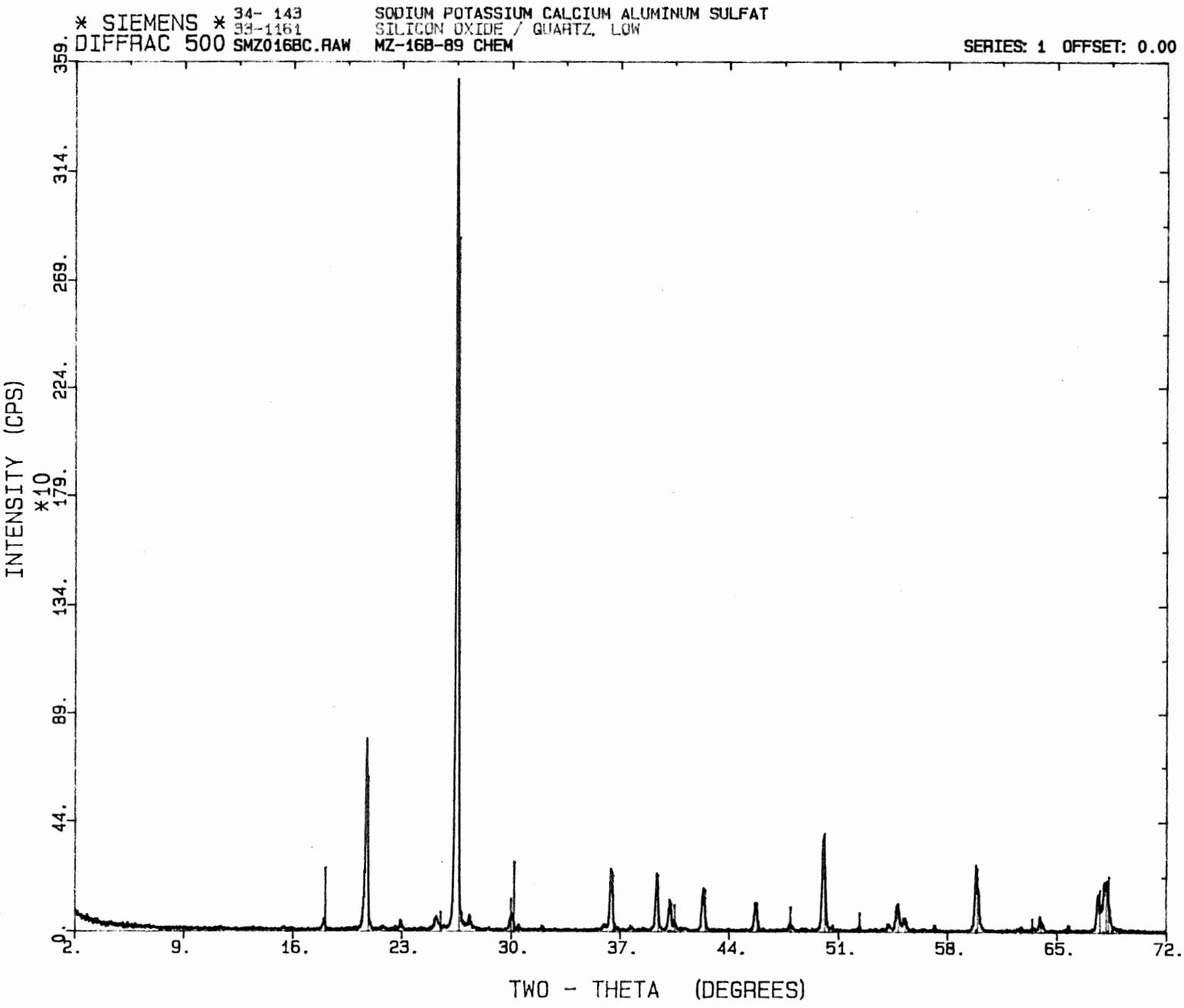
* SIEMENS * 34- 143
DIFFRAC 500 SMZ016BC.RAW
SODIUM POTASSIUM CALCIUM ALUMINUM SULFAT
SILICON OXIDE / QUARTZ, LOW
MZ-16B-89 CHEM
SERIES: 1 OFFSET: 0.00
INTENSITY (CPS)
*10
359.
314.
269.
224.
179.
134.
89.
44.
0.
2.
9.
16.
23.
30.
37.
44.
51.
58.
65.
72.
TWO - THETA (DEGREES)

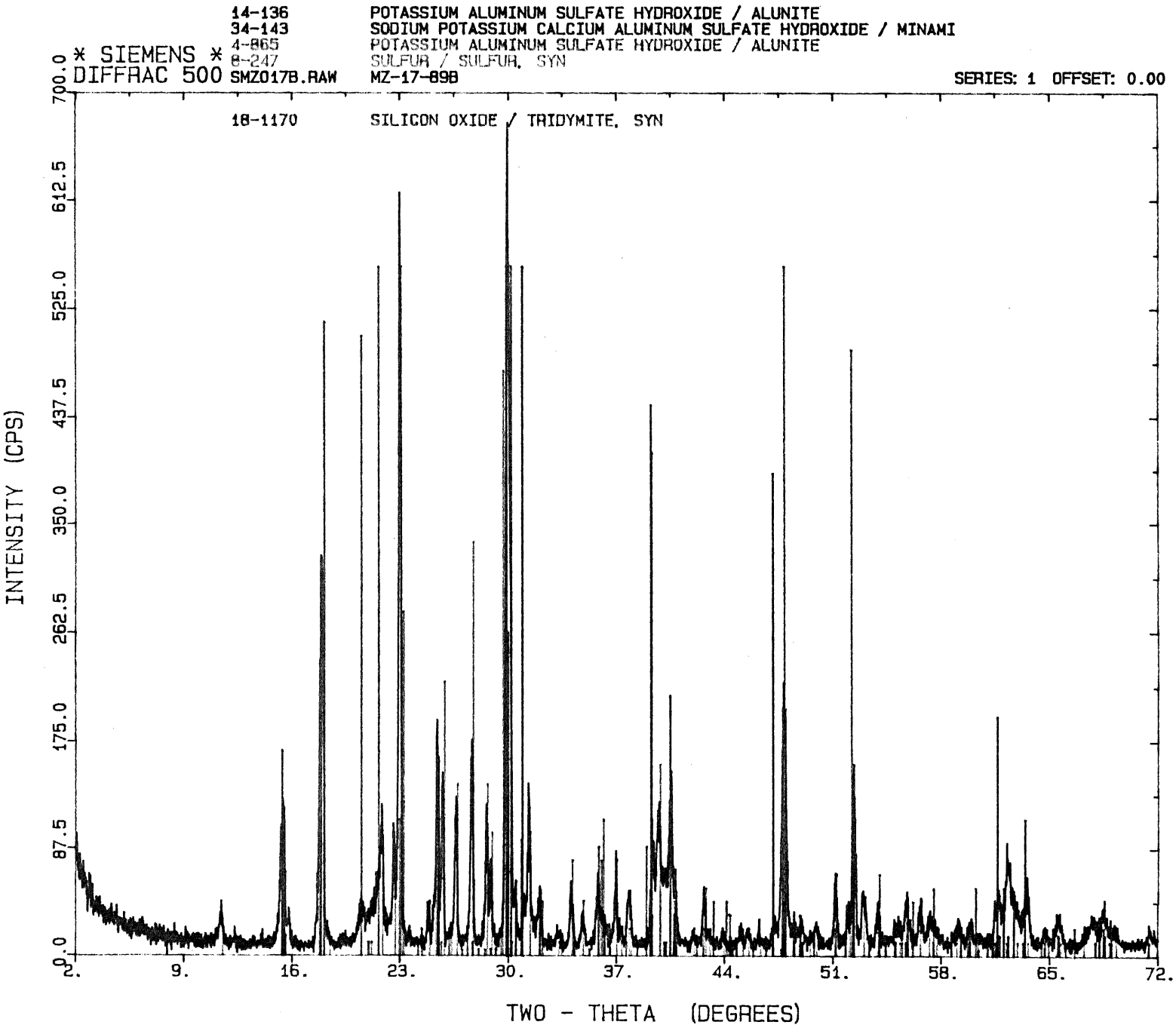
14-136 POTASSIUM ALUMINUM SULFATE HYDROXIDE / ALUNITE
34-143 SODIUM POTASSIUM CALCIUM ALUMINUM SULFATE HYDROXIDE / MINAMI
4-865 POTASSIUM ALUMINUM SULFATE HYDROXIDE / ALUNITE
8-247 SULFUR / SULFUR, SYN
* SIEMENS *
DIFFRAC 500
SMZ017B.RAW
MZ-17-89B
SERIES: 1 OFFSET: 0.00
18-1170 SILICON OXIDE / TRIDYMITE, SYN
INTENSITY (CPS)
700.0
612.5
525.0
437.5
350.0
262.5
175.0
87.5
0.0
2.
9.
16.
23.
30.
37.
44.
51.
58.
65.
72.
TWO - THETA (DEGREES)

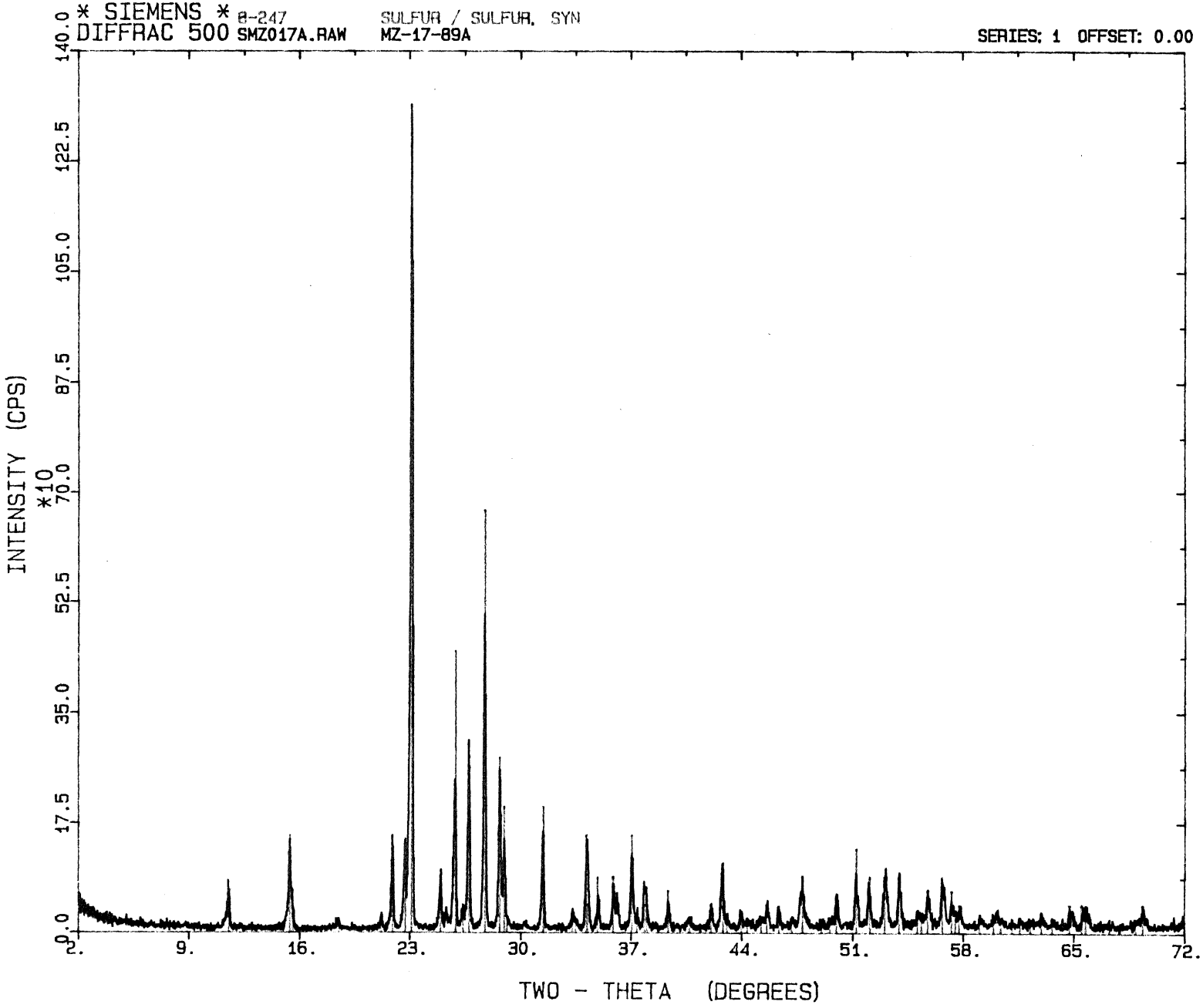
* SIEMENS * 8-247
DIFFRAC 500 SMZ017A.RAW
SULFUR / SULFUR, SYN
MZ-17-89A
SERIES: 1 OFFSET: 0.00
INTENSITY (CPS)
*10
140.0
122.5
105.0
87.5
70.0
52.5
35.0
17.5
0.0
2.
9.
16.
23.
30.
37.
44.
51.
58.
65.
72.
TWO - THETA (DEGREES)

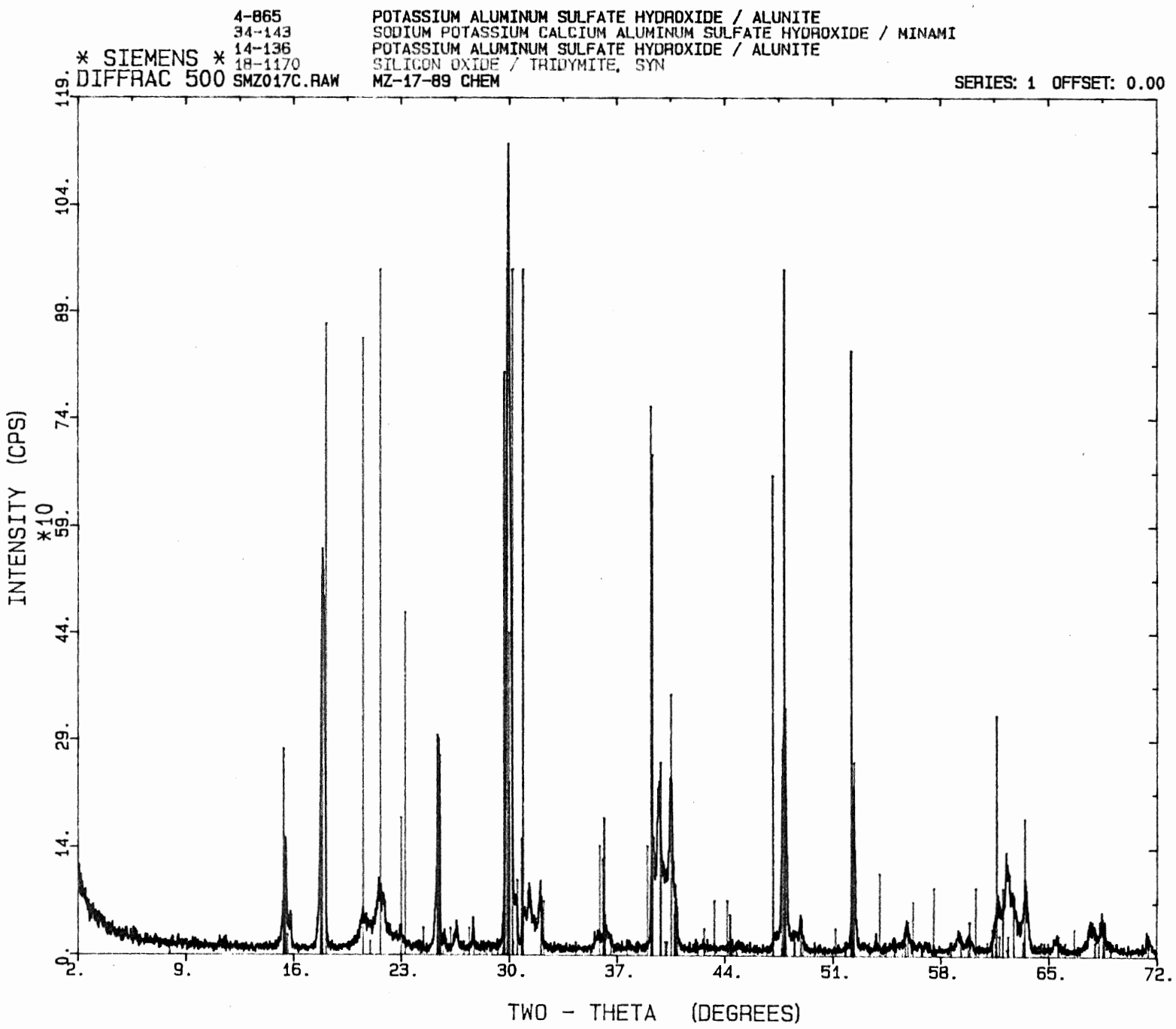
4-865 POTASSIUM ALUMINUM SULFATE HYDROXIDE / ALUNITE
34-143 SODIUM POTASSIUM CALCIUM ALUMINUM SULFATE HYDROXIDE / MINAMI
14-136 POTASSIUM ALUMINUM SULFATE HYDROXIDE / ALUNITE
18-1170 SILICON OXIDE / TRIDYMITE, SYN
* SIEMENS * DIFFRAC 500 SMZ017C.RAW MZ-17-89 CHEM
SERIES: 1 OFFSET: 0.00
INTENSITY (CPS) *10
119.
104.
89.
74.
59.
44.
29.
14.
0.
2.
9.
16.
23.
30.
37.
44.
51.
58.
65.
72.
TWO - THETA (DEGREES)

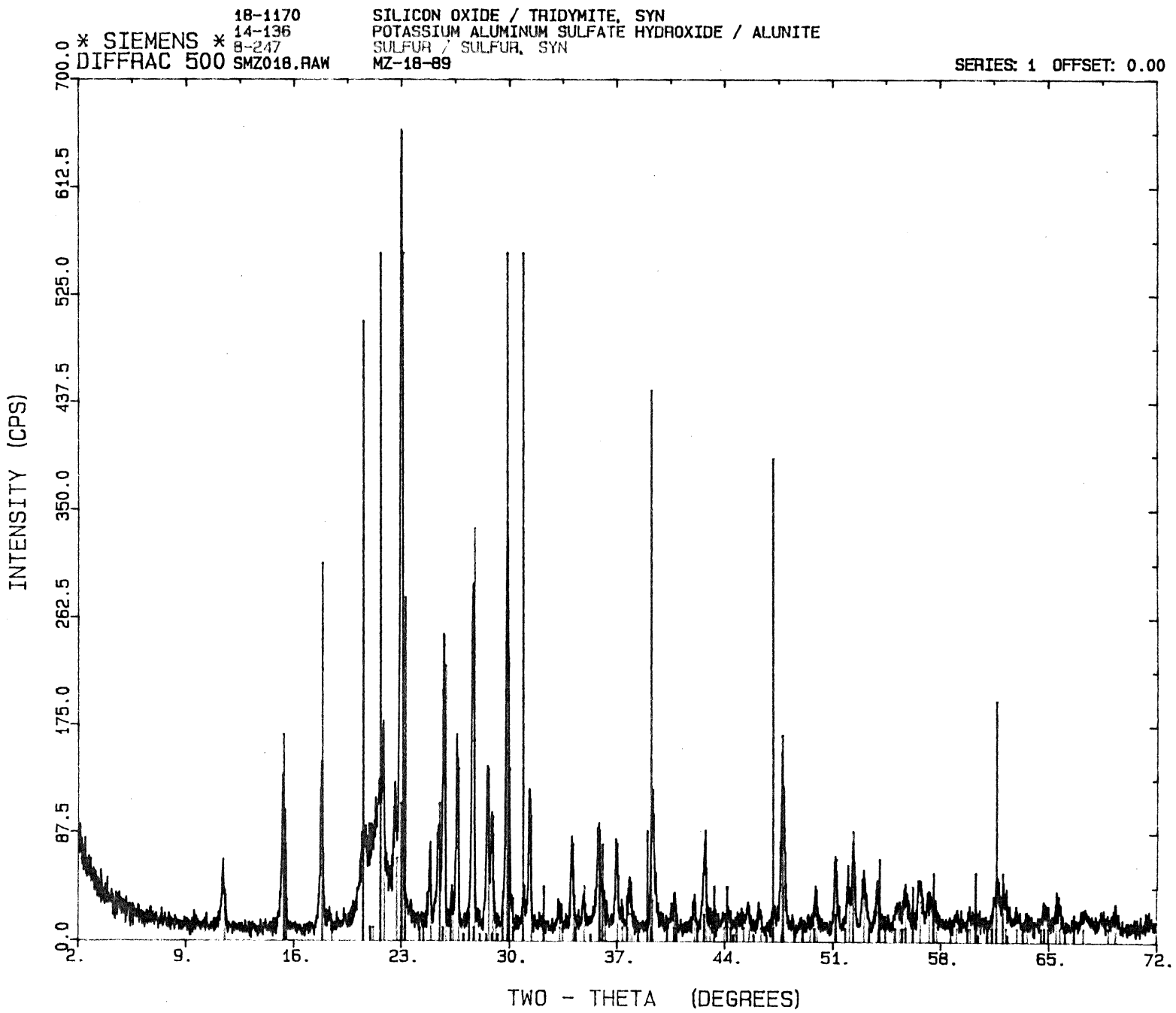
18-1170 SILICON OXIDE / TRIDYMITE, SYN
14-136 POTASSIUM ALUMINUM SULFATE HYDROXIDE / ALUNITE
8-247 SULFUR / SULFUR, SYN
* SIEMENS *
DIFFRAC 500
SMZ018.RAW
MZ-18-89
SERIES: 1 OFFSET: 0.00
INTENSITY (CPS)
700.0
612.5
525.0
437.5
350.0
262.5
175.0
87.5
0.0
2.
9.
16.
23.
30.
37.
44.
51.
58.
65.
72.
TWO - THETA (DEGREES)

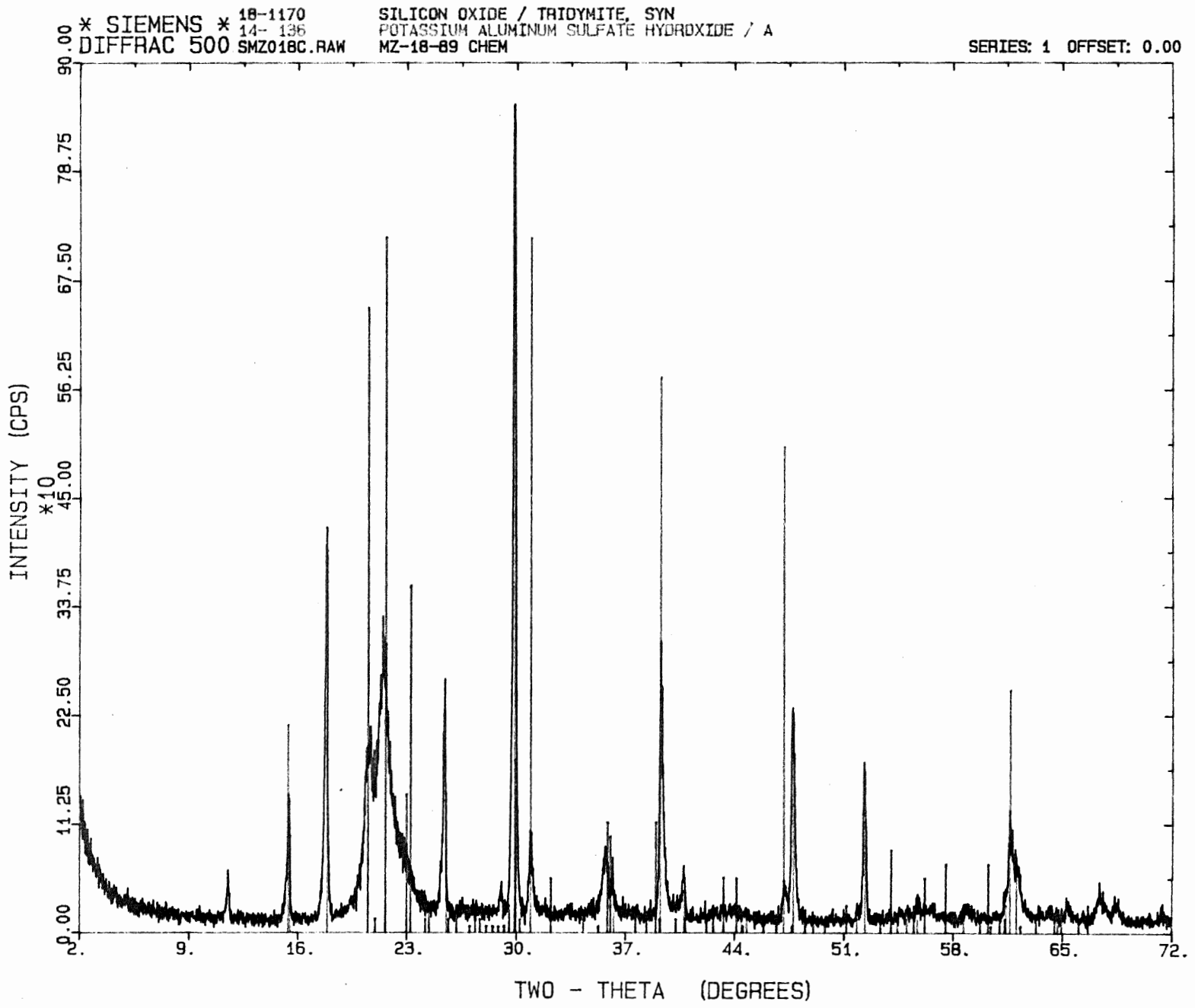
* SIEMENS *
DIFFRAC 500
18-1170
14- 136
SMZ018C.RAW
SILICON OXIDE / TRIDYMITE, SYN
POTASSIUM ALUMINUM SULFATE HYDROXIDE / A
MZ-18-89 CHEM
SERIES: 1 OFFSET: 0.00
INTENSITY (CPS)
*10
90.00
78.75
67.50
56.25
45.00
33.75
22.50
11.25
0.00
2.
9.
16.
23.
30.
37.
44.
51.
58.
65.
72.
TWO - THETA (DEGREES)

Appendix: C

Thin Section Description

Some samples are too soft and brittle to produce thin sections. However, many of the samples did produce thin sections and are in the following appendix.

Sample Number: MZ-4-89

Alteration

Hand Sample: High grade sulphur with minor earthy yellow alteration.

Thin Section: This sample contains native sulphur and some other cryptocrystalline material. XRD determines this to be tridymite.

Sample Number: MZ-5-89

Alteration

Hand Sample: Massive yellow-white alteration impregnated by native sulphur.

Thin Section: This sample is mostly cryptocrystalline, however, gypsum and native sulphur can be identified (confirmed by XRD). Gypsum and native sulphur accumulates in patches >1.4 mm in diameter. Relict structures of hornblende and plagioclase are present in this altered rock and are replaced with gypsum and native sulphur.

Sample Number: MZ-6-89

Alteration

Hand Sample: Massive earthy yellow native sulphur impregnated rock. Relict plagioclase phenocryst are observed >1.5 mm in length.

Thin Section: This sample contains very fine (>0.1 mm) irregular grains of native sulphur and quartz (confirmed by XRD) which accumulate together to form patches >1.5 mm in diameter. Relict plagioclase phenocryst are observed and are replaces with mainly quartz.

Sample Number: MZ-7-89

Alteration

Hand Sample: Cherty quartz encrusted in fibrous gypsum >0.4 cm in length.

Thin Section: Quartz (>0.3 mm in diameter) displays a chalcedonic texture and is present as one large mass. Gypsum is present as fibrous masses, up to 0.4 cm in width, rimming the quartz.

Sample Number: MZ-9-89

Alteration

Hand Sample: Cherty quartz veinlets with a rusty grossan.

Thin Section: Quartz displaying a chalcedonic texture.

Sample Number: MZ-13-89

Alteration

Hand Sample: Massive yellow earthy altered rock. Relict plagioclase phenocryst present as holes.

Thin Section: Unidentifiable material. XRD determines this material to be albite-anorthite.

Sample Number: MZ-14-89

Alteration

Hand Sample: Yellowish red altered silicified tuff. Relict plagioclase phenocryst present.

Thin Section: Unidentifiable material. XRD determines this material to be albite-anorthite.

Sample Number: MZ-16a-89

Alteration

Hand Sample: Porous and banded quartz in native sulphur impregnated breccia. Cinnabar is present as little specks >1 mm throughout the sample.

Thin Section: Anhedral quartz (>1 mm diameter) accumulating to form cm sized patches. These patches of quartz contain relict plagioclase phenocryst. Native sulphur and alunite is identified as a very fine grained (>0.1 mm) mass of up to 1.4 cm in size.

Sample Number: MZ-16b-89

Alteration

Hand Sample: Yellow, native sulphur-rich highly altered tuff containing pyroclasts of quartz (>1 cm in diameter).

Thin Section: Pyroclasts contain anhedral quartz (>2 mm diameter). A very fine grained (>0.1 mm) alteration consists of native sulphur and an unidentified material. XRD determines this to be alunite.

Sample Number: MZ-17-89

Alteration

Hand Sample: Massive earthy yellow native sulphur impregnated rock. Cinnabar is seen as small red specks >1 mm in diameter. Relict plagioclase phenocryst are present and are >2 mm in length.

Thin Section: This sample is cryptocrystalline. XRD identifies native sulphur, tridymite, and minimiite. Relict plagioclase phenocryst are observed >2 mm in length.

Sample Number: MZ-18-89

Alteration

Hand Sample: Massive earthy yellow native sulphur impregnated rock. Cinnabar is present as small red specks >1 mm in diameter.

This Section: This sample is cryptocrystalline. XRD identifies alunite, native sulphur, and minor tridymite. Relict plagioclase phenocryst are observed >1.4 mm in length.

Appendix D:

Volcan Copiapo
Chemical Results

Sample	total* [1] % S	Au*	Sb	As	W	Cu	Pb	Mo	Hg*	Ag	Zn	Ba
MZ-3-89		-	3	39	**1120**	27	9	3	540	-	22	200
MZ-5-89	**31.21**	**11**	-	19	46	4	3	1	158	-	1	660
MZ-6-89	**42.85**	-	-	3	34	2	-	1	115	-	2	850
MZ-7-89	9.25	-	-	-	110	2	-	2	86	-	-	360
MZ-9-89	0.30	-	-	-	**928**	7	-	-	317	-	2	520
MZ-10-89	2.65	-	3	42	**928**	19	8	2	61	-	11	980
MZ-12-89	2.51	-	-	13	94	16	5	-	245	-	14	1100
MZ-13a-89	3.71	-	3	38	89	20	**11**	1	72	-	17	660
MZ-13b-89	1.11	-	2	36	200	20	6	1	55	-	12	560
MZ-14-89	7.81	-	2	**63**	549	6	-	1	43	-	2	430
MZ-16a-89	**21.11**	-	**22**	7	335	2	-	1	**22960**[2]	-	-	570
MZ-16b-89	**63.51**	**18**	**27**	20	66	3	8	1	**12960**[2]	**.1**	2	460
MZ-18-89	**46.82**	-	**27**	3	31	3	4	1	**10960**[2]	-	2	510
MZ-20-89		-	3	38	2	25	9	3	166	**.2**	18	1100

Sample	% S	Au*	As	Pb	Mo	Hg*	Ag	Ba
WZ-117-84	0.36	**1560**	**108**	**122**	**33**	**1210**[2]	<2	668
WZ-120-84	2.00	**571**	**212**	**469**	**87**	90[2]	<2	
WZ-122-84	0.54	**4670**	**449**	**73**	**58**	20[2]	<2	

*Note: All elements are in ppm with the exception of S, Au and Hg. (Au and Hg are measured in ppb) (S is in %).

[1] Sulphur analysis done by Mineral Engineering Centre, Technical University of Nova Scotia. Method: Total leach; Leco Titration.

[2] Hg analysis done by Mineral Engineering Centre, Technical University of Nova Scotia. Method: Cold Vapour Atomic Adsorption.

Unless otherwise stated, all MZ samples were analyzed for Dr. Zentilli at Bondar-Clegg & Company Ltd. in Ottawa, Canada. Method: Neutron Activation Analysis for Au, Sb, As, W, and Ba. Atomic Absorptoin Analysis for Cu, Pb, Mo, Ag, Zn. Cold Vapour Atomic Adsorption for Hg.

Unless otherwise stated, all WZ geochemistry comes from Mulja (1986). Method: Neutron Activation Analysis for Au, Ag, As, Mo. X-ray Fluorescence for Ba.

Appendix E:

Sulphur Isotope Analysis

Sulphur isotope values are determined at Krueger Enterprises Inc. using an Isogas Micromass 602 D mass spectrometer. Sulphate samples are reduced by boiling in a HCl-HI-H3PO2 acid bath. The sulphur is precipitated by bubbling through a Cd(COOH)2 solution to form CdS. The CdS is filtered, dried, and burned to form SO2 gas. Native sulphur samples are simply burned to form SO2 gas. This gas is fed into the mass spectrometer for sulphur isotope value determination.

Appendix F:

Microprobe work was done by the author at Dalhousie University, Halifax, Nova Scotia, Canada.

Microprobe: raw data for Samples MZ-13-19, MZ-14-89, MZ-15-89, MZ-16a-89, MZ-18-89.

MZ-13-89

Oxide	Results wt%	Norm wt%
SIO2	95.00	99.91
TIO2	0.00	0.00
AL203	0.08	0.09
FEO	0.00	0.00
MNO	0.00	0.00
MGO	0.00	0.00
CAO	0.00	0.00
NA2O	0.00	0.00
K 2O	0.00	0.00
S O4	0.00	0.00
Total =	95.08	

MZ-14-89

Oxide	Results wt%	Norm wt%
SIO2	83.34	99.29
TIO2	0.24	0.29
AL203	0.23	0.27
FEO	0.00	0.00
MNO	0.00	0.00
MGO	0.00	0.00
CAO	0.00	0.00
NA2O	0.02	0.02
K 2O	0.00	0.00
S O4	0.11	0.13
Total =	83.94	

MZ-14-89

Oxide	Results wt%	Norm wt%
SIO2	0.36	0.42
TIO2	0.03	0.04
AL203	41.96	49.59
FEO	2.27	2.68
MNO	0.00	0.00
MGO	0.15	0.18
CAO	0.16	0.19
NA2O	1.46	1.72
K 2O	2.38	2.81
S O4	35.84	42.36
Total =	84.60	

MZ-14-89

Oxide	Results wt%	Norm wt%
SIO2	1.38	1.57
TIO2	0.00	0.00
AL203	45.42	51.73
FEO	0.35	0.40
MNO	0.00	0.00
MGO	0.02	0.02
CAO	0.06	0.06
NA2O	1.68	1.92
K 2O	1.03	1.17
S O4	37.87	43.13
Total =	87.80	

MZ-14-89

Oxide	Results wt%	Norm wt%
SIO2	60.53	61.78
TIO2	0.00	0.00
AL203	20.81	21.24
FEO	3.00	3.06
MNO	0.00	0.00
MGO	0.09	0.09
CAO	0.42	0.43
NA2O	0.14	0.15
K 2O	1.08	1.10
S O4	11.90	12.14
Total =	97.97	

MZ-15-89

Oxide	Results wt%	Norm wt%
SIO2	93.64	98.95
TIO2	0.07	0.07
AL203	0.71	0.75
FEO	0.13	0.14
MNO	0.00	0.00
MGO	0.00	0.00
CAO	0.00	0.00
NA2O	0.09	0.09
K 2O	0.00	0.00
S O4	0.00	0.00
Total =	94.64	

MZ-15-89

Oxide Results

	wt%	Norm wt%
SIO2	0.77	0.95
TIO2	0.00	0.00
AL203	39.40	48.65
FEO	2.12	2.61
MNO	0.00	0.00
MGO	0.00	0.00
CAO	0.15	0.18
NA2O	0.89	1.10
K 2O	6.19	7.65
S O4	31.47	38.85
Total =	81.00	

MZ-15-89

Oxide Results

	wt%	Norm wt%
SIO2	85.59	99.85
TIO2	0.00	0.00
AL203	0.13	0.15
FEO	0.00	0.00
MNO	0.00	0.00
MGO	0.00	0.00
CAO	0.00	0.00
NA2O	0.00	0.00
K 2O	0.00	0.00
S O4	0.00	0.00
Total =	86.02	

MZ-15-89

Oxide Results

	wt%	Norm wt%
SIO2	0.00	0.00
TIO2	0.01	0.01
AL203	54.88	56.75
FEO	0.05	0.06
MNO	0.00	0.00
MGO	0.01	0.01
CAO	0.00	0.00
NA2O	0.46	0.48
K 2O	2.01	2.08
S O4	39.26	40.60
Total =	96.70	

MZ-16a-89

Oxide Results

	wt%	Norm wt%
SIO2	89.52	98.12
TIO2	1.28	1.41
AL203	0.29	0.32
FEO	0.00	0.00
MNO	0.00	0.00
MGO	0.00	0.00
CAO	0.00	0.00
NA2O	0.01	0.01
K 2O	0.00	0.00
S O4	0.13	0.14
Total =	91.24	

MZ-16a-89

Oxide Results

	wt%	Norm wt%
SIO2	55.51	34.92
TIO2	0.15	0.09
AL203	0.14	0.09
FEO	0.00	0.00
MNO	0.00	0.00
MGO	0.00	0.00
CAO	0.00	0.00
NA2O	0.02	0.02
K 2O	0.00	0.00
S O4	103.16	64.89
Total =	159.00	

MZ-16a-89

Oxide Results

	wt%	Norm wt%
SIO2	96.97	99.96
TIO2	0.00	0.00
AL203	0.02	0.02
FEO	0.00	0.00
MNO	0.00	0.00
MGO	0.00	0.00
CAO	0.00	0.00
NA2O	0.02	0.02
K 2O	0.00	0.00
S O4	0.00	0.00
Total =	97.01	

MZ-16a-89

Oxide	Results wt%	Norm wt%
SIO2	12.52	16.13
TIO2	0.00	0.00
AL203	30.18	38.87
FEO	0.45	0.58
MNO	0.00	0.00
MGO	0.06	0.07
CAO	0.25	0.32
NA2O	8.63	11.11
K 2O	1.59	2.05
S O4	23.97	30.87
Total =	77.63	

MZ-16a-89

Oxide	Results wt%	Norm wt%
SIO2	93.81	99.27
TIO2	0.00	0.00
AL203	0.55	0.58
FEO	0.00	0.00
MNO	0.00	0.00
MGO	0.01	0.01
CAO	0.00	0.00
NA2O	0.01	0.01
K 2O	0.00	0.00
S O4	0.12	0.13
Total =	94.50	

MZ-16a-89

Oxide	Results wt%	Norm wt%
SIO2	89.92	99.27
TIO2	0.00	0.00
AL203	0.61	0.67
FEO	0.00	0.00
MNO	0.00	0.00
MGO	0.00	0.00
CAO	0.05	0.05
NA2O	0.00	0.00
K 2O	0.00	0.00
S O4	0.00	0.00
Total =	90.58	

MZ-18-89

Oxide	Results wt%	Norm wt%
SIO2	20.44	20.60
TIO2	0.00	0.00
AL203	44.98	45.34
FEO	0.00	0.00
MNO	0.00	0.00
MGO	0.02	0.02
CAO	0.13	0.13
NA2O	0.86	0.87
K 2O	2.35	2.37
S O4	30.43	30.67
Total =	99.22	

MZ-18-89

Oxide	Results wt%	Norm wt%
SIO2	3.50	3.85
TIO2	0.00	0.00
AL203	48.89	53.72
FEO	0.36	0.69
MNO	0.00	0.00
MGO	0.02	0.02
CAO	0.14	0.15
NA2O	0.68	0.42
K 2O	3.24	3.56
S O4	34.49	37.89
Total =	91.01	

MZ-18-89

Oxide	Results wt%	Norm wt%
SIO2	32.53	32.22
TIO2	0.00	0.00
AL203	41.01	40.62
FEO	0.11	0.11
MNO	0.00	0.00
MGO	0.02	0.02
CAO	0.18	0.18
NA2O	0.29	0.28
K 2O	1.95	1.94
S O4	24.87	24.63
Total =	100.95	

MZ-18-89

Oxide	Results wt%	Norm wt%
SIO2	0.91	1.11
TIO2	0.00	0.00
AL203	39.42	48.15
FEO	0.17	0.20
MNO	0.00	0.00
MGO	0.00	0.00
CAO	0.01	0.02
NA2O	0.44	0.54
K 2O	4.08	4.98
S O4	36.85	45.01
Total =	81.88	

MZ-18-89

Oxide	Results wt%	Norm wt%
SIO2	0.00	0.00
TIO2	0.00	0.00
AL203	50.23	53.98
FEO	0.17	0.18
MNO	0.00	0.00
MGO	0.00	0.00
CAO	0.06	0.06
NA2O	0.48	0.51
K 2O	2.04	2.19
S O4	40.08	43.08
Total =	93.05	

MZ-18-89

Oxide	Results wt%	Norm wt%
SIO2	0.18	0.20
TIO2	0.00	0.00
AL203	48.98	54.05
FEO	0.00	0.00
MNO	0.00	0.00
MGO	0.00	0.00
CAO	0.00	0.00
NA2O	0.63	0.69
K 2O	2.53	2.79
S O4	38.30	42.26
Total =	90.62	

MZ-18-89

Oxide	Results wt%	Norm wt%
SIO2	0.00	0.00
TIO2	0.00	0.00
AL203	42.65	51.47
FEO	1.04	1.26
MNO	0.00	0.00
MGO	0.00	0.00
CAO	0.07	0.08
NA2O	0.97	1.17
K 2O	0.69	0.84
S O4	37.45	45.19
Total =	82.87	

Appendix G:

Atomic Absorption of Potassium in CS2 Sulphur Saturated Solution:

All assumptions made below are in favour of the chemical treatment affecting the potassium content in sample MZ-18-89. This sample contains an abundant amount of the potassium-rich mineral alunite.

Atomic Absorption for K+ in this solution was conducted at the Technical University of Nova Scotia and yielded a concentration of 0.25 ppm.

Potassium Removed From Sample by Chemical Treatment:

Measured density of sulphur saturated solution = 1.23 g/ml

Volume of saturated liquid = 27.6 ml

Concentration of K+ in solution = 0.25 ppm

g of K+ = (0.25*10-6 g of K+/litre of soln)*1.23 g/ml soln

g of K+ in 1 litre = 3.075*10-4 g/l

The total amount of K+ removed from rock sample = total amount of K+ in saturated solution.

g of K+ removed from sample = K+ in 27.6 ml = 8.48*10-6 g of K+

Analysis of Potassium in Chemically Treated Sample:

Flame-photometric analysis for potassium from Krueger Enterprises Inc. is done on the chemically treated sample.

Weight of sample 7.81 g

Flame-photometric analysis = 1.392 %

Alunite is the only potassium bearing mineral identified by XRD or microprobe in the sample (molecular weight = 414.18 g/mol).

moles of alunite = 7.81 g/414.18 g/mol = 0.01883 mol.

Therefore, 7.81 g of alunite has approximately 0.10868 g of K.

Flame-Photometric Analysis for K:

A good analysis will have 0.1% error by flame-photometric analysis and is accurate to the milligram. The above calculation shows that the K removed is two orders of magnitude lower than the error of a good analysis. The insignificant difference could be from traces of K in native sulphur.

Appendix H:

K-Ar Geochronology From Krueger Enterprises Inc.

1.) Sample MZ-26-85, hornblende in an andesite.

Argon Analyses:

$^{40*}Ar$, ppm	$^{40*}Ar/Total^{40}Ar$	Ave.$^{40*}Ar$, ppm
0.001219	0.689	0.001220
0.001221	0.654	

Potassium Analyses:

% K	Ave. % K	^{40}K, ppm
2.029	2.013	2.402
1.997		

$^{40*}Ar/^{40}K$= 0.000508

AGE= 8.7 +/- 0.5 M.Y.

2.) Sample MZ-15b-89, alunite chips from a silica cap.

Argon Analyses:

$^{40*}Ar$, ppm	$^{40*}Ar/Total^{40}Ar$	Ave.^{40}Ar, ppm
0.004646	0.096	0.004513
0.004379	0.087	

Potassium Analyses:

% K	Ave. % K	$^{40*}K$, ppm
4.856	4.868	5.808
4.880		

$^{40*}Ar/^{40}K$= 0.000777

AGE= 13.3 +/- 0.5 M.Y.

3.) Sample MZ-18-89, alunite alteration associated with native sulphur near a hydrothermal breccia vent. Chemically treated with carbon disulphide.

Argon Analyses:

$^{40*}Ar$, ppm	$^{40*}Ar/Total\ ^{40}Ar$	Ave. $^{40*}Ar$, ppm
0.003678	0.033	0.003635
0.003591	0.034	

Potassium Analyses:

% K	Ave. % K	^{40}K, ppm
1.413	1.392	1.661
1.371		

$^{40*}Ar/^{40}K$= 0.002189

AGE= 37.3 +/- 1.4 M.Y.

Appendix I:

$^{40}Ar/^{39}Ar$ Heating Steps For MZ-11-89 Biotite and Hornblende.

MZ11-89B BIOTITE SUMMARY

°C	mV 39	% 39	AGE(Ma)	% ATMOS	37/39	40/36	39/36	% IIC
500	4	<1	-31.6 +/- 5.7	113	1.024	260	4.7	1
600	6	<1	-19.8 +/- -3	113	.862	262	7.1	1
650	18	<1	5.6 +/- 1.5	94	.232	314	13.4	0
700	607	18	8.5 +/- .1	39	.021	750	223.1	1
850	267	8	8.4 +/- .1	42	.018	696	198.9	1
900	796	24	8 +/- .1	44	.02	676	198.9	1
950	371	11	8.3 +/- .2	63	.049	472	89.4	1
1000	652	20	6.4 +/- .3	75	.18	392	63.2	0
1050	540	16	7.7 +/- .2	68	.235	432	74.2	0
1100	80	2	10.8 +/- .4	71	.766	414	46.2	2

TOTAL GAS AGE = 8 Ma

J = 2.34E-03

ERROR ESTIMATES AT ONE SIGMA LEVEL

37/39,40/36 AND 39/36 Ar RATIOS ARE CORRECTED FOR INTERFERING ISOTOPES

% IIC - INTERFERING ISOTOPES CORRECTION

MZ11-89B BIOTITE SUMMARY

°C	mV 39	% 39	AGE(Ma)	% ATMOS	37/39	40/36	39/36	% IIC
500	4	<1	-31.6 +/- -5.7	113	1.024	260	4.7	1
600	6	<1	-19.8 +/- -3	113	.862	262	7.1	1
650	18	<1	5.6 +/- 1.5	94	.232	314	13.4	0
700	607	18	8.5 +/- .1	39	.021	750	223.1	1
850	267	8	8.4 +/- .1	42	.018	696	198.9	1
900	796	24	8 +/- .1	44	.02	676	198.9	1
950	371	11	8.3 +/- .2	63	.049	472	89.4	1
1000	652	20	6.4 +/- .3	75	.18	392	63.2	0
1050	540	16	7.7 +/- .2	68	.235	432	74.2	0
1100	80	2	10.8 +/- .4	71	.766	414	46.2	2

TOTAL GAS AGE = 8 Ma

J = 2.34E-03

ERROR ESTIMATES AT ONE SIGMA LEVEL

37/39,40/36 AND 39/36 Ar RATIOS ARE CORRECTED FOR INTERFERING ISOTOPES

% IIC - INTERFERING ISOTOPES CORRECTION